Titre: Title:	Aeroelastic analysis of circular cylindrical and truncated conical shells subjected to a supersonic flow
Auteur: Author:	Farhad Sabri
Date:	2009
Type:	Mémoire ou thèse / Dissertation or Thesis
Référence: Citation:	Sabri, F. (2009). Aeroelastic analysis of circular cylindrical and truncated conical shells subjected to a supersonic flow [Thèse de doctorat, École Polytechnique de Montréal]. PolyPublie. https://publications.polymtl.ca/8455/

UNIVERSITÉ DE MONTRÉAL

AEROELASTIC ANALYSIS OF CIRCULAR CYLINDRICAL AND TRUNCATED CONICAL SHELLS SUBJECTED TO A SUPERSONIC FLOW

FARHAD SABRI

DÉPARTEMENT DE GÉNIE MÉCANIQUE

ÉCOLE POLYTECHNIQUE DE MONTRÉAL

THÈSE PRÉSENTÉE EN VUE DE L'OBTENTION

DU DIPLÔME DE PHILOSOPHIAE DOCTOR

(GÉNIE MÉCANIQUE)

JUIN 2009

Your file Votre référence
ISBN: 978-0-494-53806-7
Our file Notre référence
ISBN: 978-0-494-53806-7

UNIVERSITÉ DE MONTRÉAL

ÉCOLE POLYTECHNIQUE DE MONTRÉAL

Cette thèse intitulée :

AEROELASTIC ANALYSIS OF CIRCULAR CYLINDRICAL AND TRUNCATED CONICAL SHELLS SUBJECTED TO A SUPERSONIC FLOW

présentée par: SABRI Farhad

en vue de l'obtention du diplôme de : Philosophiae Doctor

a été dument acceptée par le jury d'examen constitue de :

M. KAHAWITA René, Ph.D., président

M. LAKIS Aouni A., Ph.D., membre et directeur de recherche

M. SHIRAZI-ADL Aboulfazl, Ph.D., membre

M. NEJAD ENSAN Manouchehr, Ph.D., membre externe

Dedication

To: my parents
my sister and brothers
and my wife, Hamideh

Acknowledgments

I would like to acknowledge the friendly supervision, complete support and advice given by Prof. Aouni A. Lakis, my thesis advisor, throughout the course of my PhD. He has been a great source of knowledge and inspiration during the period leading to my thesis and in all submitted papers for publication.

I express my warmest thanks to all present and former graduate students of Applied Mechanics section with whom I spent most of my non-academic time relaxing, enjoying, and discussing. They made Montreal my home away from home.

The last but not the least, I would like to thank my lovely wife, Hamideh, for her constant devotion, support, endurance and for all her love during the whole course of our stay in Montreal.

The financial support from the NSERC (Canada) is gratefully acknowledged.

Résumé

Les coques de révolution, en particulier les coques cylindrique et conique, sont l'un des principaux éléments structurels dans les structures aérospatiales. Avec l'avancement de la grande vitesse des avions, ces coques peuvent montrer de l'instabilité dynamique lorsqu'elles sont exposées à un écoulement supersonique. Par conséquent, l'analyse aéroélastique de ces éléments est l'un des principaux critères de conception que les ingénieurs aéronautiques traitent. Cette analyse peut être faite à l'aide de la méthode des éléments finis (FEM) couplée avec la dynamique des fluides computationnelle (CFD) ou avec les méthodes expérimentales qui nécessitent beaucoup de temps et qui coûtent très chères. L'objectif de cette thèse est de développer un tel outil numérique pour faire une analyse aéroélastique rapide et précise. Pendant ce temps, au cours de la phase de conception où les différentes configurations de chargement et de condition aux limites peuvent être analysées, cette méthode numérique peut être utilisée très facilement avec un niveau élevé de fiabilité. Dans cette étude, la modélisation structurelle est une combinaison de la théorie linéaire des coques minces de Sanders et de la méthode classique des éléments finis. En se basant sur la méthode de l'élément fini hybride, les déplacements des coques sont trouvés à partir des solutions exactes de la théorie de la coque plutôt que l'approximation faite par la fonction polynôme de la méthode traditionnelle des éléments finis. Ceci conduit à une convergence rapide et précise. La modélisation aérodynamique supersonique se fait sur la base de la théorie de piston et de la théorie de piston modifiée avec le terme de courbure de la coque. La rigidité du stress est due à la pression latérale et axiale de compression qui sont également prises en

compte. L'interaction fluide-structure en présence du fluide interne au repos est modélisée sur la base de la théorie du potentiel. Dans cette méthode, le fluide est considéré comme un potentiel de vitesse variable à chaque nœud de l'élément coque où son mouvement est exprimé en termes de déplacement nodal élastique à l'interface fluide-structure.

Cet élément fini hybride proposé a les capacités de faire les analyses suivantes :

i) Le flambement et les vibrations d'une coque cylindrique ou conique vide ou une partiellement remplie de fluide, qui est soumise à la pression interne et externe et le chargement de compression axiale. Ceci est un exemple typique du liquide extérieur propulsé du réservoir des navettes spatiales et de véhicules de rentrée, où ils peuvent avoir l'expérience de ce type de chargement pendant le vol. Dans le présent travail, les différentes conditions aux limites des coques cylindriques avec différents taux de remplissage ont été analysées. Pour les meilleurs auteurs connus, cette étude est la première en ce genre où ce type de chargement et de conditions aux limites complexes est traité ensemble au cours d'une telle analyse. Seulement l'instabilité statique et la divergence ont été observées où il a été montré que le taux de remplissage ne doit pas avoir d'effet sur la pression critique de flambement et de compression axiale. Juste les fréquences de vibration sont diminuées. Il a été aussi observé que les coques pressurisées perdent leurs stabilités au haut flambement axial de chargement.

ii) Analyse aéroélastique des coques cylindriques et coniques vides ou partiellement remplies de liquide. Différentes conditions aux limites et géométries de coques soumises à des écoulements d'air supersonique sont étudiées dans cette étude. Dans tous les cas,

les coques perdent leur stabilité pour le mode de battement couplé. Les résultats montrent que la pression interne a un effet stabilisateur et augmente la vitesse critique de battement. Il a été observé que la valeur critique de la pression dynamique change rapidement et augmente largement le taux de remplissage pour de petites valeurs. En outre, en augmentant le ratio de la longueur, la décroissance de la vitesse de battement disparaît et est réduite. Ce changement rapide de la pression critique dynamique à faible taux de remplissage et de son comportement presque stable au grand taux de remplissage indique que le liquide près du fond de la coque est largement influencé par la déformation élastique lorsque la coque est soumise à l'écoulement subsonique externe.

Sur la base de comparaison avec les données numériques, analytiques et expérimentales existantes et des fortes capacités de la méthode de l'élément fini hybride pour modéliser différentes conditions aux limites et de chargements complexes, cet outil des FEM peut être utilisé efficacement pour la conception de structures aérospatiales avancées. Il fournit des résultats à moindre coût de calcul comparé au logiciel commercial FEM, qui impose des limitations au moment où cette analyse est effectuée.

Abstract

Shells of revolution, particularly cylindrical and conical shells, are one of the basic structural elements in the aerospace structures. With the advent of high speed aircrafts, these shells can show dynamic instabilities when they are exposed to a supersonic flow. Therefore, aeroelastic analysis of these elements is one of the primary design criteria which aeronautical engineers are dealing with. This analysis can be done with the help of finite element method (FEM) coupled with the computational fluid dynamic (CFD) or by experimental methods but it is time consuming and very expensive. The purpose of this dissertation is to develop such a numerical tool to do aeroelastic analysis in a fast and precise way. Meanwhile during the design stage, where the different configurations, loading and boundary conditions may need to be analyzed, this numerical method can be used very easily with the high order of reliability. In this study structural modeling is a combination of linear Sanders thin shell theory and classical finite element method. Based on this hybrid finite element method, the shell displacements are found from the exact solutions of shell theory rather than approximating by polynomial function done in traditional finite element method. This leads to a precise and fast convergence. Supersonic aerodynamic modeling is done based on the piston theory and modified piston theory with the shell curvature term. The stress stiffening due to lateral pressure and axial compression are also taken into accounts. Fluid-structure interaction in the presence of inside quiescent fluid is modeled based on the potential theory. In this method, fluid is considered as a velocity potential variable at each node of the shell

element where its motion is expressed in terms of nodal elastic displacements at the fluid-structure interface.

This proposed hybrid finite element has capabilities to do following analysis:

i) Buckling and vibration of an empty or partially fluid filled circular cylindrical shell or truncated conical shell subjected to internal/external pressure and axial compression loading. This is a typical example of external liquid propellant tanks of space shuttles and re-entry vehicles where they may experience this kind of loading during the flight. In the current work, different end boundary conditions of a circular cylindrical shell with different filling ratios were analyzed. To the best author' knowledge this is the first study where this kind of complex loading and boundary conditions are treated together during such an analysis. Only static instability, divergence, was observed where it showed that the fluid filling ratio does not have any effect on the critical buckling pressure and axial compression. It only reduces the vibration frequencies. It also revealed that the pressurized shell loses its stability at a higher critical axial load.

ii) Aeroelastic analysis of empty or partially liquid filled circular cylindrical and conical shells. Different boundary conditions with different geometries of shells subjected to supersonic air flow are studied here. In all of cases shell loses its stability though the coupled mode flutter. The results showed that internal pressure has a stabilizing effect and increases the critical flutter speed. It is seen that the value of critical dynamic pressure changes rapidly and widely as the filling ratio increases from a low value. In addition, by increasing the length ratio the decrement of flutter speed is decreased and vanishes. This rapid change in critical dynamic pressure at low filling ratios and its

almost steady behaviour at large filling ratios indicate that the fluid near the bottom of the shell is largely influenced by elastic deformation when a shell is subjected to external subsonic flow.

Based on comparison with the existing numerical, analytical and experimental data and the power of capabilities of this hybrid finite element method to model different boundary conditions and complex loadings, this FEM package can be used effectively for the design of advanced aerospace structures. It provides the results at less computational cost compare to the commercial FEM software, which imposes some restrictions when such an analysis is done.

Condensé en Français

Introduction

Les coques de révolutions sont l'une des principales composantes dans les structures des vaisseaux spatiaux. Leurs applications comprennent la cuve ou le propulseur à gaz déployées dans la jupe des vaisseaux spatiaux. En raison de l'épaisseur mince de paroi, les coques conique et cylindrique sont plus sensibles à la l'instabilité dynamique ou du battement induit par le nombre de Mach de haut débit de gaz. En outre, les navettes spatiales ont besoin d'une grande poussée dans un court intervalle de temps, donc un grand réservoir de propulsion est nécessaire.

En revanche la stabilité hydroelastique, pour les parois minces du réservoir est un aspect important dans sa conception. Ces liquides propulsés des lanceurs et des navettes spatiales sont sujet à une importante perturbation pendant la poussée longitudinale développée et aussi en raison de l'effet du mécanisme de lancement. Les conditions de flambement dû à la combinaison de la compression axiale et la pression extérieure ou intérieure de la coque peut provoquer la séparation du matériau de la protection thermique du réservoir et de conduire ainsi à la défaillance de la navette spatiale. L'analyse de stabilité dynamique et statique, d'un tel problème en présence d'interaction fluide-structure est l'un des sujets difficiles en génie aérospatial. Un grand soin doit être pris au cours de la conception des navettes spatiales pour empêcher l'instabilité statique (flambement) ou dynamique (battement). Depuis le siècle dernier, les ingénieurs en aéronautique ont appliqué une telle simple analyse, comme la théorie linéaire de poutre couplée avec une quasi-stabilité aérodynamique unidimensionnelle (1D) jusqu'à nos

jours, où plus d'avancement fondé sur le couplage de la méthode des éléments finis (FEM) et de la dynamique des fluides computationnelle (CFD) est utilisé. La puissance des ordinateurs moderne et des outils de calcul ont juste amélioré le temps des solutions. La vibration hydroelastique développée a comme conséquence l'interaction entre la pression hydrodynamique du liquide au repos et la déformation élastique d'une coque sous pression soumise à une compression axiale à ses côtés, est un problème complexe. Par conséquent, des méthodes numériques telles que les FEM est un outil puissant et proposé pour notre étude, ces méthodes peuvent décrire adéquatement la stabilité dynamique d'un tel système contenant des structures, des conditions aux limites et de chargement complexes.

Objectifs

Dans toutes les littératures, mais quelques-unes d'entre elles portent sur le même objectif proposé par notre étude, soit ils n'ont pas une structure ou une modélisation suffisamment puissante pour contenir tous les éléments en même temps. Il ya quelques analyse aéroélectriques très précise basées sur le couplage des FEM et les CFD, mais ils imposent des restrictions sur les comptes de tous les facteurs affectant le battement frontalier. Ils sont aussi coûteux en calcul, où il n'est pas souhaitable le long de la conception préliminaire de la structure d'avion.

Pour le cas de la coque partiellement remplie soumise à des écoulements supersonique, pour les meilleurs auteurs connus, il n'existe pas de données publiées. Ainsi, il est intéressant pour les ingénieurs aéronautiques de comprendre clairement la nature des

effets à l'intérieur des fluides sur le comportement de battement de la coque conique et cylindrique. C'est un exemple typique des réservoirs d'oxygène liquide de la navette spatiale, où le plus grand soin doit être pris pendant le processus de conception afin de prévenir toute instabilité statique ou dynamique.

Par conséquent, la motivation de notre projet de doctorat découle de l'absence d'une convergence rapide et précise de l'outil de la méthode des éléments finis pour l'analyse aéroélectriques de la coque de révolution utilisée efficacement pour la conception de structures aérospatiales qui ont les capacités suivantes:

- capable de modéliser le flambement en raison de la pression hydrostatique et de compression axiale ou une combinaison de ces chargements.
- capable de modéliser l'effet fluide-structure en présence du la coque remplie de liquide.
- capable de modéliser la pression aérodynamique du chargement autour de la coque sans la complexité de la méthode des CFD.
- Capable d'obtenir suffisamment un haut degré de fidélité pour s'assurer que le modèle fournit une bonne idée de la physique du comportement aéroélectriques des coques.
- Capable d'être facilement adoptée pour les différents fluides et conditions aux limites de la structure afin de reproduire différentes données expérimentales existantes pour des fins de vérification.

Les objectifs de ce travail nécessitent l'utilisation de l'état de l'art, du modèle hybride en éléments finis.

Méthodologie

Cette thèse comporte six chapitres qui traitent des objectifs mentionnés dans un format d'articles ayant leur propre résumé, introduction et recherche de littérature, méthodologie, résultats, discussion et liste de références. Suite à ces articles, une discussion et conclusion générale, concernant la réussite de l'objectif, ainsi qu'un certain nombre de recommandations pour des études futures sont présentés.

La liste des articles soumis au cours de ce doctorat considérés pour la publication sont :

Sabri F, Lakis A A. Hydroelastic Vibration of Partially Liquid-Filled Circular Cylindrical Shells under Combined Internal Pressure and Axial Compression, *Aerospace Science and Technology,* (submitted Feb. 2009).

Sabri F, Lakis A A. Hybrid Finite Element Method Applied to Supersonic Flutter of a Circular Cylindrical Shell, *AIAA Journal,* (submitted Jul. 2008).

Sabri F, Lakis A A. Hybrid Finite Element Method Applied to Supersonic Flutter of an Empty or Partially Liquid-Filled Truncated Conical Shell, Journal of Sound and Vibration, (submitted Apr. 2009)

Modélisation structurale

Le modèle structurel est basé sur une combinaison de la théorie linéaire de Sanders pour les coques minces et de la théorie classique des éléments finis. La théorie des coques de Sander est basée sur la première approximation de Love où la contradiction liée au fait que les déformations des petites rotations du corps rigide de la coque qui ne

disparaissent pas, a été enlevée. Un tronc cylindrique circulaire est appliqué pour générer les matrices de masse et de rigidité du modèle structurel. Ce type d'élément à deux lignes de nœuds circulaires. Il existe quatre degrés de liberté à chaque nœud; axial, radial, déplacement circonférentiel, et de rotation. Ce type d'élément permet d'utiliser facilement des équations de la coque mince, afin de trouver la solution exacte des fonctions de déplacement plutôt que d'un rapprochement avec les fonctions polynomiales, comme c'est le cas des éléments finis classique. Cette sélection de l'élément résulte dans un élément hybride où le critère de convergence de la méthode des éléments finis est fourni avec plus de précision.

Rigidité du stress

L'influence des forces de membrane sur la stabilité dynamique d'une coque cylindrique en présence d'écoulement d'air supersonique est étudiée. Ces forces de membranes sont dus à des forces de pression différentielle à travers la coque et la compression axiale. La contribution de l'énergie de déformation est introduite dans la formulation. Il est supposé que la coque est sous les conditions d'équilibre et quelle n'a pas atteint son état de flambage. Ces forces initiales de membrane résulte d'une matrice de rigidité ajoutée à la géométrie de la matrice de rigidité déjà développée.

Modélisation aérodynamique

La théorie Piston est un outil puissant pour la modélisation aérodynamique de

L'aéroélasticité. Pour un cylindre soumis à un écoulement d'air supersonique parallèle à l'axe de la coque, l'effet fluide-structure est dû à la pression externe du chargement peut être pris en compte à l'aide de la théorie du potentiel du premier ordre linéaire, avec ou sans correction du terme de la courbure. Le vecteur de la force en raison de la pression résulte dans l'amortissement aérodynamique, et la rigidité des matrices en fonction de la vitesse d'écoulement supersonique.

Modélisation Fluide

Pour le cas d'une coque remplie du liquide, il est supposé que le fluide est incompressible et n'a pas d'effet de la surface libre du fluide. Ce dernier est considéré comme un potentiel de vitesse variable à chaque nœud de l'élément coque où son mouvement est exprimé en termes de déplacement nodal élastique à l'interface fluide-structure. Sur la base de l'équation de Laplace, l'équation de Bernoulli et la condition de l'imperméabilité, la pression hydrodynamique en termes de déplacements nodaux est trouvés et finalement aboutit à une matrice de masse du liquide qui est introduit dans la formulation.

Modélisation Aéroélastiques

La gouvernance de l'équation du mouvement dans un système global d'un liquide d'une coque remplie conique et cylindrique circulaire soumise à l'écoulement d'air extérieur supersonique est dérivée. L'équation Aéroélastiques du mouvement est due à un problème de valeurs propres standard. La stabilité Aéroélastiques est investiguée en

étudiant les valeurs propres dans le plan complexe. Le début de battement se produit lorsque la partie imaginaire de la valeur propre passe de positive à négative. Le flambement est trouvé quand la partie réelle devient zéro.

Résultats et Discussion

Cette étude présente un battement supersonique, les vibrations et le flambement de d'une coque circulaire cylindrique et tronquée conique.

Lorsque la coque est complètement ou partiellement remplie du liquide, le flambement critique des charges n'est pas modifié par rapport au cas de la coque vide. Le Remplissage avec le liquide affecte seulement les fréquences de vibrations de la coque, lorsque, en augmentant la portion du liquide intérieur, les fréquences d'oscillation sont diminuées. Le flambement est constaté lorsque les fréquences d'oscillation disparaissent. Il a été également observé que la coque pressurisée montre plus de résistance en flambement lorsqu'il est en compression axiale. Si elle est soumise à une pression extérieure, le flambement aura lieu à une petite valeur critique de compression axiale par rapport au premier cas. Dans tous ces résultats obtenus l'effet du pré-flambement et l'imperfection de la coque est négligé, et il est recommandé pour les futures études.

Pour une coque partiellement remplie, quand elle est soumise à l'écoulement supersonique, il en révèle que le fluide intérieur a de l'influence sur l'apparition du battement. Cet effet est plus important pour les faibles taux de remplissage et de faible rapport L/R, où la vitesse critique du battement est augmentée pour cette condition aux limites et de la configuration de la géométrie.

La dynamique de l'instabilité se produit sous forme de mode de battement couplé, pour une coque conique et cylindrique à la fois placé dans un écoulement externe supersonique. La coque pressurisée montre plus de résistance au battement que celle non pressurisée où elle devrait indiquer et sur la base de résultats expérimentaux, que la pression interne modérée peut réduire la dynamique de la stabilité de la coque au niveau inférieur d'une coque non pressurisée. En revanche pour des petites est grandes pressions être indiqué que sur la base des. Mais pour les petites et les grandes pressions cette simulation numérique elle est en bon accord avec d'autres résultats théoriques et numériques.

Lorsque la coque est en état de vibration libre, les formes des modes sont dans les ondes restantes alors que pour la vitesse supersonique avant l'apparition du battement, la forme des modes contiennent des composantes d'onde transitoires comme cela a été rapporté dans un essai expérimental. Dans ce cas, les nœuds et la les anti-nœuds voyagent circonférencielement le long de la coque. Différents bords des conditions aux limites ont été testés pour les coques cylindriques et coniques. Dans tous les cas, les coques perdent leur stabilité à travers le mode du battement couplé, sauf pour le bord libre-libre de la coque conique. Tout d'abord elle perd sa stabilité par des modes de divergence (flambement) et en augmentant la vitesse d'écoulement, il devient instable dynamiquement par le mode de battement couplé.

Conclusion

Un code d'élément fini hybride efficace pour une analyse Aéroélastiques et le flambement de la coque de révolution a été développé. Cet outil des FEM peut être utilisé efficacement pour la conception de structures aérospatiales avancées. Il a été montré que la solution de convergence est très rapide et précise. Pendant ce temps, le comportement des coques soumises à l'écoulement supersonique avec différentes conditions aux limites et géométries complexes sont bien prédits.

Dans cette thèse les modélisations et les capacités d'analyse suivantes ont été réalisés :

- Modélisation Linéaire de coque avec la méthode des éléments finis hybrides.
- Les déformations initiales et la rigidité du stress dû à la pression latérale et axiale du chargement.
- La théorie Piston pour la pression aérodynamique supersonique du chargement.
- La théorie de l'écoulement potentiel pour la pression interne hydrodynamique.

Avec une telle capacité de modélisations, différents problèmes et une meilleure prédiction sont obtenus. Ils comprennent :

- Le flambement pour les coques vide et partiellement rempli de fluide.
- L'instabilité Aéroélastique, battement.
- L'effet de la déformation initiale sur la stabilité Aéroélastiques.

La contribution la plus importante de ce travail est la formulation par éléments finis et la solution. La formulation des éléments finis est conçue de manière à inclure toute formulation analytique ou numérique pour la coque cylindrique ou conique, basée sur la théorie de Sanders des coques minces couplée avec la théorie de Piston. Cet élément

finis hybride est très bien réussi pour la prédiction de l'instabilité Aéroélastiques. L'efficacité et la performance de calcul de cette méthode a également été prouvé d'être plus efficace que le couplage CFD et l'outil des FEM.

Les futurs travaux doivent inclure l'effet de la géométrie et la non-linéarité aérodynamique où elles doivent prouver la rentabilité de cet outil en FEM. Il est également recommandé d'inclure l'effet du chauffage aérodynamique dans le plan de distribution et le gradient de la température le long de l'épaisseur de la coque, sur la stabilité Aéroélastiques.

La paroi extérieure de la plupart des véhicules aérospatiaux modernes met l'expérience dans des environnements à très haute température; à cause de cela, l'utilisation de fonctions de grade du martiaux (FGM) peut être efficace. À la suite de ce travail sera traitant de le battement supersonique FG de la coque cylindrique et conique, qui leurs propriétés sont supposées être dépendante de la température et du classement dans l'ensemble de l'épaisseur de la coque en fonction de différentes théories (c'est-à-dire simple loi de puissance).

Table of Contents

List of Tables

List of Figures

Chapter 1: Introduction and Literature Review

1.1 Overview

Understanding the stability features of thin cylindrical shells has been one of the more challenging of all classic problems in the theory of elasticity and in the field of experimental mechanics. For almost half a century, the large discrepancy between experimental and theoretical analysis for the buckling of cylindrical shells under lateral pressure and axial compression has been known to researchers. As evidenced by Yamaki (Yamaki, 1984) in his book, this problem now seems to be reasonably well understood. Since cylindrical and conical shells represent the basic structural element in both aircraft and aerospace systems, the question arises as to how the shell's basic stability features are affected by an external field of supersonic flow parallel to its axis. This question is investigated here using theoretical and numerical analysis. Many of the older challenges are found along with some recent results which are brought about specifically by the presence of the external supersonic flow. Past experience gained in resolving classic shell stability features was beneficial to understanding of the problem. In spite of this however, the problem is not completely solved and several of its features remain as a challenge for future research.

The general study is of practical interest as it can be applied during the design of skin panels on high-performance aircraft, space shuttles, rocket-launched boosters and re-entry vehicles. Although preliminary design criteria include use of a flat panel element subjected to supersonic flow, very little design information is currently available for

thin-walled shell structures. Further research is necessary to obtain a better understanding of the stability and also of the response characteristics of thin shells subjected to a high-velocity fluid environment which may include aerodynamic noise, boundary layer turbulence, and buffeting conditions or large-scale turbulence. The present investigation is concerned only with the stability characteristics of such structures (thin circular cylindrical and truncated conical shells) when influenced by a high-velocity external flow environment parallel to the shell axis under combined internal/external pressure and axial compression. For such an analysis, applying commercial finite element software imposes some restrictions and is very costly. The objective of this dissertation is to provide new insights into an approach using a hybrid finite element solution for analysis of supersonic flutter of cylindrical and conical shells. This approach provides very fast and precise convergence with less numerical computation and cost compared to current commercial finite element packages.

1.2 The Flutter Phenomenon

Flutter is a self-excited dynamic instability phenomenon comprising an odd interaction between aerodynamic, elastic and inertial forces. This unwanted oscillation often results in structural failure. Although one cannot define a safe velocity regime for flutter instability, advanced aircraft flying at supersonic or hypersonic speeds are aerospace structures which are most influenced by the flutter phenomenon. The first flutter incident was recorded in 1916 on a twin engine biplane British heavy bomber (Barnes, 1987). During World War I, wing-aileron flutter was also reported and solved by conducting

mass balance about the control surface hinge line (Collar, 1978). Technological advancement led to the manufacture of new high speed aircraft and wing flutter was again reported during flight tests in the 1920s and 1930s. After 1947, aircraft could reach supersonic flight speeds and a new type of flutter called panel flutter was observed. This type of flutter appears as a constant amplitude standing or traveling wave on the skin panels of the aircraft structure. The first panel flutter was reported on the skin shell (Circular Cylindrical shell) of a V-2 rocket. Since then, extensive theoretical and experimental investigations have been performed on the subject.

1.3 Literature Review

Aeroelasticity is a vast field in aerospace engineering. Flutter (a dynamic instability) and divergence (a static instability) are aeroelastic instabilities that are of serious concern to aeronautical engineers who are always trying to resolve these conditions during design of high-speed and high-performance aircrafts. Since the last century, analysis to their resolution has involved application of simple methods such as linear beam theory coupled with 1D quasi-steady aerodynamics. Currently, more advanced analytical methods are used combining the Finite Element Method (FEM) and Computational Fluid Dynamics (CFD). Modern powered computers and computation tools have reduced the computation time to calculate solutions. In the following paragraphs a survey of research literature on the subject of aeroelastic stability of shells of revolution, particularly circular cylindrical and truncated conical shells, is presented. This survey is categorized into three subjects: *i)* buckling and vibration of liquid-filled cylindrical

shells, *ii)* supersonic flutter of circular cylindrical shells and *iii)* supersonic flutter of truncated conical shells.

1.4 Buckling and Vibration of Liquid-Filled Cylindrical Shells

A liquid-filled cylindrical shell is a typical model for a liquid propellant tank of a space shuttle. These launched vehicles experience significant loads due to thrust and launch mechanisms. This disturbance can bring the shell to the buckling state which may cause thermal protection material to separate from the tank. An extensive literature review revealed that a large number of papers deal with the buckling of circular cylindrical shells. A comprehensive study was done by Yamaki (Yamaki, 1984). To the best knowledge of the authors there is no record in the literature concerning the effect of the filled fluid while the structure is under a pre-stress condition (combined external/internal pressure and axial compression). However, the fluid-structure interaction problem has received much attention among researchers. Paidousiss (Paidoussis, 1998, 2004) and Amabili (Marco Amabili, 2008) have addressed this subject in more detail in their books. A short review including the buckling state of circular cylindrical shells and fluid-structure interaction are presented here.

Lakis and Paidoussis (Lakis & Paidoussis, 1971) studied the free vibration of a partially liquid-filled cylindrical shell using a hybrid finite element method. An experimental attempt was reported by Mistry and Menezes (Mistry & Menezes, 1995) for coupled cylindrical shell-fluid dynamic interaction, which was verified using an axisymetric finite element mode. Mazuch et al (Mazuch et al., 1996) also measured experimentally

the natural frequencies and vibration modes of a water filled circular cylindrical shell. Amabili et al (M. Amabili et al., 1998) considered the effect of sloshing and bulging modes due to the fluid free surface effect for dynamic analysis of a circular cylindrical shell. In this study the shell was filled partially with liquid and the bottom plate of the tank was considered to be rigid. Jeong and Lee (Jeong & Lee, 1998) applied Sander's shell theory to analytically investigate the hydroelastic vibration of a partially fluid-filled cylindrical shell. In all of these mentioned works the shell was free of any pre-stress condition.

Pellicano and Amabili (Pellicano & Amabili, 2003) applied Donnell's nonlinear shallow shell theory to analyze the parametric instability and dynamic behavior of a fluid-filled circular cylindrical shell subjected to static and dynamic axial loads. In another study they (Pellicano & Amabili, 2006) used Sanders-Koiter shell theory to investigate the chaotic dynamic stability of a pre-compressed cylindrical shell. Nemeth et al (Nemeth et al., 1996; Nemeth et al., 2002) investigated the buckling behavior of a space shuttle liquid-oxygen tank. The results showed that the stability of a fluid-filled tank can be very sensitive to initial imperfections. Buckling of an empty shell has also been investigated by several researchers. For example Vodenitcharova and Ansourian (Vodenitcharova & Ansourian, 1996) reported a theoretical method for buckling of a cylindrical shell under lateral pressure and axial compression based on Flugge's stability equation.

Hydroelastic vibration developed as a consequence of interaction between hydrodynamic pressure of quiescent liquid and elastic deformation of a pressurized shell

subjected to an axial compression at its edges, is a complex problem. Numerical methods such as FEM are powerful tools which are capable of adequately describing the dynamic stability of such a system containing complex structures, boundary conditions and loading. This method is proposed here.

1.5 Supersonic Flutter of Circular Cylindrical Shells

Ashley and Zartarian (Ashley & Zartarian, 1956) introduced piston theory into the aeroelastic system to model the coupled pressure loading in a supersonic flow regime. In late 1960s, researchers began to investigate supersonic flutter of circular cylindrical shells. In general, they focused on the development of an analytical relation to describe the effect of shell and flow parameters on the flutter boundaries. The structural model was based on classical shell theories coupled with the piston theory to account for pressure. The resulting governing equations were treated numerically using the Galerkin method. In most cases they did not successfully verify their results with experimental data (Horn et al., 1974). Dowell is one of the main contributors in this domain and has summarized these research works in his book (Dowell, 1975). Olson and Fung (Olson & Fung, 1966, 1967) performed a comprehensive experimental study of supersonic flutter for a circular cylindrical shell. Their results revealed that a pressurized shell loses its stability at a lower level of freestream static pressure than predicted by theory. Later Evensen and Olson (Evensen & Olson, 1967, 1968) tested a nonlinear model to calculate the limit cycle amplitude of shell deflection. Their work also presented the existence of a traveling wave flutter the same as that observed during the experimental study in Ref.

(Olson & Fung, 1966). In cases with a small amount of static preload acting on the shell, the discrepancy between experimental and theoretical results is decreased. Bar and Stearman (Barr & Stearman, 1969, 1970) presented an overall improvement in the correlation between theoretical analysis and experimental data by applying an initial imperfection. Amabili and Pellicano (M. Amabili & Pellicano, 2001, 2002) used nonlinear theory for both structural and fluid modeling considering shell imperfection. They succeed in correctly capturing the nonlinear behavior of a shell subjected to supersonic airflow. It is also indicated that the information calculated by nonlinear piston theory has no influence on the onset of flutter however knowledge of axisymmetric imperfections can help to correctly predict this point of onset.

This problem has also been treated numerically by several researchers using a finite element method. Bismarck-Nasr has reviewed all the works conducted in this domain (Bismarck-Nasr, 1996). For example, Bismarck-Nasr (Bismarck-Nasr, 1976) developed an FEM solution for supersonic flutter of a cylindrical shell. Ganapathi et al (Ganapathi et al., 1994) modeled an orthotropic and laminated anisotropic circular cylindrical shell in supersonic flow using FEM.

The intention of this present study is to adequately describe supersonic flutter of a circular cylindrical shell and also represent a more precise numerical model for existing experimental data. An efficient choice of shell theory for developing FEM solutions is also tested.

1.6 Supersonic Flutter of Conical Shells

As it was summarized in the preceding section, most of the aeroelastic analyses for shell of revolutions have been devoted to circular cylindrical shells while truncated conical shells are also considered as primary structural elements in advanced aircraft structures. Conical shells have received little attention relative to aeroelastic stability in supersonic flow. The earliest work for supersonic flutter of a truncated conical shell was addressed by Shulman (Shulman, 1959). Ueda et al (Ueda et al., 1977) investigated this problem theoretically and experimentally. In the case of an orthotropic conical shell, vibration and flutter analysis was done by Dixon and Hudson (Dixon & Hudson, 1970). A pressurized conical shell subjected to supersonic flow was also tested by Miserentino and Dixon (Miserentino & Dixon, 1971). Bismarck-Nasr and Costa-Savio (Bismarck-Nasr & Costa Savio, 1979) found an FEM solution for the supersonic flutter of an isotropic conical shell. Sunder et al (Sunder et al., 1983a) found the flutter boundaries for a laminated conical shell using FEM. In a subsequent study they found the optimum semivertex angle for a conical shell in aeroelastic flutter (Sunder et al., 1983b). Most of the mentioned works were only concerned with the simply supported boundary condition of the shell and other boundary conditions were not solved using these methods. Mason and Bolter (Mason & Blotter, 1986) used a finite element technique to predict the flutter boundaries for a conical shell subjected to an internal supersonic gas flow.

For the case of a partially liquid-filled shell subjected to supersonic flow, to the best knowledge of the authors there is no published data. It is useful for aeronautic engineers

to clearly understand what kind of effects the inside fluid has on the flutter behavior of a conical shell. A typical example is space shuttle liquid oxygen tanks. For these structures, great care must be taken during the design process to prevent any static or dynamic instability.

1.7 Objectives

A few of the works mentioned in the literature survey address the same objective proposed here, however they either lack a consistent structural model or a sufficiently a powerful method to contain all the features at the same time. There are some very accurate aeroelastic analyses based on the coupling of FEM and CFD but they impose restrictions to account for all of the factors affecting the flutter boundaries. Also they are computationally expensive, which is not desired during the preliminary design of an aircraft structure.

The motivation for the proposed Ph.D. thesis therefore stems from the need for a precise and fast convergence FEM package for aeroelastic analysis of shell of revolutions used effectively for the design of aerospace structures. The proposed analysis package must have the following capabilities:

- able to model the buckling state due to hydrostatic pressure, axial compression or a combination of these loadings
- able to model the fluid-structure effect in the presence of fluid inside the container

- able to model the aerodynamic pressure loading around the shell without the complexity of CFD method.
- able to obtain a sufficiently high degree of fidelity to ensure that the model provides an accurate physical insight into the aeroelastic behavior of shells.
- able to be adapted easily for different fluids and structure boundary conditions to reproduce different existing experimental data for verification.

The goals of the present work necessitate the use of a state-of-the-art hybrid finite element model.

1.8 Plan of Thesis

This dissertation includes six Chapters which address the mentioned objectives in the format of articles, each having their own abstract, introduction and literature reviews, method, results, discussion and list of references. Following these articles a general discussion and conclusion regarding the success of objective achievements with some recommendations for future study is presented. The following articles were submitted for publication during the course of the Ph.D. study:

Sabri F, Lakis A A. Hydroelastic Vibration of Partially Liquid-Filled Circular Cylindrical Shells under Combined Internal Pressure and Axial Compression, *Aerospace Science and Technology,* (submitted Feb. 2009).

Sabri F, Lakis A A. Hybrid Finite Element Method Applied to Supersonic Flutter of a Circular Cylindrical Shell, *AIAA Journal,* (submitted Jul. 2008).

Sabri F, Lakis A A. Hybrid Finite Element Method Applied to Supersonic Flutter of an Empty or Partially Liquid-Filled Truncated Conical Shell, Journal of Sound and Vibration, (submitted Apr. 2009)

Chapter 2: Article I - Hydroelastic Vibration of Partially Liquid-Filled Circular Cylindrical Shells under Combined Internal Pressure and Axial Compression.

2.1 Abstract

In the present study, a hybrid finite element method is applied to investigate the dynamic stability of a partially fluid-filled circular cylindrical shell under constant lateral pressure and compressive load. The structural formulation is a combination of Sanders shell theory and the classic finite element method. Nodal displacements are derived from exact solution of Sanders shell theory. Initial stress stiffness in the presence of shell lateral pressure and axial compression is taken into account. It is assumed that the fluid is incompressible and has no free-surface effect. Fluid is considered as a velocity potential variable at each node of the shell element where its motion is expressed in terms of nodal elastic displacement at the fluid-structure interface. Numerical simulation is done and vibration frequencies for different filling ratios of pre-stressed cylindrical shells are obtained and compared with existing experimental and theoretical results. The stability for different shell geometries, filling ratios and boundary conditions with different combinations of lateral pressure and axial compression is summarized. This proposed hybrid finite element method can be used effectively for analyzing the dynamic stability of aerospace structures at less computational cost than other commercial FEM software.

2.2 Nomenclature

[A]	=	defined in Appendix
[B]	=	defined by Eq. (20)
D	=	defined by Eq. (6)
E	=	Young's modulus
$\{F_p\}$	=	force vector due to the aerodynamic pressure field
h	=	shell thickness
i	=	complex number, $\sqrt{-1}$
K	=	bending stiffness of shell, defined by Eq. (6)
[K]	=	global stiffness matrix for a shell
$[K_I]$	=	global initial stiffness matrix for a shell
$[k_s]$	=	stiffness matrix for a shell element
$[k_I]$	=	initial stiffness matrix for a shell element
L	=	shell length
l	=	element length
M_x M_θ, $M_{x\theta}$	=	stress couples for a circular cylindrical shell
$[M_s]$	=	global mass matrix for a shell
$[m_f]$	=	mass matrix for a fluid element
$[m_s]$	=	mass matrix for a shell element
N_x N_θ, $N_{x\theta}$	=	stress resultant for a circular cylindrical shell
$\overline{N}_x$, $\overline{N}_\theta$	=	stress resultant due to shell internal pressure and axial compression

[N]	=	defined by Eq. (19)
P	=	hydrodynamic pressure
P_m, P_x	=	shell internal pressure and axial compression
[P]	=	elasticity matrix
Q_x, Q_θ	=	transverse stress resultant for a circular cylindrical shell
[Q]	=	defined in Appendix
R	=	shell radius
r	=	radial coordinate
{r}	=	vector defined by Eq. (27)
[R]	=	defined in Appendix
$[R_f]$	=	defined by Eq. (45)
[T]	=	defined in Appendix
U	=	axial displacement
U_i	=	potential energy due to initial strain
U_∞	=	free stream velocity
u_n	=	component of U associated with the n^{th} circumferential wave number
V	=	circumferential displacement
v_n	=	component of V associated with the n^{th} circumferential wave number
W	=	radial displacement

w_n = component of W associated with the n^{th} circumferential wave number

x = longitudinal coordinate

δ_i, δ_j = displacement at node i and j

ε_x, ε_θ, $\varepsilon_{x\theta}$ = axial, circumferential and shear strains for a circular cylindrical shell

κ_x, κ_θ, = bending strains for a circular cylindrical shell

$\kappa_{x\theta}$ = twisting strain for a circular cylindrical shell

λ_j = complex roots of the characteristic equation associated with Eq. (5)

υ = Poisson's ratio

Γ = defined by Eq. (51)

θ = circumferential coordinate

ρ = shell density

ρ_f = fluid density

ω = oscillation frequency

φ_{xx}, $\varphi_{x\theta}$, φ_n = elastic rotations for a circular cylindrical shell

$\{\varepsilon\}$ = strain vector

$\{\sigma\}$ = stress vector

2.3 Introduction

Shells of revolution are one of the key components in spacecraft structures. Space shuttles need a large thrust within a short time interval; thus a large propellant tank is required. Hydroelastic stability in the lightweight, thin-walled tank is an important aspect in its design. These liquid propelled space launch vehicles experience a significant longitudinal disturbance during thrust build up and also due to the effect of the launch mechanism. A buckling condition due to the combination of axial compressions and shell external or internal pressure can cause the thermal protection materials to separate from the liquid tank and lead to failure of the space shuttle. Dynamic and static stability analysis of such a problem in the presence of fluid-structure interaction is one of the challenging subjects in aerospace engineering. Great care must be taken during the design of spacecraft vehicles to prevent static (buckling) or dynamic (flutter) instabilities.

Vibration analysis of a cylindrical shell immersed or containing fluid has been investigated by a large number of researchers. A comprehensive study of fluid-structure interaction (FSI) has been addressed by Paidoussis in his books(Paidoussis, 1998, 2004). A short review of studies on this subject is presented in the following paragraph.

Lakis and Paidousiss (Lakis & Paidoussis, 1971) investigated the free vibration of a cylindrical shell partially filled with liquid using a hybrid finite element method. This method led to fast and precise results. In another study, the effect of a fluid free-surface was investigated by Lakis and Neagu (Lakis & Neagu, 1997). Mistry and Menezes (Mistry & Menezes, 1995) developed a mathematical model for a coupled cylindrical

shell-fluid dynamic interaction based on an axisymetric finite element and verified their results with experimental analysis. Mazuch et al (Mazuch et al., 1996) also did an experimental and numerical study to measure the natural frequencies and modes of vibration for a water filled cylindrical shell. Amabili et al. (Amabili et al., 1998) analytically studied the dynamic behavior of a circular cylindrical shell partially filled with liquid. In this study, the bottom plate of the tank was considered to be flexible and the fluid free-surface was taken into account, so both sloshing and bulging modes were calculated. Jeong and Lee (Jeong & Lee, 1998) developed an analytical method based on Sander's shell theory and applied it to hydroelastic vibration of a partially fluid-filled cylindrical shell. They compared their results to those obtained using finite element analysis to investigate the validity of the proposed model. In all of these mentioned studies the shell was not under any pre-stress condition due to axial compression or internal pressure. Pellicano and Amabili (Pellicano & Amabili, 2003) used Donnell's nonlinear shallow shell theory to analyze the parametric instability and dynamic behavior of a fluid-filled circular cylindrical shell subjected to static and dynamic axial loads. In another study, Pellicano and Amabili(Pellicano & Amabili, 2006) used the Sanders-Koiter shell theory to investigate the chaotic dynamic of a pre-compressed cylindrical shell. Nemeth et al. (Nemeth et al., 1996; Nemeth et al., 2002) investigated buckling of a space shuttle super lightweight liquid-oxygen tank. The results showed that the stability of a fluid-filled tank can be very sensitive to initial imperfections. Buckling of empty circular cylindrical shells under this loading condition has been also investigated by several researchers. For example, Vodenitcharova and Ansourian

(Vodenitcharova & Ansourian, 1996) presented a theoretical investigation of buckling of a cylindrical shell under lateral pressure and compression loading based on Flugge's stability equation in coupled form; this method provides very good accuracy.

For a pressurized shell that is partially liquid-filled and subjected to an axial compression at its edges, if one wishes to consider the hydroelastic vibration developed as a consequence of interaction between hydrodynamic pressure of quiescent liquid and elastic deformation of the shell, this is a complex problem. Numerical methods such as the finite element method (FEM) are therefore used since they are powerful tools that can adequately describe the dynamic stability of such a system which contains complex structures, boundary conditions, materials, and loadings. Some powerful commercial FEM software exists, such as ANSYS, ABAQUS and NASTRAN. When using these tools to model such a complex FSI problem, a large number of elements are required in order to get good convergence. The hybrid approach presented in this study provides very fast and precise convergence with less numerical cost compared to these commercial FEM software packages.

In this work a combined formulation of Sanders shell theory and the standard finite element method (FEM) is applied to model the shell structure. Nodal displacements are found from exact solution of Sanders shell theory. This hybrid FEM has been applied to produce efficient and robust models during dynamic analysis of cylindrical shells (Lakis & Paidoussis, 1971, 1972). A circular cylindrical shell which has been pre-stressed due to shell internal pressure and axial compression, filled partially with incompressible and inviscid fluid is modeled in this study. The fluid is characterized as a velocity potential

variable at each node of the shell finite element mesh; then fluid and structure are coupled through the linearized Bernoulli's equation and an impermeable boundary condition at the fluid-structure interface. Dynamic stability of the structure under various geometries, boundary conditions and filling ratios is analyzed.

2.4 Formulation

2.4.1 Structural Modeling

Based on Love's first approximation, Sanders (Sanders, 1959) developed an improved thin shell theory, where all strains vanish for small rigid-body motion. In this study, the structure is modeled using a hybrid finite element method which is a combination of Sanders shell theory and classic finite element formulation. The displacement functions are found from exact solution of Sanders shell theory rather than approximated using a polynomial function. The finite element used here is a circumferential frustum shown in Figure 1. It has two nodal circles with nodal points i and j and there are four degrees of freedom at each node.

According to Sanders linear thin shell theory (Sanders, 1959) the equilibrium equations for a circular cylindrical shell in a cylindrical coordinate system are:

$$
\begin{aligned}
&\frac{\partial N_x}{\partial x}+\frac{1}{R}\frac{\partial N_{x\theta}}{\partial \theta}-\frac{1}{2R^2}\frac{\partial M_{x\theta}}{\partial \theta}=0\\
&\frac{\partial N_{x\theta}}{\partial x}+\frac{1}{R}\frac{\partial N_{\theta}}{\partial \theta}+\frac{1}{2R}\frac{\partial M_{x\theta}}{\partial x}+\frac{1}{R}Q_{\theta}=0\\
&\frac{\partial Q_x}{\partial x}+\frac{1}{R}\frac{\partial Q_{\theta}}{\partial \theta}-\frac{1}{R}N_{\theta}=0\\
&\frac{\partial M_x}{\partial x}+\frac{1}{R}\frac{\partial M_{x\theta}}{\partial \theta}-Q_x=0\\
&\frac{\partial M_{x\theta}}{\partial x}+\frac{1}{R}\frac{\partial M_{\theta}}{\partial \theta}-Q_{\theta}=0
\end{aligned}
\qquad (1)
$$

where R represents the shell radius; N_x and N_θ are the normal stress resultants in axial and circumferential directions respectively and $N_{x\theta}$ is the shear stress resultant in the $x-\theta$ plane ; M_x and M_θ are stress couples in axial and circumferential directions respectively and $M_{x\theta}$ is the couple in $x-\theta$ plane; Q_x and Q_θ are the transverse stress resultants in axial and circumferential directions respectively.

The linear strain-displacement equations in terms of axial U, radial W and circumferential V displacements are:

$$\begin{Bmatrix} \varepsilon_x \\ \varepsilon_\theta \\ \varepsilon_{x\theta} \\ \kappa_x \\ \kappa_\theta \\ \kappa_{x\theta} \end{Bmatrix} = \begin{Bmatrix} \dfrac{\partial U}{\partial x} \\ \dfrac{1}{R}\dfrac{\partial V}{\partial \theta} + \dfrac{W}{R} \\ \dfrac{1}{2}\left(\dfrac{\partial V}{\partial x} + \dfrac{1}{R}\dfrac{\partial U}{\partial \theta}\right) \\ -\dfrac{\partial^2 W}{\partial x^2} \\ -\dfrac{1}{R^2}\dfrac{\partial^2 W}{\partial \theta^2} + \dfrac{1}{R^2}\dfrac{\partial V}{\partial \theta} \\ -\dfrac{1}{R}\dfrac{\partial^2 W}{\partial \theta \partial x} + \dfrac{3}{4R}\dfrac{\partial V}{\partial x} - \dfrac{1}{4R^2}\dfrac{\partial U}{\partial \theta} \end{Bmatrix} \tag{2}$$

The stress-strain relation for an anisotropic shell is expressed by:

$$[\sigma] = [P]\{\varepsilon\} \tag{3}$$

where $[P]$ is the elasticity matrix for an anisotropic shell (Toorani & Lakis, 2000). By introducing Equations (2) and (3) into Equation (1), the following system of equations is obtained:

$$L_J(U, W, V, P_{ij}) = 0 \tag{4}$$

where $L_J (J = 1,2,3)$ are three equations of an anisotropic shell presented in the Appendix.

In the case of an isotropic shell, matrix $[P]$ becomes:

$$[p]=\begin{bmatrix} D & \upsilon D & 0 & 0 & 0 & 0 \\ \upsilon D & D & 0 & 0 & 0 & 0 \\ 0 & 0 & \frac{D(1-\upsilon)}{2} & 0 & 0 & 0 \\ 0 & 0 & 0 & K & \upsilon K & 0 \\ 0 & 0 & 0 & \upsilon K & K & 0 \\ 0 & 0 & 0 & 0 & 0 & \frac{K(1-\upsilon)}{2} \end{bmatrix} \tag{5}$$

where:

$$K=\frac{Eh^3}{12(1-\upsilon^2)}$$
$$D=\frac{Eh}{1-\upsilon^2} \tag{6}$$

E is Young's modulus, υ is Poisson's ratio and h is shell thickness.

Considering the displacements as periodic functions, they can be expressed in Fourier series form as:

$$U(r,x,\theta)=\sum_{n=0}^{\infty} u_n(x)\cos(n\theta)$$
$$W(r,x,\theta)=\sum_{n=0}^{\infty} w_n(x)\cos(n\theta) \tag{7}$$
$$V(r,x,\theta)=\sum_{n=0}^{\infty} v_n(x)\sin(n\theta)$$

where n is the circumferential wave number and u_n, v_n and w_n are the magnitudes of deflections and depend only on x. They can be assumed as:

$$u_n(x) = Ae^{\lambda x/R}$$
$$v_n(x) = Be^{\lambda x/R} \tag{8}$$
$$w_n(x) = Ce^{\lambda x/R}$$

Upon substitution of Equations (7) and (8) into Equation (4) one obtains the following three linear differential equations:

$$[H]\begin{Bmatrix} A \\ B \\ C \end{Bmatrix} = 0 \tag{9}$$

In order to have a nontrivial solution the determinant of matrix $[H]$ must be zero, thus it yields the following characteristic equation:

$$\lambda^8 - 4n^2\lambda^6 + [\frac{1-\upsilon^2}{K} + 6n^2(n^2-1)]\lambda^4 \\ -4n^2(n^2-1)^2\lambda^2 + n^4(n^2-1)^2 = 0 \tag{10}$$

Each root λ of the above equation leads to the solution of Equations (4). The complete solution is obtained by summation of each single root and constants A_i, B_i and C_i $(i = 1,2,...,8)$ as follows:

$$u_n(x) = \sum_{i=1}^{8} A_i e^{\lambda_i x/R}$$
$$v_n(x) = \sum_{i=1}^{8} B_i e^{\lambda_i x/R} \quad (11) \tag{11}$$
$$w_n(x) = \sum_{i=1}^{8} C_i e^{\lambda_i x/R}$$

The independent constants A_i and B_i can be expressed in terms of C_i as:

$$\begin{aligned} A_i &= \alpha_i C_i \\ B_i &= \beta_i C_i \end{aligned} \tag{12}$$

where α_i and β_i are complex numbers. Substituting Equation (12) into Equation (9), α_i and β_i can be found by solving the following equation:

$$\begin{bmatrix} H_{11} & H_{12} \\ H_{21} & H_{22} \end{bmatrix} \begin{Bmatrix} \alpha_i \\ \beta_i \end{Bmatrix} = \begin{bmatrix} -H_{13} \\ -H_{23} \end{bmatrix} \tag{13}$$

where H_{ij} are the elements of matrix $[H]$. The final form for the magnitude of displacement functions can be written as:

$$\begin{Bmatrix} u_n(x) \\ w_n(x) \\ v_n(x) \end{Bmatrix} = [R]\{C_i\} \tag{14}$$

where matrix $[R]_{3\times 8}$ are given in the Appendix and constants C_i must be determined by applying the boundary conditions. The displacement vector that corresponds to the circumferential wave number n is given by (Equation (7))

$$\begin{Bmatrix} U(x,\theta) \\ W(x,\theta) \\ V(x,\theta) \end{Bmatrix} = [T][R]\{C_i\} \tag{15}$$

where matrix $[T]_{3\times 3}$ is defined in the Appendix.

The vector of displacements (axial, radial, rotation and circumferential) at each node is defined by:

$$\{\delta_i\} = \{u_{ni}, w_{ni}, \partial w_{ni}/\partial x, v_{ni}\}^T \tag{16}$$

Each element has two nodes and so eight degrees of freedom. The nodal displacement vector will be:

$$\begin{Bmatrix}\delta_i \\ \delta_j\end{Bmatrix} = \{u_{ni}, w_{ni}, \partial w_{ni}/\partial x, v_{ni}, u_{nj}, w_{nj}, \partial w_{nj}/\partial x, v_{nj}\}^T = [A]\{C\} \tag{17}$$

where matrix $[A]_{8\times 8}$ is given in the Appendix and is obtained from the terms of matrix $[R]$. Now pre-multiplying Equation (17) by $[A]^{-1}$, constants $\{C\}$ are found:

$$\{C\} = [A]^{-1}\begin{Bmatrix}\delta_i \\ \delta_j\end{Bmatrix} \tag{18}$$

Substituting into Equation (15), the nodal displacement vector is found in terms of degrees of freedom as:

$$\begin{Bmatrix}U(x,\theta) \\ W(x,\theta) \\ V(x,\theta)\end{Bmatrix} = [T][R][A]^{-1}\begin{Bmatrix}\delta_i \\ \delta_j\end{Bmatrix} = [N]\begin{Bmatrix}\delta_i \\ \delta_j\end{Bmatrix} \tag{19}$$

Replacing Equation (19) into Equation (2), the strain vector is written as

$$\{\varepsilon\} = \begin{bmatrix}[T] & [0] \\ [0] & [T]\end{bmatrix}[Q][A^{-1}]\begin{Bmatrix}\delta_i \\ \delta_j\end{Bmatrix} = [B]\begin{Bmatrix}\delta_i \\ \delta_j\end{Bmatrix} \tag{20}$$

where matrix $[Q]_{6\times 8}$ is given in the Appendix. The stress resultant vector can now be found from Equations (3) and (20) as:

$$\{\sigma\} = [P][B]\begin{Bmatrix}\delta_i \\ \delta_j\end{Bmatrix} \tag{21}$$

According to the standard finite element formulation the mass and stiffness matrix for each element can be found as:

$$\begin{aligned}[m_s] &= \rho h \iint [N]^T [N] dA \\ [k_s] &= \iint [B]^T [P][B] dA\end{aligned} \tag{22}$$

where ρ is the shell density and $dA = rd\theta\, dx$. Finally, the global mass $[M]$ and stiffness matrix $[K]$ for the entire shell based on standard assembling technique for different boundary conditions are found.

2.4.2 Stress Stiffening

The influence of axial compression and shell internal pressure appears through the stress stiffening matrix in the above equations. It is assumed that the shell is under equilibrium condition and has not reached its buckling state. The initial in-plane shear, static bending and transverse shear are not considered either. The stress resultants of internal pressure P_m and axial compression P_x are

$$\begin{aligned}\overline{N}_x &= -\frac{P_x}{2\pi R} \\ \overline{N}_\theta &= P_m R\end{aligned} \tag{23}$$

The potential energy due to this initial strain can be found as (MacNeal, 1972)

$$U_i = 1/2 \int_0^l \int_0^{2\pi} [\overline{N}_x \phi_{\theta\theta}^2 + \overline{N}_\theta \phi_{xx}^2 + (\overline{N}_x + \overline{N}_\theta)\phi_n^2] R d\theta dx \qquad (24)$$

where ϕ_{xx}, ϕ_{xx} and ϕ_{xx} are the strain rotations (Sanders, 1959):

$$\begin{aligned} \phi_{00} &= -\frac{\partial W}{\partial x} \\ \phi_{xx} &= \frac{1}{R}(V - \frac{\partial W}{\partial \theta}) \\ \phi_n &= \frac{1}{2}(-\frac{1}{R}\frac{\partial U}{\partial \theta} + \frac{\partial V}{\partial x}) \end{aligned} \qquad (25)$$

If the displacements are replaced by Equation (19), the potential energy in terms of nodal degrees of freedom is generated as:

$$U_i = 1/2 \int_0^l \int_0^{2\pi} \{r\}^T \begin{bmatrix} \overline{N}_x & 0 & 0 \\ 0 & \overline{N}_\theta & 0 \\ 0 & 0 & \overline{N}_x + \overline{N}_\theta \end{bmatrix} \{r\} R d\theta dx \qquad (26)$$

where vector $\{r\}$ is defined as:

$$\{r\} = \begin{bmatrix} 0 & -\frac{\partial}{\partial x} & 0 \\ 0 & -\frac{1}{R}\frac{\partial}{\partial \theta} & 0 \\ -\frac{1}{2R}\frac{\partial}{\partial \theta} & 0 & \frac{1}{2}\frac{\partial}{\partial x} \end{bmatrix} \begin{Bmatrix} U \\ W \\ V \end{Bmatrix} = [C_0][N] \begin{Bmatrix} \delta_i \\ \delta_j \end{Bmatrix} \qquad (27)$$

Therefore, the initial stiffness matrix for each element becomes:

$$[k_I] = \int_0^l \int_0^{2\pi} [N]^T [C_0]^T \begin{bmatrix} \overline{N}_x & 0 & 0 \\ 0 & \overline{N}_\theta & 0 \\ 0 & 0 & \overline{N}_x + \overline{N}_\theta \end{bmatrix} [C_0]^T [N]^T R d\theta dx \qquad (28)$$

Analytical integration of above equation is done with the help of MAPLE. After assembling the whole stress stiffness matrix, it is added to the stiffness matrix developed in Equation (22).

2.4.3 Fluid Modeling

It is assumed that fluid is inviscid, incompressible and irrotational. In a cylindrical coordinate system the governing equation for velocity potential ϕ satisfying the Laplace equation is expressed as:

$$\frac{\partial^2\phi}{\partial r^2}+\frac{1}{r}\frac{\partial\phi}{\partial r}+\frac{1}{r}\frac{\partial^2\phi}{\partial\theta^2}+\frac{\partial^2\phi}{\partial x^2}=0 \tag{29}$$

The velocity components in the axial, radial and circumferential directions are defined as:

$$\begin{aligned} V_x &= U_x+\frac{\partial\phi}{\partial x} \\ V_\theta &= \frac{1}{r}\frac{\partial\phi}{\partial\theta} \\ V_r &= \frac{\partial\phi}{\partial r} \end{aligned} \tag{30}$$

where U_x is the free stream velocity; for quiescent fluid $U_x = 0$.

From the Bernoulli equation the hydrodynamic pressure is found as:

$$P=\rho_f\frac{\partial\phi}{\partial t} \tag{31}$$

where ρ_f is the fluid density.

The impermeability condition ensures contact between the shell surface and the fluid. For a fluid at rest it can be written as:

$$V_{r=R} = \frac{\partial \phi}{\partial r}|_{r=R} = \frac{\partial W}{\partial t}|_{r=R} \tag{32}$$

where W is the radial deflection of shell.

Solution of potential velocity by applying the method of separation of variables can be found as:

$$\phi(x,r,\theta,t) = R(r)S(\theta,x,t) \tag{33}$$

Considering the radial displacement from Equation (15) equal to:

$$W = \sum_{j=1}^{8} C_j e^{i(\lambda_j x/R+\omega t)} \cos(n\theta) = \sum_{j=1}^{8} W_j \tag{34}$$

which satisfies the governing equations (Equations (4)), the impermeability condition can be expressed through substitution of Equation (33) into Equation (32):

$$\frac{\partial \phi}{\partial r}|_{r=R} = \sum_{j=1}^{8} \frac{\partial W_j}{\partial t}|_{r=R} = \sum_{j=1}^{8} R_j'(R) S_j(x,\theta,t) \tag{35}$$

or

$$S_j(x,\theta,t) = \sum_{j=1}^{8} \frac{1}{R_j'(R)} \dot{W}_j \tag{36}$$

So the potential velocity can be written as:

$$\phi(x,r,\theta,t)=\sum_{j=1}^{8}\frac{R_j(r)}{R_j'(R)}\dot{W}_j \tag{37}$$

and from the Bernoulli equation (Equation (31)) the pressure acting on the internal surface of the shell is

$$p\,|_{r=R}=-\rho\sum_{j=1}^{8}\frac{R_j(r)}{R_j'(R)}\ddot{W}_j \tag{38}$$

In order to find the function $R(r)$ and its derivative at $r=R$, Equation (37) with the help of Equation (34) is substituted into the Laplace equation (Equation (29)). This leads to the following expression of the Bessel function:

$$r^2R_j''(r)+rR_j'(r)+R_j(r)[i^2m_j^2r^2-n^2]=0 \tag{39}$$

where $i^2=-1$ and $m_j^2=(\frac{\lambda_j^2}{R})^2$. The solution of this Bessel function will be:

$$R_j(r)=AJ_n(im_jr) \tag{40}$$

where $J_n(z)$ is the Bessel function of the first kind of order n and its derivative is defined as:

$$J_n'(u)=z'[\frac{n}{z}J_n(u)-J_{n+1}(u)] \tag{41}$$

Finally, the hydrodynamic pressure in Equation (31) is written as:

$$p\,|_{r=R}=-\rho\sum_{j=1}^{8}Z_j(im_jr)[\ddot{W}_j]_{r=R} \tag{42}$$

where,

$$z_j(im_j r) = \frac{R_j(r)}{R_j'(r)} = \frac{r}{n - (imr)\dfrac{J_{n+1}(im_j r)}{J_n(im_j r)} R_j'(R)} \tag{43}$$

The pressure field vector in terms of nodal degrees of freedom is found by replacing Equation (19) into Equation (42):

$$\begin{Bmatrix} 0 \\ P \\ 0 \end{Bmatrix} = -\rho_f [T][R_f][A^{-1}] \begin{Bmatrix} \ddot{\delta}_i \\ \ddot{\delta}_j \end{Bmatrix} \tag{44}$$

where matrix $[R_f]_{3\times 8}$ is given by:

$$[R_f] = \begin{bmatrix} 0 & \cdots & 0 \\ e^{i\lambda_{1x}/R} & e^{i\lambda_{jx}/R} & e^{i\lambda_{8x}/R} \\ 0 & \cdots & 0 \end{bmatrix}_{3\times 8} \begin{bmatrix} Z_1 & & 0 \\ & Z_j & \\ 0 & & Z_8 \end{bmatrix}_{8\times 8} \tag{45}$$

The general force vector due to the fluid pressure loading is given by:

$$\{F_p\} = \iint [N]\{P\} dA \tag{46}$$

After substituting the expressions for pressure field vector and matrix $[N]$ in the above equation, the local mass matrix $[m_f]$ can be found from the following:

$$[m_f] = -\rho_f [A^{-1}]^T [S_f][A^{-1}] \tag{47}$$

where;

$$[S_f] = \pi r \int_0^l [R]^T [R_f] dx \tag{48}$$

2.4.4 Hydroelastic Modeling

The governing equation which accounts for fluid-structure interaction in the presence of axial compression and internal pressure is derived as:

$$[[M_s] - [M_f]] \begin{Bmatrix} \ddot{\delta}_i \\ \ddot{\delta}_j \end{Bmatrix} + [\,[K_s] + [K_I]\,] \begin{Bmatrix} \delta_i \\ \delta_j \end{Bmatrix} = 0 \tag{49}$$

where subscripts *s* and *f* refer to shells in vacua and fluid, respectively and *I* refers to the case in which the shell is under axial compression and pressurized. In general, mass and stiffness matrices are square symmetric matrices of order *NDF(N+1)* where *NDF* is the number of degrees of freedom at each node (*NDF=4*) and *N* is the number of elements required to discretize the shell geometry. The hydroelastic instability conditions of the shell are elaborated by finding the eigenvalues of Equation (49).

2.5 Results and Discussion

In this section numerical results are presented and compared with existing experimental, analytical and numerical data. There different materials and geometries of circular cylindrical shells listed in Table 1. In all cases the Poisson ratio was $\upsilon=0.3$ and the modulus of elasticity $E=200\ GPa$.

2.5.1 Validation and Comparison

The main advantages of this proposed hybrid finite element method is its fast and precise convergence. This can be seen in Figure 2; 15 elements were required for convergence of the frequency for a clamped-free cylindrical shell.

For the three sets of data mentioned in Table 1, the predicted dimensionless frequencies are expressed by the following relation:

$$\lambda^2 = \omega^2 \frac{(1-\nu^2)\rho R^2}{E} \tag{50}$$

Results for different filling ratios and mode numbers compared to experimental, theoretical and numerical analyses are presented in Table 2. These data are obtained by applying the clamped-free boundary condition which is an adequate condition for liquid storage tanks. Very good agreement can be seen.

2.5.2 Buckling of a Partially Liquid-Filled Shell

Hydroelastic stability of a pressurized shell under axial compression for different filling ratios and simply supported boundary conditions is presented here. Figure 3 shows that internal pressure tends to increase the natural frequency while external pressure has a decreasing effect. In other words, internal pressure has a stabilizing influence. This behavior is seen in Figure 4. A simply supported shell (case A of Table 1) was subjected to a constant axial compression force at different levels of internal or external pressures. In order to see the effect of the contained fluid ($\rho_f = 1000\ kg/m^3$) on the critical load, the frequency of the first axial mode number for different filling ratios (*H/L*) has been

computed. It is seen that as the compressive load increases from zero, the frequency associated with all filling ratios decrease; they remain real until a sufficiently high compressive load is reached, then vanish, indicating the existence of buckling (divergence) instability. In fact this loading generates a self-adjoint problem and its effect on the system stability can produce only a static mode of instability. These figures also reveal that the contained fluid has no influence on the buckling compressive load but affects only the inertial properties of the system where it reduces the natural frequencies. For a pressurized shell this buckling point occurs at a higher load value than an unpressurized shell or a shell subjected to external pressure. Buckling load for an unpressurized shell, Figure 4a, is $P_{critical} = 1.68 \times 10^6 N$. For a pressurized shell, Figure 4b, this critical buckling load is increased to $P_{critical} = 2.05 \times 10^6 N$ and for a shell subjected to an external pressure, Figure 4c, buckling occurs at $P_{critical} = 1.27 \times 10^6 N$. It should be noted that when the shell is subjected to a lateral pressure, the effects of pre-buckling and imperfections are neglected for this stability computation.

2.5.3 Critical Buckling Loading

The contained fluid has no effect on the magnitude of the critical buckling load based on the previously mentioned results. For this reason, in this section the critical buckling loads for an empty circular cylindrical shell with different boundary conditions and geometries are reported. In all cases, loading is either lateral pressure or axial compression. Table 3 shows the results for a clamped-clamped shell under lateral pressure. Critical lateral pressures obtained in this study were compared with those in

Reference (Vodenitcharova & Ansourian, 1996) . As the L/R ratio increases, or the R/t ratio decreases, the difference between the two sets of results increases. Our results for an axial compression loading with a clamped-clamped boundary condition are compared with those given by Yamaki (Yamaki, 1984) in Figure 5. The variable Γ represents the ratio between the critical axial compression stress found by present study and the classical buckling stress. This ratio can be expressed by the following relation:

$$\Gamma = \frac{\sigma}{\sigma_{cr}} = \frac{R\sigma}{Eh}\left[3\left(1-\vartheta^2\right)\right]^{\frac{1}{2}} \tag{51}$$

The ratio is plotted versus different L/R ratios at a constant $R/h = 100$. Similar comparisons for the case of simply-simply supported boundary conditions are presented in the Table 4 and Figure 6. It is seen that an increase in the L/R ratio leads to a decrease in the differences between the two sets of results. It is evident from the results that these two different boundary conditions somehow impose the same buckling loads.

2.6 Conclusions

The problem of buckling of a partially liquid-filled cylindrical shell under combined uniform lateral pressure and axial compressive load is investigated. The system loses its stability through divergence due to these conservative loads. The critical buckling loads and corresponding modes are found. Results show good agreement with other numerical, analytical and experimental data. The proposed hybrid finite element method provides the capability to analyze cases involving application of different complex boundaries and loading patterns for circular cylindrical shells. It can be used effectively in the

design and analysis of aerospace structures and provides very fast and precise convergence at less computational cost compared to commercial FEM software, which imposes some restrictions when such an analysis is done.

2.7 Acknowledgments

The authors acknowledge the financial support of the NSERC of Canada, grant No. A8814.

2.8 Appendix

Sanders linear equation for thin cylindrical shells in terms of axial, tangential and circumferential displacements is (Equation (4)):

$$
\begin{aligned}
L_1(U,V,W,P_{ij}) = {} & P_{11}\frac{\partial^2 U}{\partial x^2} + \frac{P_{12}}{R}\frac{\partial^2 U}{\partial x^2}\left(\frac{\partial^2 V}{\partial x \partial \theta} + \frac{\partial W}{\partial x}\right) - P_{14}\frac{\partial^3 W}{\partial x^3} \\
& + \frac{P_{15}}{R^2}\left(\frac{\partial^3 W}{\partial x \partial \theta^2} + \frac{\partial^2 V}{\partial x \partial \theta}\right) + \left(\frac{P_{33}}{R} - \frac{P_{63}}{2R^2}\right)\left(\frac{\partial^2 V}{\partial x \partial \theta} + \frac{1}{R}\frac{\partial^2 U}{\partial \theta^2}\right) \\
& + \left(\frac{P_{36}}{R^2} - \frac{P_{66}}{2R^3}\right)\left(-2\frac{\partial^3 W}{\partial x \partial \theta^2} + \frac{3}{2}\frac{\partial^2 V}{\partial x \partial \theta} - \frac{1}{2R}\frac{\partial^2 U}{\partial \theta^2}\right)
\end{aligned}
$$

$$
\begin{aligned}
L_2(U,V,W,P_{ij}) = {} & \left(\frac{P_{21}}{R} - \frac{P_{51}}{R^2}\right)\frac{\partial^2 U}{\partial x \partial \theta} + \frac{1}{R}\left(\frac{P_{22}}{R} + \frac{P_{52}}{R^2}\right)\left(\frac{\partial^2 V}{\partial \theta^2} + \frac{\partial W}{\partial \theta}\right) \\
& - \left(\frac{P_{24}}{R} + \frac{P_{54}}{R^2}\right)\frac{\partial^3 W}{\partial x^2 \partial \theta} + \frac{1}{R^2}\left(\frac{P_{25}}{R} + \frac{P_{55}}{R^2}\right)\left(-\frac{\partial^3 W}{\partial \theta^3} + \frac{\partial^2 V}{\partial \theta^2}\right) \\
& + \left(P_{33} + \frac{3P_{63}}{2R}\right)\left(\frac{\partial^2 V}{\partial x^2} + \frac{\partial^2 U}{R \partial x \partial \theta}\right) \\
& + \frac{1}{R}\left(P_{36} + \frac{3P_{66}}{2R}\right)\left(-2\frac{\partial^3 W}{\partial x^2 \partial \theta} + \frac{3}{2}\frac{\partial^2 V}{\partial x^2} - \frac{1}{2R}\frac{\partial^2 U}{\partial x \partial \theta}\right)
\end{aligned}
\qquad \text{(A.1)}
$$

$$L_3(U,V,W,P_{ij}) = P_{41}\frac{\partial^3 U}{\partial x^3} + \frac{P_{42}}{R}\left(\frac{\partial^3 V}{\partial x^2 \partial\theta} + \frac{\partial^2 W}{\partial x^2}\right) - P_{44}\frac{\partial^4 W}{\partial x^4}$$
$$+ \frac{P_{45}}{R^2}\left(-\frac{\partial^4 W}{\partial x^2 \partial\theta^2} + \frac{\partial^3 V}{\partial x^2 \partial\theta}\right) + \frac{2P_{63}}{R}\left(\frac{1}{R}\frac{\partial^3 U}{\partial x \partial\theta^2} + \frac{\partial^3 V}{\partial x^2 \partial\theta}\right)$$
$$+ \frac{2P_{66}}{R^2}\left(-2\frac{\partial^4 W}{\partial x^2 \partial\theta^2} + \frac{3}{2}\frac{\partial^3 V}{\partial x^2 \partial\theta} - \frac{1}{2R}\frac{\partial^3 U}{\partial x \partial\theta^2}\right) + \frac{P_{51}}{R^2}\frac{\partial^3 U}{\partial x \partial\theta^2}$$
$$+ \frac{P_{52}}{R^3}\left(\frac{\partial^3 V}{\partial\theta^3} + \frac{\partial^2 W}{\partial\theta^2}\right) + \frac{P_{55}}{R^4}\left(-\frac{\partial^4 W}{\partial\theta^4} + \frac{\partial^3 V}{\partial\theta^3}\right) - \frac{P_{21}}{R}\frac{\partial U}{\partial x} - \frac{P_{54}}{R^2}\frac{\partial^4 W}{\partial x^2 \partial\theta^2}$$
$$+ \frac{P_{22}}{R^2}\left(\frac{\partial V}{\partial\theta} + W\right) + \frac{P_{24}}{R^2}\frac{\partial^2 W}{\partial\theta^2} - \frac{P_{25}}{R^3}\left(-\frac{\partial^2 W}{\partial\theta^2} + \frac{\partial V}{\partial\theta}\right)$$

Matrices $[T]_{3\times3}$, $[R]_{3\times8}$, and $[A]_{8\times8}$ are defined as:

$$[T] = \begin{bmatrix} \cos(n\theta) & 0 & 0 \\ 0 & \cos(n\theta) & 0 \\ 0 & 0 & \sin(n\theta) \end{bmatrix} \qquad \text{(A.2)}$$

$$R(1,i) = \alpha_i e^{\lambda_i x/R}\ ,\ R(2,i) = e^{\lambda_i x/R}\ ,\ R(1,i) = \beta_i e^{\lambda_i x/R} \qquad i = 1,2,...,8$$

(A.3)

$$A(1,i) = \alpha_i,\quad A(2,i) = 1,\quad A(3,i) = \frac{\lambda_i}{R},\quad A(4,i) = \beta_i,\quad A(5,i) = \alpha_i e^{\lambda_i l/R}$$
$$A(6,i) = e^{\lambda_i l/R},\quad A(7,i) = \frac{\lambda_i}{R}e^{\lambda_i l/R},\quad A(8,i) = \beta_i e^{\lambda_i l/R} \qquad i = 1,2,...8$$

(A.4)

2.9 References

Amabili, M., Paidoussis, M. P., and Lakis, A. A. (1998). Vibrations of partially filled cylindrical tanks with ring-stiffeners and flexible bottom. *Journal of Sound and Vibration, 213*(2), 259-298.

Jeong, K.-H., and Lee, S.-C. (1998). Hydroelastic vibration of a liquid-filled circular cylindrical shell. *Computers and Structures, 66*(2-3), 173-185.

Lakis, A. A., and Neagu, S. (1997). Free surface effects on the dynamics of cylindrical shells partially filled with liquid. *Journal of Sound and Vibration, 207*(2), 175-205.

Lakis, A. A., and Paidoussis, M. P. (1971). Free Vibration of Cylindrical Shells Partially Filled with Liquid. *journal of Sound and Vibration, 19*(1), 1-15.

Lakis, A. A., and Paidoussis, M. P. (1972). Dynamic analysis of axially non-uniform thin cylindrical shells. *Journal of Mechanical Engineering Science, 14*(1), 49-71.

MacNeal, R. H. (1972). *Nastran Theoretical manual.*

Mazuch, T., Horacek, J., Trnka, J., and Vesely, J. (1996). Natural modes and frequencies of a thin clamped-free steel cylindrical storage tank partially filled with water: FEM and measurement. *Journal of Sound and Vibration, 193*(3), 669-690.

Mistry, J., and Menezes, J. C. (1995). Vibration of cylinders partially-filled with liquids. *Journal of Vibration and Acoustics, Transactions of the ASME, 117*(1), 87-93.

Nemeth, M. P., Britt, V. O., Collins, T. J., and Starnes, J. H., Jr. (1996). Nonlinear analysis of the space shuttle super-lightweight external fuel tank. *NASA Technical Paper 3616.*

Nemeth, M. P., Young, R. D., Collins, T. J., and Starnes J.H, Jr. (2002). Effects of initial geometric imperfections on the non-linear response of the Space Shuttle superlightweight liquid-oxygen tank. *International Journal of Non-Linear Mechanics, 37*(4-5), 723-744.

Paidoussis, M. P. (1998). *Fluid-Structure Interactions: Slender Structures and Axial Flow; Volume 1* (Vol. 1). Bridgend, Mid Glamorgan,UK: Academic Press.

Paidoussis, M. P. (2004). *Fluid-Structure Interactions: Slender Structures and Axial Flow; Volume 2* (Vol. 2). Amsterdam: Elsevier Academic Press.

Pellicano, F., and Amabili, M. (2003). Stability and vibration of empty and fluid-filled circular cylindrical shells under static and periodic axial loads. *International Journal of Solids and Structures, 40*(13-14), 3229-3251.

Pellicano, F., and Amabili, M. (2006). Dynamic instability and chaos of empty and fluid-filled circular cylindrical shells under periodic axial loads. *Journal of Sound and Vibration, 293*(1-2), 227-252.

Sanders, J. L. (1959). An Improved First-Approximation Theory for Thin Shell. *NASA R-24.*

Toorani, M. H., and Lakis, A. A. (2000). General equations of anisotropic plates and shells including transverse shear deformations, rotary inertia and initial curvature effects. *Journal of Sound and Vibration, 237*(4), 561-615.

Vodenitcharova, T., and Ansourian, P. (1996). Buckling of circular cylindrical shells subject to uniform lateral pressure. *Engineering Structures, 18*(8), 604-614.

Yamaki, N. (1984). *Elastic Stability or Circular Cylindrical Shells*: North Holland.

2.10 List of Figures and Tables

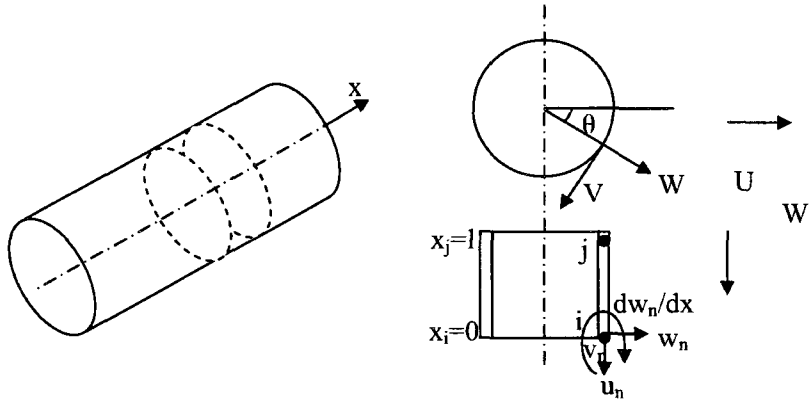

Figure1: cylindrical frustum element

Table 1: Material and geometry data for three type cylinders

	Cylinder A	Cylinder B	Cylinder C
Density (kg/m^3)	7800	7750	7750
t (mm)	1.5	1.16	0.65
R (mm)	77.25	99.58	99.33
L (mm)	231	398	280

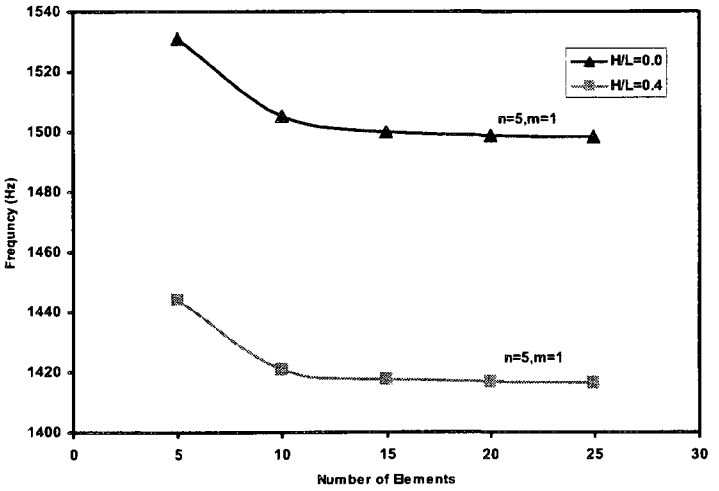

Figure 2: Convergence test for empty and partially liquid-filled cylindrical shells

Table 2: Dimensionless natural frequency of partially liquid-filled cylindrical shells, Clamped-Free ends

Cylinder	H/L (%)	(n,m)	Frequency(10^{-2})		
			Theory(Mazuch et al., 1996)	Present work	Experiment(Mazuch et al., 1996)
A	0	3,1	5.721	5.724	5.563
		4,1	8.554	8.560	8.533
		5,1	13.374	13.373	13.361
	100	3,1	3.618	3.337	3.504
		4,1	5.718	5.388	5.671
		4,2	10.030	9.499	9.880
			Theory(Mistry & Menezes, 1995)	Present work	Experiment(Mistry & Menezes, 1995)
B	80	2,1	2.832	2.556	2.356
		3,1	2.275	2.152	2.205
		4,1	2.913	3.354	3.435
C	50	2,1	6.297	5.915	5.672
		3,1	3.693	3.620	3.635
		4,1	3.183	3.220	3.195

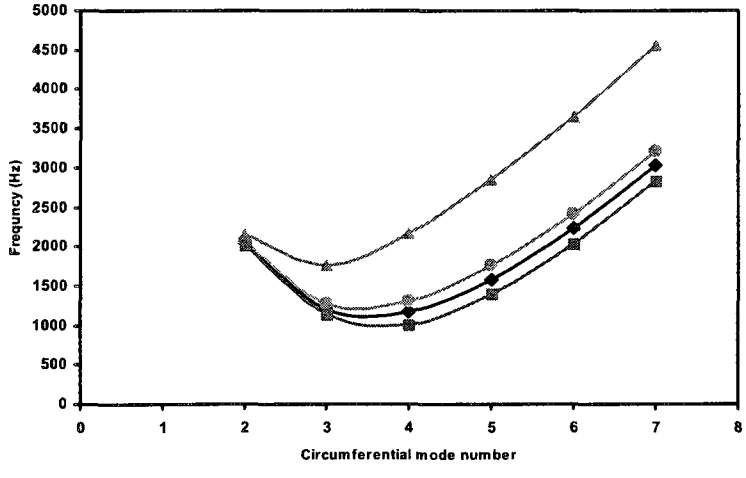

Figure 3: Vibration frequency of an empty shell under an external pressure loading; ●, $P_m = 900\times10^3\ Pa$; ■, $P_m = -900\times10^3\ Pa$; ♦, $P_m = 0.0Pa$; ▲, $P_m = 900\times10^4\ Pa$

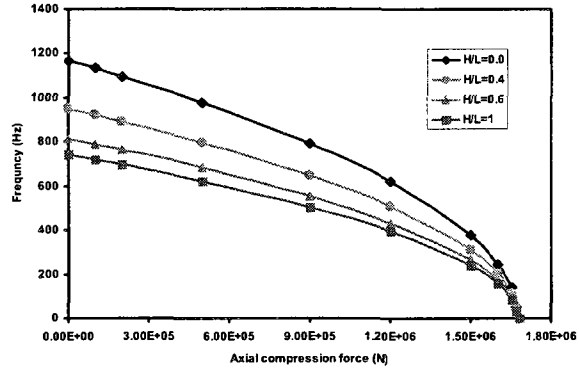

a)

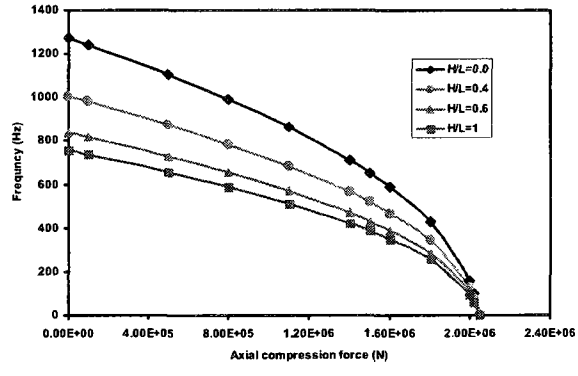

b)

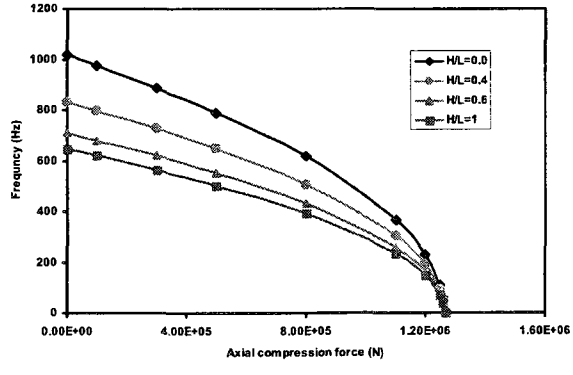

c)

Figure 4: Variation of frequency versus axial compression load for different filling ratios and internal pressures; a) $P_m = 0.0\,Pa$; **b)** $P_m = 900\times10^3\,Pa$; **c)** $P_m = -900\times10^3\,Pa$

Table 3: Buckling pressure and mode number for clamped-clamped ends

L/R	R/t	n, circumferential wave number	P_{cr} (pa)	P_{cr} (pa) Ref. 14
0.5	300	17	243730	361790
	3000	33	1141	1095
1	300	13	173124	172580
	500	15	49900	48114
	1000	18	8930	8536
	1500	20	3231	3107
	2000	22	1570	1518
	3000	24	562	552
2	300	10	92610	87610
	3000	17	270	278
3	300	8	60110	57851
	3000	14	172	185
5	300	6	35360	34830
	3000	11	95	111.4

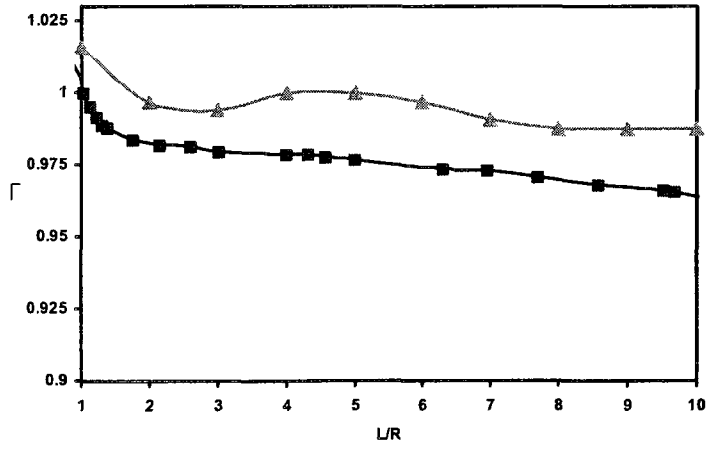

Figure 5: Comparison of results for the clamped-clamped case under axial compression; ▲, present study; ■, Yamaki (Yamaki, 1984)

Table 4: Buckling pressure and mode number for simply-simply supported ends

L/R	R/t	n, circumferential wave number	P_{cr} (pa)	P_{cr} (pa) Ref. 14
0.5	300	17	234135	332430
	3000	33	1129.9	1083.1
1	300	13	169581	168520
	500	15	49234	47412
	1000	18	8862	8468.1
	1500	20	3215	3089.7
	2000	22	1564	1512
	3000	24	561.3	550.4
2	300	10	91136	86917
	3000	17	270.2	277.9
3	300	8	59948	57674
	3000	14	172.5	185.6
5	300	6	35311	34769
	3000	11	95.1	111.3

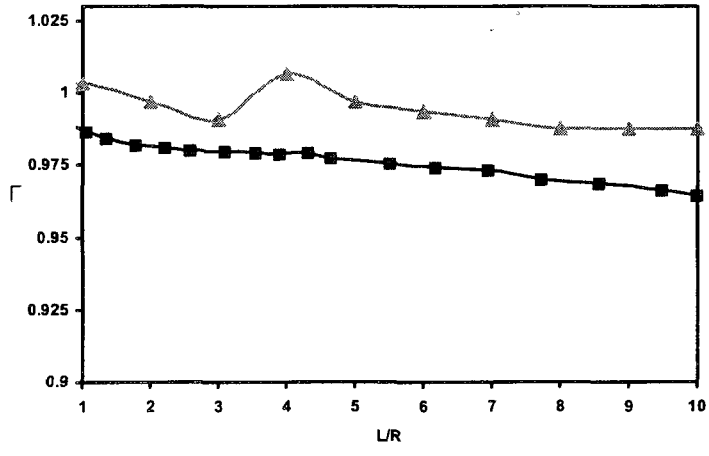

Figure 6: Comparison of results for the simply supported case under axial compression; ▲, present study; ■, Yamaki (Yamaki, 1984)

Chapter 3: Article II - Hybrid Finite Element Method Applied to Supersonic Flutter of a Circular Cylindrical Shell.

3.1 Abstract

This study is focused on the aeroelastic behavior of a circular cylindrical shell in a supersonic airflow. The method of analysis is a combination of Sander's thin shell theory and the classic finite element method. Potential and piston theories with and without a correction factor for curvature are applied to derive aerodynamic damping and stiffness matrices. The influence of stress stiffness due to internal pressure on the shell and axial loading is also taken into account. Aeroelastic equations in the hybrid finite element formulation are derived and solved numerically. Different boundary conditions of the shell, geometry and flow parameters are investigated. In all study cases the shell loses its stability due to coupled-mode flutter and a traveling wave is observed during this dynamic instability. The results are compared with existing experimental data and other analytical and finite element solutions. The presented study shows efficient and reliable results which can be applied for aeroelastic design and analysis of shells of revolution in aerospace vehicles.

3.2 Nomenclature

a_∞	=	freestream speed of sound
[A]	=	defined in Appendix
[B]	=	defined by Equation (11)

$[C_f]$	=	global aerodynamic damping matrix
$[c_f]$	=	local aerodynamic damping matrix
D	=	defined by Equation (4)
E	=	Young's modulus
$\{F_p\}$	=	force vector due to the aerodynamic pressure field
h	=	shell thickness
i	=	complex number, $\sqrt{-1}$
k	=	bending stiffness of shell, defined by Equation (4)
$[K]$	=	global stiffness matrix for a shell
$[K_f]$	=	global aerodynamic damping matrix
$[K_l]$	=	global initial stiffness matrix for a shell
$[k]$	=	stiffness matrix for a shell element
$[k_f]$	=	local aerodynamic stiffness matrix
$[k_l]$	=	initial stiffness matrix for a shell element
L	=	shell length
l	=	element length
M	=	Mach number
$M_x\ M_\theta,\ M_{x\theta}$	=	stress couples for a circular cylindrical shell
$[M_s]$	=	global mass matrix for a shell
$[m]$	=	mass matrix for a shell element
$N_x\ N_\theta,\ N_{x\theta}$	=	stress resultant for a circular cylindrical shell

$\overline{N}_x, \overline{N}_\theta$ = stress resultant due to shell internal pressure and axial compression

$[N]$ = defined by Equation (10)

P_a = aerodynamic pressure

P_∞ = freestream static pressure

P_m, P_x = shell internal pressure and axial compression

$[P]$ = elasticity matrix

Q_x, Q_θ = transverse stress resultant for a circular cylindrical shell

$[Q]$ = defined in Appendix

R = shell radius

r = radial coordinate

$\{r\}$ = vector defined by Equation (18)

$[R]$ = defined in Appendix

$[R_f]$ = defined in Appendix

$T_{t\infty}$ = stagnation temperature

$[T]$ = defined in Appendix

U = axial displacement

U_i = potential energy due to initial strain

U_∞ = freestream velocity

u_n = component of U associated with the n^{th} circumferential wave number

V = circumferential displacement

v_n = component of V associated with the n^{th} circumferential wave number

W = radial displacement

w_n = component of W associated with the n^{th} circumferential wave number

x = longitudinal coordinate

δ_i, δ_j = displacement at node i and j

ε_x, ε_θ, $\varepsilon_{x\theta}$ = axial, circumferential and shear strains for a circular cylindrical shell

κ_x, κ_θ, = bending strains for a circular cylindrical shell

$\kappa_{x\theta}$ = twisting strain for a circular cylindrical shell

λ_j = complex roots of the characteristic equation associated with Equations (5)

υ = Poisson's ratio

γ = adiabatic exponent

θ = circumferential coordinate

ρ = shell density

ρ_f = fluid density

ω = oscillation frequency

φ_{xx}, $\varphi_{x\theta}$, φ_n = elastic rotations for a circular cylindrical shell

$\{\varepsilon\}$ = strain vector

$\{\sigma\}$ = stress vector

3.3 Introduction

Shells and plates are key structures in aerospace vehicles. For example, these elements are frequently used in the fuselage and engine nacelles of airplanes and the skin of space shuttles. As they are exposed to external airflow and particularly supersonic flow, dynamic instability and flutter become key considerations in the design and analysis of skin panels. Cylindrical shells can also show this kind of aeroelastic instability and prevention of this behavior is one of the primary design criterions faced by aeronautical engineers.

After introducing the application of piston theory in the aeroelastic modeling presented by Ashley and Zartarian (Ashley & Zartarian, 1956), a number of interesting experimental and theoretical studies[3-11] were conducted to investigate supersonic flutter of a cylindrical shell in the late 1960s. In general, all of this research was concerned with the development of an analytical relation to describe the effect of shell and flow parameters on the critical flutter frequency. Aeroelastic models were developed by applying the theory of shells (i.e., linear or nonlinear Donells shallow-shell theory) in conjunction with linear or nonlinear piston theory to account for fluid-structure interaction. The resulting governing equations were treated numerically using the Galerkin method. In most cases the theory did not agree well with experimentally obtained results (Horn et al., 1974). A comprehensive experimental test was done by Olson and Fung (Olson & Fung, 1966). They examined the effects caused by shell boundary conditions and the initial strain state due to internal pressure and axial load. It was observed that a pressurized cylindrical shell fluttered at a lower level of freestream

static pressure than predicted by theory (Olson & Fung, 1967). Later, Evensen and Olson (Evensen & Olson, 1967) (Evensen & Olson, 1968) presented a nonlinear analysis for calculating the limit cycle amplitude of a cylindrical shell using a four-mode approximation for the shell deflection. They observed a circumferentially traveling wave flutter similar to that occurring during the experimental study in Ref. 2. Dowell (Dowell, 1966) also investigated the behavior of a cylindrical shell in supersonic flow for different flow and shell parameters. An extensive description of panel flutter modeling has been reported in his book (Dowell, 1975). A study by Carter and Stearman (Carter & Stearman, 1968) showed that agreement between the theory and experiments reported in the literature exists in cases which involve a small amount of static preload acting on the shell. In an effort to compensate for the disagreement of other cases, Bar and Stearman (Barr & Stearman, 1969) presented an overall improvement in the correlation between theoretical analysis and experimental data by applying an initial imperfection and prestability deformation caused by static loading. In a follow-up study (Barr & Stearman, 1970) they found that supersonic flow has no influence on the critical buckling load of a cylindrical shell while a small amount of axial load significantly decreases the flutter speed of the shell. Amabili and Pellicano (Amabili & Pellicano, 2001) included geometric nonlinearities in their study which modeled the supersonic flutter of a circular cylindrical shell. Based on the selection of expansion modes to discretize the aeroelastic equations to facilitate their solution, they succeeded in capturing the nonlinear behavior of the shell correctly. Amabili and Pellicano (Amabili & Pellicano, 2002) also applied the nonlinear piston theory with a shell imperfection to

reproduce the experimental data for a pressurized cylindrical shell. In this case results show that the nonlinear piston theory has no influence on the onset of flutter but knowledge of axisymmetric imperfections can help to predict it correctly.

There are also some researchers who focused on numerical solution of this problem. They developed their solutions using a variational formulation. For example, the equations of virtual displacements were solved using the finite element method (FEM). Aeroelastic governing equations were derived by applying classical shell theory based on the Kirchchoff-Love hypothesis coupled with the piston theory for evaluation of aerodynamic forces. For example, Bismarck-Nasr (Bismarck-Nasr, 1976) developed a FEM applied to supersonic flutter of a circular shell subjected to internal pressure and axial loading. The numerical results were compared with experimental and analytical solutions. Ganapathi et al (Ganapathi et al., 1994) modeled an orthotropic and laminated anisotropic circular cylindrical shell in supersonic flow using FEM and did a parametric study to see the effect of different shell geometries on the flutter boundaries. For more details interested readers can refer to the review paper presented by Bismarck-Nasr (Bismarck-Nasr, 1996).

For such a problem that contains complex structures, boundary conditions, materials, and loading, an analytical model becomes very complicated to undergo for change of factors affecting the flutter boundaries; therefore, numerical methods like FEM are considered such as powerful tools. The first objective of the study presented in this article was to adequately describe supersonic flutter of a circular cylindrical shell and present a numerical model of existing experimental data. The second objective was to

determine an efficient choice of shell theory for developing a finite element model. Most of the published papers in the literature have applied general linear or nonlinear shell theory based on the Kirchhof-Love hypothesis. These developments can only be applied to thin and uniform shells. In cases of multi-layered shells or shells of non-uniform thickness (i.e. allowing for axial variation in thickness), difficulties occur during the calculation of panel flutter. This study is focused on the development of a circumferential hybrid element for a circular cylindrical shell in supersonic flow. The procedure is similar to the finite element development done for vertical shells by Lakis and Paidoussis (Lakis & Paidoussis, 1972) and for horizontal open shells by Selmane and Lakis (Selmane & Lakis, 1997). These developments resulted in precise and fast convergence with few numerical difficulties. The element is a cylindrical frustum instead of the usual rectangular shell element. The linear Sander's shell theory where all the strains vanish for rigid body motions but the other theories are incapable of this attribute, is coupled with the linearized first-order piston theory (Ashley & Zartarian, 1956) including the curvature correction term (Krumhaar, 1963) and also the potential theory (Lakis & Laveau, 1991) to take into account fluid-structure interaction. Initial stress stiffening in the presence of shell internal pressure and axial compression is also applied in the formulation. Finally, the linear mass, damping and stiffness matrices of the aeroelastic system are obtained and solved numerically. The linear theory developed here is adequate to predict the onset of flutter, however nonlinear shell theory required to capture the actual limit cycle amplitudes of flutter, is left for future study.

3.4 Structural Modeling

3.4.1 Hybrid Element

Sander's shell theory (J. L. Sanders, 1959) is based on Love's first approximation where the inconsistency related to the fact that strains for small rigid-body rotations of the shell do not vanish, has been removed. Using a cylindrical coordinate system, the equilibrium equations for a cylindrical shell according to this theory (J. L. Sanders, 1959) are:

$$\begin{aligned}
&\frac{\partial N_x}{\partial x}+\frac{1}{R}\frac{\partial N_{x\theta}}{\partial \theta}-\frac{1}{2R^2}\frac{\partial M_{x\theta}}{\partial \theta}=0\\
&\frac{\partial N_{x\theta}}{\partial x}+\frac{1}{R}\frac{\partial N_{\theta}}{\partial \theta}+\frac{1}{2R}\frac{\partial M_{x\theta}}{\partial x}+\frac{1}{R}Q_{\theta}=0\\
&\frac{\partial Q_x}{\partial x}+\frac{1}{R}\frac{\partial Q_{\theta}}{\partial \theta}-\frac{1}{R}N_{\theta}=0\\
&\frac{\partial M_x}{\partial x}+\frac{1}{R}\frac{\partial M_{x\theta}}{\partial \theta}-Q_x=0\\
&\frac{\partial M_{x\theta}}{\partial x}+\frac{1}{R}\frac{\partial M_{\theta}}{\partial \theta}-Q_{\theta}=0
\end{aligned} \qquad (1)$$

where; R is the mean shell radius, N_x, N_θ are the normal stress resultants in axial and circumferential directions, respectively and $N_{x\theta}$ represents the shear stress resultant in the $x\theta$ plane. M_x , M_θ are the stress couples in axial, circumferential directions, respectively and $M_{x\theta}$ is the couple in the $x\theta$ plane. In the above equation Q_x is the transverse stress resultant in the axial direction and Q_θ represents the transverse stress resultant in the circumferential direction. The strain-displacement equations for three infinitesimal displacements in axial U, radial W and circumferential V directions are: (J. L. Sanders, 1959)

$$\begin{Bmatrix} \varepsilon_x \\ \varepsilon_\theta \\ \varepsilon_{x\theta} \\ \kappa_x \\ \kappa_\theta \\ \kappa_{x\theta} \end{Bmatrix} = \begin{Bmatrix} \dfrac{\partial U}{\partial x} \\ \dfrac{1}{R}\dfrac{\partial V}{\partial \theta} + \dfrac{W}{R} \\ \dfrac{1}{2}\left(\dfrac{\partial V}{\partial x} + \dfrac{1}{R}\dfrac{\partial U}{\partial \theta}\right) \\ -\dfrac{\partial^2 W}{\partial x^2} \\ -\dfrac{1}{R^2}\dfrac{\partial^2 W}{\partial \theta^2} + \dfrac{1}{R^2}\dfrac{\partial V}{\partial \theta} \\ -\dfrac{1}{R}\dfrac{\partial^2 W}{\partial \theta \partial x} + \dfrac{3}{4R}\dfrac{\partial V}{\partial x} - \dfrac{1}{4R^2}\dfrac{\partial U}{\partial \theta} \end{Bmatrix} \tag{2}$$

In Equation (2), ε_x and ε_θ are the strains in axial, circumferential directions, respectively and $\varepsilon_{x\theta}$ represents the strain in the $x\theta$ plane. κ_x and κ_θ are the axial and circumferential strains, respectively and $\kappa_{x\theta}$ is the twisting strain for a circular cylindrical shell.

The stress-strain relations for anisotropic shells are given by:

$$[\sigma] = [P]\{\varepsilon\} \tag{3}$$

where $[P]$ is the elasticity matrix for an anisotropic shell (Toorani & Lakis, 2000). Upon substitution of Equation (2) and (3) into Equation (1) a system of equilibrium equations can be obtained as a function of displacements (Toorani & Lakis, 2000):

$$L_J(U, W, V, P_{ij}) = 0 \tag{4}$$

where $L_J\,(J = 1,2,3)$ are three linear partial differential equations presented in the Appendix, and P_{ij} are elements of the elasticity matrix which, for an isotropic shell are given by:

$$[p]=\begin{bmatrix} D & \upsilon D & 0 & 0 & 0 & 0 \\ \upsilon D & D & 0 & 0 & 0 & 0 \\ 0 & 0 & \frac{D(1-\upsilon)}{2} & 0 & 0 & 0 \\ 0 & 0 & 0 & K & \upsilon K & 0 \\ 0 & 0 & 0 & \upsilon K & K & 0 \\ 0 & 0 & 0 & 0 & 0 & \frac{K(1-\upsilon)}{2} \end{bmatrix} \tag{5}$$

where;

$$K=\frac{Eh^3}{12(1-\upsilon^2)}$$
$$D=\frac{Eh}{1-\upsilon^2} \tag{6}$$

and E is Young's modulus, υ is Poisson's ratio and h is the shell thickness.

A circumferential cylindrical frustum based on the development done by Lakis and Paidoussis(Lakis & Paidoussis, 1972) is applied to generate the mass and stiffness matrices of the structural model. This element type (see Fig. 1) has two nodal circles with two nodal points; i and j. There are four degrees of freedom at each node; axial, radial, circumferential displacement, and rotation. This kind of element makes it possible to use thin shell equations easily in order to find the exact solution of displacement functions rather than an approximation with polynomial functions as is done in classic FEM. This element selection results in a hybrid element where the convergence criterion of the finite element method is provided with greater accuracy. Considering the displacement in the normal manner, as:

$$
\begin{aligned}
U(r,x,\theta) &= \sum_n u_n(x)\cos(n\theta) \\
W(r,x,\theta) &= \sum_n w_n(x)\cos(n\theta) \\
V(r,x,\theta) &= \sum_n v_n(x)\sin(n\theta)
\end{aligned} \tag{7}
$$

where n is the circumferential wave number, Lakis and Paidoussis (Lakis & Paidoussis, 1972) found the exact analytical solution for displacements based on the characteristic equation associated with a system of Eqs. (4). The final form of the displacement functions was obtained as:

$$
\begin{Bmatrix} U(x,r,\theta) \\ W(x,r,\theta) \\ V(x,r,\theta) \end{Bmatrix} = [N] \begin{Bmatrix} \delta_i \\ \delta_j \end{Bmatrix} \tag{8}
$$

where the nodal displacement vector $\{\delta\}$ and matrix $[N]$ are defined by:

$$
\{\delta_i\} = \begin{Bmatrix} u_{ni} \\ w_{ni} \\ (dw_n/dx)_i \\ v_{ni} \end{Bmatrix} \tag{9}
$$

$$
[N] = [T][R][A]^{-1} \tag{10}
$$

In the above equation the matrices $[T]$, $[R]$ and $[A]$ are shown in the Appendix. By introducing Equation (8) into Equation (2) the strain vector can be found:

$$
\{\varepsilon\} = \begin{bmatrix} [T] & [0] \\ [0] & [T] \end{bmatrix} [Q][A^{-1}] \begin{Bmatrix} \delta_i \\ \delta_j \end{Bmatrix} = [B] \begin{Bmatrix} \delta_i \\ \delta_j \end{Bmatrix} \tag{11}
$$

where Matrix $[Q]$ is given in the Appendix. Now the stress resultant is found from Equations (11) and (3):

$$\{\sigma\} = [P][B]\begin{Bmatrix}\delta_i \\ \delta_j\end{Bmatrix} \tag{12}$$

Therefore, the mass and stiffness matrices for each element are derived (Zienkiewicz & Taylor, 2000):

$$\begin{aligned}[m] &= \rho h \iint [N]^T [N] dA \\ [k] &= \iint [B]^T [P][B] dA\end{aligned} \tag{13}$$

where ρ is the shell density and $dA = rdxd\theta$. For the entire shell geometry, the standard assembly technique in FEM can be used along with application of the appropriate boundary conditions to find the global mass and stiffness matrices. Further information regarding derivation of stiffness and mass matrix equations for this combined finite element analysis with classic thin shell theory can be found in Ref. 17.

3.4.2 Initial Stress Stiffness

The influence of membrane forces on the dynamic stability of a cylindrical shell in the presence of supersonic airflow is investigated here. These membrane forces are due to pressure differential across the shell P_m and axial compression P_x. It is assumed that the shell is in an equilibrium condition and also that it has not reached its buckling state. The initial in-plane shear, static bending and transverse shear are also ignored for this analysis. The stress resultants due to internal pressure P_m and axial compression P_x are:

$$\begin{aligned} \overline{N}_x &= -\frac{P_x}{2\pi R} \\ \overline{N}_\theta &= P_m R \end{aligned} \tag{14}$$

The potential energy due to this initial strain is equal to (MacNeal, 1972):

$$U_i = 1/2 \int_0^l \int_0^{2\pi} [\overline{N}_x \phi_{00}^2 + \overline{N}_\theta \phi_{xx}^2 + (\overline{N}_x + \overline{N}_\theta)\phi_n^2] R d\theta dx \tag{15}$$

where l is the element length, ϕ_{xx} is the strain rotation about the x axis, $\phi_{\theta\theta}$ is about the normal to $x\theta$ plane and ϕ_n is the rotation about the normal to the shell element. This rotation vector is given by (J. L. Sanders, 1959):

$$\begin{aligned} \phi_{00} &= -\frac{\partial W}{\partial x} \\ \phi_{xx} &= \frac{1}{R}(V - \frac{\partial W}{\partial \theta}) \\ \phi_n &= \frac{1}{2}(-\frac{1}{R}\frac{\partial U}{\partial \theta} + \frac{\partial V}{\partial x}) \end{aligned} \tag{16}$$

If the displacements are replaced by Equation (8), the potential energy in terms of nodal degrees of freedom is generated:

$$U_i = 1/2 \int_0^l \int_0^{2\pi} \{r\}^T \begin{bmatrix} \overline{N}_x & 0 & 0 \\ 0 & \overline{N}_\theta & 0 \\ 0 & 0 & \overline{N}_x + \overline{N}_\theta \end{bmatrix} \{r\} R d\theta dx \tag{17}$$

where vector $\{r\}$ is defined as:

$$\{r\}=\begin{bmatrix} 0 & -\frac{\partial}{\partial x} & 0 \\ 0 & -\frac{1}{R}\frac{\partial}{\partial \theta} & 0 \\ -\frac{1}{2R}\frac{\partial}{\partial \theta} & 0 & \frac{1}{2}\frac{\partial}{\partial x} \end{bmatrix}\begin{Bmatrix} U \\ W \\ V \end{Bmatrix}=[C_0][N]\begin{Bmatrix} \delta_i \\ \delta_j \end{Bmatrix} \quad (18)$$

The initial stiffness matrix for each element becomes:

$$[k_l]=\int_0^{2\pi}\int_0^{\pi}[N]^T[C_0]^T\begin{bmatrix} \overline{N}_x & 0 & 0 \\ 0 & \overline{N}_\theta & 0 \\ 0 & 0 & \overline{N}_x+\overline{N}_\theta \end{bmatrix}[C_0]^T[N]^T R d\theta dx \quad (19)$$

With the help of Maple software, analytical integration of Equation (19) for each element is done. After assembling the whole initial stiffness matrix it is added to the global stiffness matrix calculated in Equation (13).

3.5 Aerodynamic Modeling

Piston theory is a powerful tool for aerodynamic modeling in aeroelasticity. For a cylinder subjected to an external supersonic airflow parallel to the centerline of the shell, the fluid-structure effect due to external pressure loading can be taken into account using linearized first-order potential theory (Dowell, 1975) with (or without) the curvature correction term (Krumhaar, 1963):

$$P_a=\frac{\gamma p_\infty M^2}{(M^2-1)^{1/2}}\left[\frac{\partial W}{\partial x}+\frac{M^2-2}{M^2-1}\frac{1}{U_\infty}\frac{\partial W}{\partial t}-\frac{W}{2R(M^2-1)^{1/2}}\right] \quad (20)$$

where p_∞, U_∞, M and γ are the freestream static pressure, freestream velocity, Mach number and adiabatic exponent of air, respectively. If the Mach number is sufficiently

high ($M \geq 2$) and neglecting the curvature term $\frac{W}{2R(M^2-1)^{1/2}}$, this equation simplifies to yield the so-called linear piston theory (Ashley & Zartarian, 1956)

$$P_a = -\gamma p_\infty \left[M \frac{\partial W}{\partial x} + \frac{1}{a_\infty} \frac{\partial W}{\partial t} \right] \tag{21}$$

where a_∞ is the freestream speed of sound. In order to show the compatibility and power of this development with different loading conditions a potential solution proposed by Lakis and Laveau (Lakis & Laveau, 1991) is applied to account for the pressure field. They have developed an exact expression for the nonlinearized aerodynamic pressure acting on a cylindrical shell which is exposed to external or internal incompressible flow. In this study, the effect of compressibility has been taken into account. Its effect is entered through the application of Bessel functions to find the velocity potential. Using Laplace equations for potential flow accompanied by boundary conditions defined by an impermeability condition and Bernoulli's equation, the linear pressure loading on the shell wall is given by:

$$P_a = -\rho_f Z \left[\frac{\partial^2 W}{\partial t^2} + 2U_\infty \frac{\partial^2 W}{\partial x \partial t} + U_\infty^2 \frac{\partial^2 W}{\partial x^2} \right] \tag{22}$$

where ρ_f is fluid density. In the above equation, Z which is expressed in terms of Bessel functions of the first and second kind, is detailed in the Appendix.

The radial displacement can be developed based on an analytical solution(Lakis & Paidoussis, 1972) in terms of λ_j, complex roots of a characteristic equation related to Eq. (5) and the oscillation frequency of the shell, ω. It can be written as:

$$W = \sum_{j=1}^{8} e^{i(\lambda_j \frac{x}{R} + \omega t)} \cos(n\theta) = \sum_{j=1}^{8} W_j \tag{23}$$

In the following subsection the pressure field for each aerodynamic loading model is expressed in terms of nodal displacements.

3.5.1 Piston Theory

The pressure field expressed by Equation (21) can be rewritten as:

$$P_a = -\gamma p_\infty \sum_{j=1}^{8} \left(\frac{1}{a_\infty}\frac{\partial W_j}{\partial t} + M\frac{\partial W_j}{\partial x}\right) \tag{24}$$

Introducing Equations (8) and (23) into Equation (24), the aerodynamic pressure may be defined:

$$\{P_a\} = \begin{Bmatrix} 0 \\ p_{radial} \\ 0 \end{Bmatrix} = -\gamma \frac{p_\infty}{a_\infty}[T][R_f][A^{-1}]\begin{Bmatrix} \dot{\delta}_i \\ \dot{\delta}_j \end{Bmatrix} - (i\frac{\lambda_j}{R})\gamma p_\infty M[T][R_f][A^{-1}]\begin{Bmatrix} \delta_i \\ \delta_j \end{Bmatrix} \tag{25}$$

where elements of matrix $[R_f]$ are shown in the Appendix.

3.5.2 Piston Theory with the Curvature Term

Equation (20) includes the curvature term and can be used to describe the aerodynamic pressure field as following:

$$\{P_a\}=\begin{Bmatrix}0\\ p_{radial}\\ 0\end{Bmatrix}=\frac{-\rho_\infty U_\infty^2}{(M^2-1)^{1/2}}\frac{1}{U_\infty}\left(\frac{M^2-2}{M^2-1}\right)[T][R_f][A^{-1}]\begin{Bmatrix}\dot{\delta}_i\\ \dot{\delta}_j\end{Bmatrix}$$
$$+\left(i\frac{\lambda_j}{R}\right)\frac{-\rho_\infty U_\infty^2}{(M^2-1)^{1/2}}[T][R_f][A^{-1}]\begin{Bmatrix}\delta_i\\ \delta_j\end{Bmatrix}$$
$$-\frac{-\rho_\infty U_\infty^2}{(M^2-1)^{1/2}}\left(\frac{1}{2(M^2-1)^{1/2}R}\right)[T][R_f][A^{-1}]\begin{Bmatrix}\delta_i\\ \delta_j\end{Bmatrix} \quad (26)$$

where ρ_∞ is the freestream air density. It is seen that the freestream static pressure and velocity can be linked using the following equations:

$$U_\infty = M.a_\infty \quad (27)$$

$$a_\infty = \sqrt{\gamma\frac{p_\infty}{\rho_\infty}} \quad (28)$$

3.5.3 Potential Theory

For the potential theory, the final form for the pressure field will be:

$$\{P_a\}=\begin{Bmatrix}0\\ p_{radial}\\ 0\end{Bmatrix}=-\rho_\infty Z[T][R_f]\begin{Bmatrix}\ddot{\delta}_i\\ \ddot{\delta}_j\end{Bmatrix}-2(i\frac{\lambda_j}{R})\rho_\infty U_\infty Z[T][R_f]\begin{Bmatrix}\dot{\delta}_i\\ \dot{\delta}_j\end{Bmatrix} \quad (29)$$
$$+(\frac{\lambda_j}{R})^2\rho_\infty U_\infty^2 Z[T][R_f]\begin{Bmatrix}\delta_i\\ \delta_j\end{Bmatrix}$$

3.6 Aerodynamic Damping and Stiffness

The general force vector due to the pressure field is written as:

$$\{F_p\}=\iint[N]^T\{p_a\}dA \quad (30)$$

For example, using the piston theory to account for pressure loading, Eqs. (10) and (25) can be substituted into Eq. (30) and the aerodynamic damping,$[c_f]$, and stiffness, $[k_f]$, for each element can be found:

$$[c_f]=[A^{-1}]^T[D_f][A^{-1}]$$
$$[k_f]=[A^{-1}]^T[G_f][A^{-1}] \quad (31)$$

where;

$$[D_f]=-\frac{\gamma}{a_\infty}p_\infty\pi r\int_0^l[R]^T[R_f]dx$$
$$[G_f]=-i\frac{\lambda_j}{r}\gamma p_\infty M\pi r\int_0^l[R]^T[R_f]dx \quad (32)$$

The same procedures can be done to derive the local damping and stiffness matrices by inserting the different pressure fields mentioned in Sec. 3.5.2 and 3.5.3 into Eq. (30).

Finally, global aerodynamic damping $[C_f]$and aerodynamic stiffness $[K_f]$ matrices are found using the assembling procedure.

3.7 Aeroelastic Model in FEM

The governing equation of motion in a global system for a cylindrical shell exposed to an external supersonic flow is:

$$[M_s]\begin{Bmatrix}\ddot{\delta}_i\\ \ddot{\delta}_j\end{Bmatrix}-[C_f]\begin{Bmatrix}\dot{\delta}_i\\ \dot{\delta}_j\end{Bmatrix}+[\,[K_s]+[K_I]-[K_f]\,]\begin{Bmatrix}\delta_i\\ \delta_j\end{Bmatrix}=0 \qquad (33)$$

where subscripts s and f refer to a shell in vacuo and fluid, respectively and I refers to a shell under axial compression and/or pressurized. It should be noted that in the case of applying potential theory to account for aerodynamic loading, the mass matrix is modified using the mass of the fluid. For air this equivalent mass is negligible compared to damping and stiffness. In order to find the aeroelastic behavior of a shell, eigenvalues and eigenvectors of Eq. (33) are found by means of the equation reduction method. Equation (33) is therefore rewritten as:

$$\begin{bmatrix}[0] & \frac{1}{\omega_0}[M_s]\\ \frac{1}{\omega^2{}_0}[M_s] & \frac{1}{\omega_0}[C_f]\end{bmatrix}\begin{Bmatrix}\ddot{\delta}\\ \dot{\delta}\end{Bmatrix}+\begin{bmatrix}-\frac{1}{\omega_0}[M_s] & [0]\\ [0] & [K]\end{bmatrix}\begin{Bmatrix}\dot{\delta}\\ \delta\end{Bmatrix}=0 \qquad (34)$$

Where ω_0 is the first element of the elasticity matrix in Eq. (5) and the total stiffness matrix is:

$$[K]=[K_s]+[K_l]-[K_f] \tag{35}$$

The corresponding eigenvalue problem is given by:

$$|[DD]-\frac{1}{\omega_0\Lambda}[I]|=0 \tag{35}$$

where $[I]$ is the identity matrix, Λ is the eigenvalue (complex frequency of the system) and $[DD]$ is:

$$[DD]=\begin{bmatrix} [0] & [I] \\ \frac{1}{\omega^2{}_0}[K^{-1}][M_s] & -\frac{1}{\omega_0}[K^{-1}][C_f] \end{bmatrix} \tag{36}$$

Matrices$[M_s]$, $[C_f]$ and $[K]$ are square matrices of order *NDF(N+1)* where *NDF* is the number of degrees of freedom at each node and N is the number of elements used to discretize the shell geometry. Dynamic stability of the shell is investigated by studying the eigenvalues in the complex plane. The flutter onset occurs when the imaginary part of the eigenvalue changes from positive to negative.

3.8 Numerical Results and Discussion

In this section, numerical results are compared with existing experimental data (Evensen & Olson, 1968; Olson & Fung, 1966, 1967), analytical (Evensen & Olson, 1967, 1968) and numerical (Bismarck-Nasr, 1976; Ganapathi et al., 1994) solutions. In all of these studies shell geometry and flow parameters have the following similar features:

$$E = 16 \times 10^6 \ lb/in \quad (11 \times 10^{10} N/m^2)$$
$$\upsilon = 0.35$$
$$h = 0.0040 \ in \quad (0.0001015 \ m)$$
$$L = 15.4 \ in \quad (0.381 \ m)$$
$$R = 8.00 \ in \quad (0.203 \ m)$$
$$\rho_s = 0.000833 \ lb - s^2/in^4 \quad (8900 \ kg/m^3)$$
$$M = 3.00$$
$$a_\infty = 8400 \ in/s \quad (213 \ m/s)$$
$$T_{t\infty} = 120^\circ \ F \quad (48.90^\circ \ C)$$

where $T_{t\infty}$ is the freestream stagnation temperature and ρ_s is the shell density . This set of data was taken from the experiments done by Olson and Fung (Olson & Fung, 1966, 1967) in the NASA Ames Research Center (here referred to as case-I). It is necessary to mention that in some of references (Carter & Stearman, 1968; Selmane & Lakis, 1997) different values for $L = 16 \ in, E = 13 \times 10^6 \ lb/in^2$ and $\upsilon = 0.33$ have been used (referred to as case-II). As a consequence, in the present analysis comparison of numerical results was sought for each given set of data.

3.8.1 Convergence Test

In finite element analysis, the number of elements has a significant influence on the final results. Therefore, a set of calculations (for case-I) was done to find the appropriate number of elements for shell discretizing. As shown in Table 1, convergence of the natural frequency using 20 elements is sufficient for further analysis.

3.8.2 Boundary Condition

For the test case in Ref 3, the shell tested in a supersonic wind tunnel had complex boundary conditions. In order to obtain reliable numerical results, two different boundary conditions were applied to find the effective ends. The numerical prediction of natural frequencies is shown in Fig. 2 along with the experimental data of Olson and Fung(Olson & Fung, 1966). For low values of n the free simply supported boundary ($V = W = 0$) lies between the experimental and simply supported ends ($V = W = U = 0$). For high values of n these two conditions approach each other and the experimental results lie above both of them. This discrepancy has been reported because of errors during measurement of the shell thickness (Olson & Fung, 1966). It seems that the free simply supported case offers a good approximation to present effective ends of the shell during the flutter calculation particularly for large values of the circumferential wave number.

3.8.3 Validation and Comparison of Aerodynamic Theories

For both sets of data (case-I and II), numerical results of this study compared to experimental, theoretical and numerical analyses are presented in Table 2. In all of the cases, instability occurred in the form of coupled-mode flutter. The proposed FEM shows very good agreement with experimental and analytical results and also has better capabilities for aeroelastic stability prediction in terms of critical p_{∞} and n compared to the other FEM methods. In Fig. 3 the results of flutter boundary for two different

aerodynamic theories; piston (Eq. (21)) and potential theory (Eq. (22)), have been presented and compared with the experimental data of Ref. 3. It can be seen that both theories predict a larger stabilizing effect of the shell internal pressure than the experiments. It also indicates that the potential solution for flutter boundary is higher than that found using piston theory, and the critical value of the circumferential wave number n is somewhat smaller than predicted by piston theory. This is due to the dependency of the pressure field on n in potential theory. As n increases, the pressure decreases significantly. In piston theory the pressure field and n are independent. Therefore, a lower value of n is reached at the flutter boundary. As an example, for unpressurized shells $P_m = 0$, and $n = 20$ the complex frequencies based on the potential theory solution for the first three longitudinal modes have been plotted in Fig. 4. The real parts of the frequencies decrease as p_∞ increases, and the imaginary parts change their sign with the variation of p_∞ values. The condition for flutter is that the damping of the system (or imaginary part) vanishes in one of the modes. This occurs for axial wave number $m = 2$ at $p_\infty = 1.05$ *psi* where the first and second modes pass through zero at a much higher value of freestream static pressure. The same behavior was found by Olson and Fung (Olson & Fung, 1967) in their calculation using potential theory. A detailed comparison between piston and potential theory indicates that piston theory has the closest prediction for both stability boundary and for critical values of circumferential wave numbers, n. The further analysis in this study is therefore done by

applying the piston theory as an aerodynamic model to account for fluid structure interaction.

3.8.4 Effect of the Curvature Term of Piston Theory

Figure 5 shows some typical complex frequencies versus freestream static pressure, p_∞ for $n = 25$. Only the first and second modes are shown ($m = 1,2$). Aerodynamic pressure is evaluated using Eq. (20). In Fig. 5a the real part of the complex frequency for the first mode increases while for the second mode it decreases as p_∞ increases. For higher values of p_∞ these real parts eventually merge into a single mode. If p_∞ is increased still further, the shell loses stability at $p_\infty = 0.521\ psi$. This instability is due to coupled-mode flutter because the imaginary part of the complex frequency (which represents the damping of the system) crosses the zero value (see Fig. 5b) and makes the vibration amplitude grow. Figure 6 presents the complex frequencies of the aerodynamic pressure if Eq. (21) is used for the calculation. The real and imaginary parts of the first and second modes show the same behavior as the freestream static pressure increases, but the onset of flutter is at $p_\infty \approx 0.60\ psi$. Prediction of the critical freestream static pressure using Eq. (20) provides a closer match to experimental results (Olson & Fung, 1966) than evaluating the pressure field using Eq. (21). As expected, the piston theory with the correction term to account for shell curvature produces a better approximation for the pressure loading acting on a shell exposed to supersonic flow.

3.8.5 Effect of Initial Strain and Aspect Ratio (L/R)

In order to investigate the effect of shell internal pressure, complex frequencies for the critical circumferential wave number $n = 23$ with shell internal pressure $p_m = 0.50\ psi$ were calculated and are shown in Fig. 7. In this case the critical freestream static pressure is $p_\infty = 1.00\ psi$; due to the increase in stiffness of the shell because of applied internal pressure, flutter onset occurred at a higher value of p_∞. In Fig. 8, the flutter boundary for the shell geometry of case-II under different internal pressures is shown. The lowest critical value of freestream static pressure for each circumferential wave number becomes larger when P_m is increased. It is observed that shell internal pressure has a stabilizing influence. Note that experiments (Olson & Fung, 1966) demonstrated that for moderate values of P_m the shell loses it dynamic stability up to even unpressurized level while small and high values of P_m stabilize the shell completely. This behavior is explained quite well by considering shell imperfections during the analysis (Carter & Stearman, 1968). The effect of axial compression on the flutter boundary is also shown in Fig. 8. The axial load P_x decreases the stiffness of the shell which results in a lower critical freestream static pressure than an unstressed shell. Figure 9 shows the case of different L/R ratios. The critical freestream static pressure for a lower ratio of L/R increases rapidly and the critical circumferential wave number also increases. For $L/R = 4$ the shell loses it stability at $n = 18$ and $P_\infty = 0.171\ psi$ while for $L/R = 1$ the onset of flutter is at $n = 31$ and $P_\infty = 1.535\ psi$.

3.8.6 Effect of Freestream Static Pressure on the Mode Shape

The normalized radial, axial and circumferential mode shapes for different values of p_∞ are shown in Fig. 10. Here Eq. (20) is used to account for aerodynamic loading. When $p_\infty = 0.0$ the eigenvectors are pure real and represent the free vibration of the shell in standing wave forms. For low values of freestream static pressure the eigenvectors are complex in regions where the imaginary part is close to zero and become negligible but as p_∞ increases each eigenvalue takes a complex mode shape which can be represented by two real mode shapes. They are commonly called cosine and sine modes and are phase shifted by 90 degrees. As a result, nodes and antinodes travel along the shell circumferentially and this means that the mode shapes contain traveling wave components. This behavior was also observed in the experiments (Olson & Fung, 1966); the flutter motions were traveling wave forms with moving node lines.

3.8.7 Effect of Shell Boundary Conditions

To establish the effects of shell boundary conditions on the critical freestream static pressures some typical data is shown in Table 3. For the same shell geometry and flow parameters the shell with one end free and the other end simply supported loses its dynamic stability first. When both ends are free, flutter onset occurs with second and third mode coupling. For the other boundary conditions flutter onset starts by coalescence of first and second longitudinal modes.

3.9 Conclusion

An efficient hybrid finite element method is used to analyze the dynamic stability of circular cylindrical shells subjected to external supersonic flow. Linear Sander's shell theory with two different potential and piston theories to account for the aerodynamic pressure field is used in a combined approach to derive the aeroelastic equation of motion. It is observed that piston theory provides a better approximation to account for fluid–structure interaction in supersonic airflow conditions. Numerical results are obtained for different shell boundary conditions and geometries. In all the study cases, only one type of instability is found, namely coupled-mode flutter in the form of traveling wave flutter, mostly in the first and second longitudinal modes. There is a good agreement for prediction of flutter onset with existing experiments and other analytical and FEM analyses. Shell internal pressure has a stabilizing effect while axial compression lowers the flutter boundary. Large L/R ratios result in lower critical freestream static pressure with lower values of associated circumferential wave numbers. This proposed hybrid FEM provides the capability to apply different theories with different complex boundaries and geometries for a cylindrical shell. This can be used effectively in the design and analysis of aerospace structures. Reliable results can be obtained at less computational cost compared to commercial FEM software, which imposes some restrictions when such analysis is done.

Subsequent work to this study is presently being prepared to deal with the effect of geometry and aerodynamic nonlinearities on flutter boundaries. This should improve the reliability of the FEM package.

3.10 Appendix

Sander's linear equation for thin cylindrical shells in terms of axial, tangential and circumferential displacements is (Eq. (4)):

$$
\begin{aligned}
L_1(U,V,W,P_{ij}) = {} & P_{11}\frac{\partial^2 U}{\partial x^2} + \frac{P_{12}}{R}\frac{\partial^2 U}{\partial x^2}\left(\frac{\partial^2 V}{\partial x \partial \theta} + \frac{\partial W}{\partial x}\right) - P_{14}\frac{\partial^3 W}{\partial x^3} \\
& + \frac{P_{15}}{R^2}\left(\frac{\partial^3 W}{\partial x \partial \theta^2} + \frac{\partial^2 V}{\partial x \partial \theta}\right) + \left(\frac{P_{33}}{R} - \frac{P_{63}}{2R^2}\right)\left(\frac{\partial^2 V}{\partial x \partial \theta} + \frac{1}{R}\frac{\partial^2 U}{\partial \theta^2}\right) \\
& + \left(\frac{P_{36}}{R^2} - \frac{P_{66}}{2R^3}\right)\left(-2\frac{\partial^3 W}{\partial x \partial \theta^2} + \frac{3}{2}\frac{\partial^2 V}{\partial x \partial \theta} - \frac{1}{2R}\frac{\partial^2 U}{\partial \theta^2}\right)
\end{aligned}
$$

$$
\begin{aligned}
L_2(U,V,W,P_{ij}) = {} & \left(\frac{P_{21}}{R} - \frac{P_{51}}{R^2}\right)\frac{\partial^2 U}{\partial x \partial \theta} + \frac{1}{R}\left(\frac{P_{22}}{R} + \frac{P_{52}}{R^2}\right)\left(\frac{\partial^2 V}{\partial \theta^2} + \frac{\partial W}{\partial \theta}\right) \\
& - \left(\frac{P_{24}}{R} + \frac{P_{54}}{R^2}\right)\frac{\partial^3 W}{\partial x^2 \partial \theta} + \frac{1}{R^2}\left(\frac{P_{25}}{R} + \frac{P_{55}}{R^2}\right)\left(-\frac{\partial^3 W}{\partial \theta^3} + \frac{\partial^2 V}{\partial \theta^2}\right) \\
& + \left(P_{33} + \frac{3P_{63}}{2R}\right)\left(\frac{\partial^2 V}{\partial x^2} + \frac{\partial^2 U}{R \partial x \partial \theta}\right) \\
& + \frac{1}{R}\left(P_{36} + \frac{3P_{66}}{2R}\right)\left(-2\frac{\partial^3 W}{\partial x^2 \partial \theta} + \frac{3}{2}\frac{\partial^2 V}{\partial x^2} - \frac{1}{2R}\frac{\partial^2 U}{\partial x \partial \theta}\right)
\end{aligned}
$$

(A.1)

$$
\begin{aligned}
L_3(U,V,W,P_{ij}) = {} & P_{41}\frac{\partial^3 U}{\partial x^3} + \frac{P_{42}}{R}\left(\frac{\partial^3 V}{\partial x^2 \partial \theta} + \frac{\partial^2 W}{\partial x^2}\right) - P_{44}\frac{\partial^4 W}{\partial x^4} \\
& + \frac{P_{45}}{R^2}\left(-\frac{\partial^4 W}{\partial x^2 \partial \theta^2} + \frac{\partial^3 V}{\partial x^2 \partial \theta}\right) + \frac{2P_{63}}{R}\left(\frac{1}{R}\frac{\partial^3 U}{\partial x \partial \theta^2} + \frac{\partial^3 V}{\partial x^2 \partial \theta}\right) \\
& + \frac{2P_{66}}{R^2}\left(-2\frac{\partial^4 W}{\partial x^2 \partial \theta^2} + \frac{3}{2}\frac{\partial^3 V}{\partial x^2 \partial \theta} - \frac{1}{2R}\frac{\partial^3 U}{\partial x \partial \theta^2}\right) + \frac{P_{51}}{R^2}\frac{\partial^3 U}{\partial x \partial \theta^2} \\
& + \frac{P_{52}}{R^3}\left(\frac{\partial^3 V}{\partial \theta^3} + \frac{\partial^2 W}{\partial \theta^2}\right) + \frac{P_{55}}{R^4}\left(-\frac{\partial^4 W}{\partial \theta^4} + \frac{\partial^3 V}{\partial \theta^3}\right) - \frac{P_{21}}{R}\frac{\partial U}{\partial x} - \frac{P_{54}}{R^2}\frac{\partial^4 W}{\partial x^2 \partial \theta^2} \\
& + \frac{P_{22}}{R^2}\left(\frac{\partial V}{\partial \theta} + W\right) + \frac{P_{24}}{R^2}\frac{\partial^2 W}{\partial \theta^2} - \frac{P_{25}}{R^3}\left(-\frac{\partial^2 W}{\partial \theta^2} + \frac{\partial V}{\partial \theta}\right)
\end{aligned}
$$

Matrices $[T]_{3\times3}$, $[R]_{3\times8}$, and $[A]_{8\times8}$ are defined as:

$$[T]=\begin{bmatrix}\cos(n\theta) & 0 & 0\\ 0 & \cos(n\theta) & 0\\ 0 & 0 & \sin(n\theta)\end{bmatrix}$$

$$R(1,i)=\alpha_i e^{\lambda_i x/R}\quad,\quad R(2,i)=e^{\lambda_i x/R}\quad,\quad R(1,i)=\beta_i e^{\lambda_i x/R}\qquad i=1,2,...,8 \tag{A.2}$$

$$A(1,i)=\alpha_i,\quad A(2,i)=1,\quad A(3,i)=\frac{\lambda_i}{R},\quad A(4,i)=\beta_i,\quad A(5,i)=\alpha_i e^{\lambda_i l/R}$$
$$A(6,i)=e^{\lambda_i l/R},\quad A(7,i)=\frac{\lambda_i}{R}e^{\lambda_i l/R},\quad A(8,i)=\beta_i e^{\lambda_i l/R}\qquad i=1,2,...8$$

The elements of matrix $[Q]$ of order 6×8 are given by:

$$Q(1,i)=\alpha_i\frac{\lambda_i}{R}e^{\lambda_i x/R},\quad Q(2,i)=\frac{1}{R}(n\beta_i+1)e^{\lambda_i x/R},\quad Q(3,i)=\frac{1}{R}(\beta_i\lambda_i-n\alpha_i)e^{\lambda_i x/R}$$
$$Q(4,i)=-(\frac{\lambda_i}{R})^2 e^{\lambda_i x/R},\quad Q(5,i)=\frac{1}{R^2}(n^2+\beta_i n)e^{\lambda_i x/R},$$
$$Q(6,i)=\frac{1}{R^2}(2n\lambda_i+\frac{3}{2}\beta_i\lambda_i+\frac{1}{2}n\alpha_i)e^{\lambda_i x/R}\qquad i=1,2,...8 \tag{A.3}$$

The expression Z in Eq. (22) for each element of the shell in external flow is:

$$Z=\sum_{j=1}^{8} Z_j(im_j r_{ext})=\frac{1}{n-im_j r_{ext}\dfrac{Y_{n+1}(im_j r_{ext})}{Y_n(im_j r_{ext})}} \tag{A.4}$$

where Y_n and Y_{n+1} are Bessel functions of the 2nd order n and $n+1$; respectively and m_j and r_{ext} are given by:

$$r_{ext} = R + h/2$$
$$m_j = (\frac{\lambda_j}{r_{ext}})^2 - \frac{1}{a_\infty^2}(\omega + U_\infty \frac{\lambda_j}{r_{ext}})^2 \qquad \text{(A.5)}$$

The elements of matrix R_f of order 3 × 8 in Eq. (25) are:

$$[R_f] = \begin{bmatrix} 0 & \dots & 0 \\ e^{i(\lambda_1 x/R)} & \dots & e^{i(\lambda_8 x/R)} \\ 0 & \dots & 0 \end{bmatrix} \qquad \text{(A.6)}$$

3.11 Acknowledgments

The authors acknowledge the financial support of NSERC of Canada, grant No. A8814.

3.12 References

Amabili, M., and Pellicano, F. (2001). Nonlinear supersonic flutter of circular cylindrical shells. *AIAA Journal, 39*(4), 564-573.

Amabili, M., and Pellicano, F. (2002). Multimode approach to nonlinear supersonic flutter of imperfect circular cylindrical shells. *Journal of Applied Mechanics, Transactions ASME, 69*(2), 117-129.

Ashley, H., and Zartarian, G. (1956). Piston theory-New aerodynamic tool for aeroelastician. *Journal of the Aeronautical Sciences, 23*(12), 1109-1118.

Barr, G. W., and Stearman, R. O. (1969). Aeroelastic stability characteristics of cylindrical shells considering imperfections and edge constraint. *AIAA Journal, 7*(5), 912-919.

Barr, G. W., and Stearman, R. O. (1970). Influence of a supersonic flowfield on the elastic stability of cylindrical shells. *AIAA Journal, 8*(6), 993-1000.

Bismarck-Nasr, M. N. (1976). Finite element method applied to the supersonic flutter of circular cylindrical shells. *International Journal for Numerical Methods in Engineering, 10*(2), 423-435.

Bismarck-Nasr, M. N. (1996). Finite elements in aeroelasticity of plates and shells. *Applied Mechanics Reviews, 49*(10 pt 2), 17-24.

Carter, L. L., and Stearman, R. O. (1968). Some aspects of cylindrical shell panel flutter. *AIAA Journal, 6*(1), 37-43.

Dowell, E. H. (1966). Flutter of infinitely long plates and shells. Part II. *AIAA Journal, 4*(9), 1510-1518.

Dowell, E. H. (1975). *Aeroelasticity of plates and shells.* Leyden: Noordhoff International Publishing.

Evensen, D. A., and Olson, M. D. (1967). *Nonlinear Flutter of a Circular Cylindrical shell in Supersonic Flow.*

Evensen, D. A., and Olson, M. D. (1968). Circumferentially traveling wave flutter of circular cylindrical shell. *AIAA Journal, 6*(8), 1522-1527.

Ganapathi, M., Varadan, T. K., and Jijen, J. (1994). Field-consistent element applied to flutter analysis of circular cylindrical shells. *Journal of Sound and Vibration, 171*(4), 509-527.

Horn, W., Barr, G., Carter, L., and Stearman, R. (1974). Recent contributions to experiments on cylindrical shell panel flutter. *AIAA Journal, 12*(11), 1481-1490.

Krumhaar, H. (1963). The accuracy of linear piston theory when applied to cylindrical shells. *AIAA Journal, 1*(6), 1448-1449.

Lakis, A. A., and Paidoussis, M. P. (1972). Dynamic analysis of axially non-uniform thin cylindrical shells. *Journal of Mechanical Engineering Science, 14*(1), 49-71.

MacNeal, R. H. (1972). *Nastran Theoretical manual.* NASA sp-221

Mason, D. R., and Blotter, P. T. (1986). Finite-Element Application to Rocket Nozzle Aeroelasticity. *Journal of Propulsion and Power, 2*(6), 499-507.

Olson, M. D., and Fung, Y. C. (1966). Supersonic flutter of circular cylindrical shells subjected to internal pressure and axial compression. *AIAA Journal, 4*(5), 858-864.

Olson, M. D., and Fung, Y. C. (1967). Comparing theory and experiment for supersonic flutter of circular cylindrical shells. *AIAA Journal, 5*(10), 1849-1856.

Sanders. (1959). *An improved first-approximation theory for thin shell.* NASA R-24.

Selmane, A., and Lakis, A. A. (1997). Non-linear dynamic analysis of orthotropic open cylindrical shells subjected to a flowing fluid. *Journal of Sound and Vibration, 202*(1), 67-93.

Toorani, M. H., and Lakis, A. A. (2000). General equations of anisotropic plates and shells including transverse shear deformations, rotary inertia and initial curvature effects. *Journal of Sound and Vibration, 237*(4), 561-615.

Zienkiewicz, O. C., and Taylor, R. L. (2000). *The finite element method,Volume:2 Solid Mechanics* (5th edition ed.). Oxford: Butterworht-Heinemann.

3.13 List of Figures and Tables

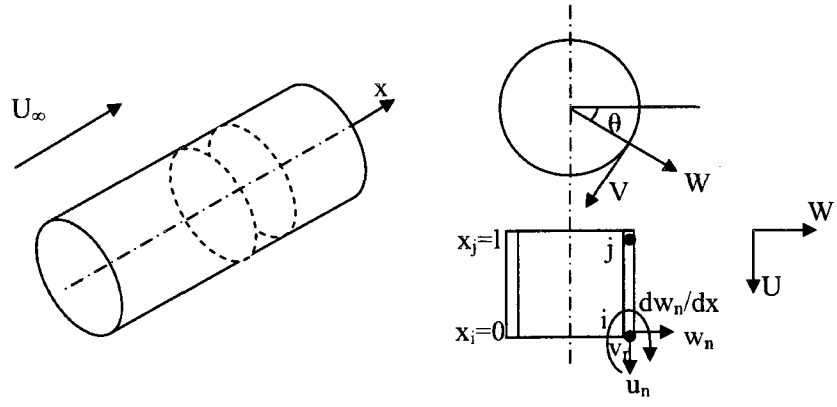

Figure 1 Geometry of cylindrical frustum element

Table 1 Convergence test for shell case-I

No. of elements	ω_1, Hz	ω_2, Hz	ω_3, Hz	ω_4, Hz	p_{cr}, psi	$n_{critical}$
6	318.836	320.253	333.286	367.256	0.100	26
8	303.339	307.551	323.062	357.826	0.333	26
10	297.195	302.330	318.605	353.346	0.425	26
13	293.237	298.898	315.574	350.165	0.481	26
15	291.922	297.747	314.549	349.079	0.499	26
16	291.455	297.343	314.204	348.744	0.506	26
19	268.218	275.048	294.877	335.063	0.519	25
20	268.047	274.899	294.742	334.912	0.521	25

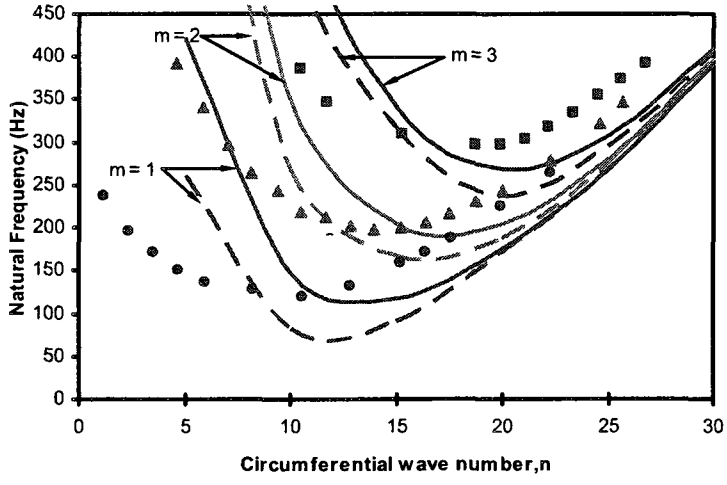

Figure 2 Natural frequencies of unstressed shell, case-I:—, simply supported ends; ---, freely simply supported ends. Experiment: •, m=1; ▲, m=2; and ■, m=3.

Table 2 Comparison of shell flutter boundary at $M = 3$ and $p_x = p_m = 0$

	p_∞, psi	$n_{critical}$	L, in	υ	$E, lb/in^2$
Experimental results(Olson & Fung, 1966)	0.380-0.420	20	15.40	0.35	16×10^6
Analytical results(Carter & Stearman, 1968)	0.420	24	16.00	0.33	13×10^6
Analytical results(Olson & Fung, 1967)	0.550	25	15.40	0.35	16×10^6
Analytical results(Amabili & Pellicano, 2001)	0.330	27	15.40	0.35	16×10^6
FEM results(Bismarck-Nasr, 1976)	0.5621	34	16.00	0.33	13×10^6
FEM results(Ganapathi et al., 1994)	0.5621	25	16.00	0.33	13×10^6
FEM results(Ganapathi et al., 1994)	0.5621	26	15.40	0.35	16×10^6
Present results	0.522	26	15.40	0.35	16×10^6
Present results	0.382	25	16.00	0.33	13×10^6

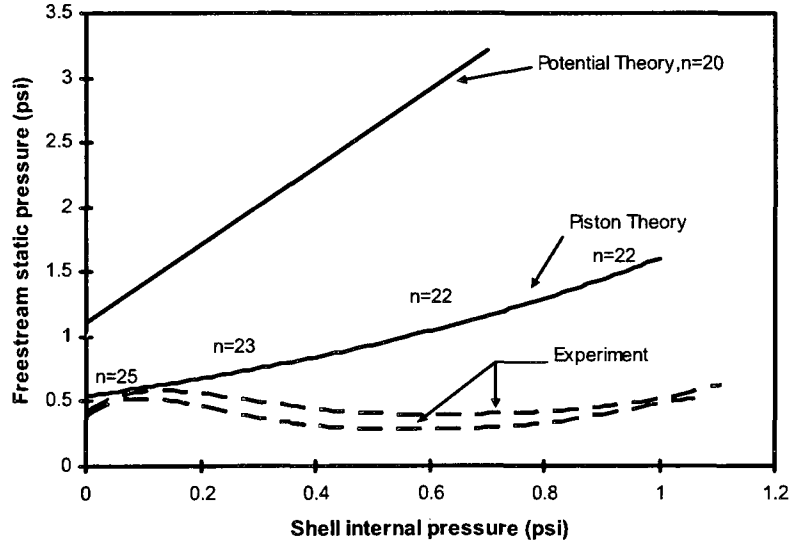

Figure 3 Cylindrical shell flutter boundaries

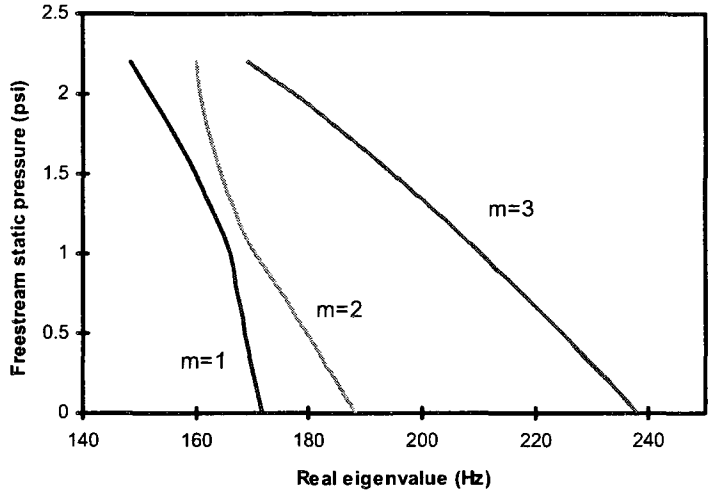

a)

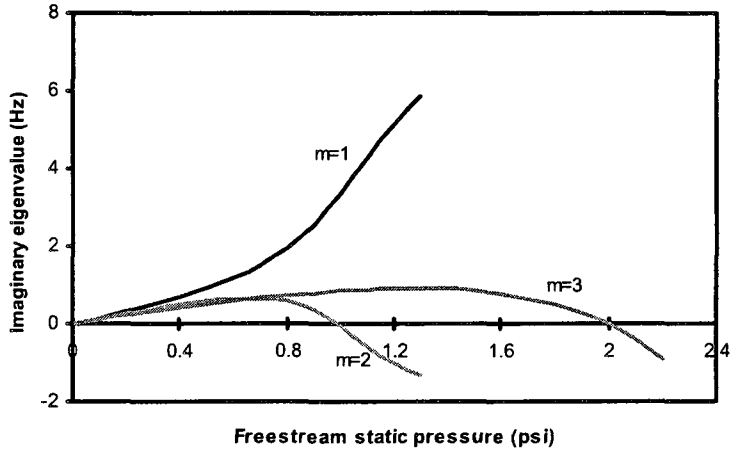

b)

Figure 4 a) Real part and b) imaginary part of the eigenvalues of system vs freestream static pressure, shell case-I, aerodynamic pressure evaluated Equation (22), $n = 20$,

$$p_m = p_x = 0.0 \ \ psi$$

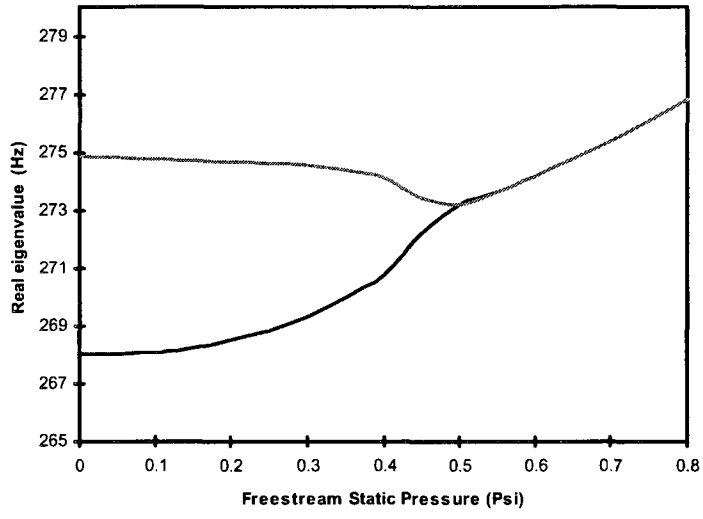

a)

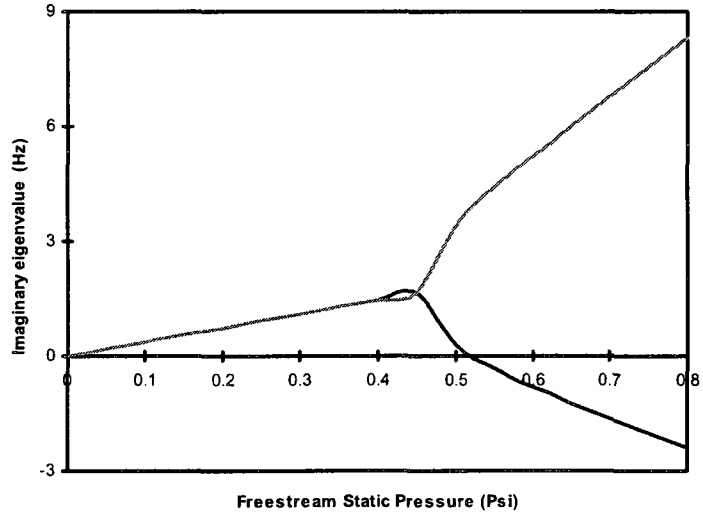

b)

Figure 5 a) Real part and b) imaginary part of the eigenvalues of system vs freestream static pressure, shell case-I, aerodynamic pressure evaluated by Equation (20),

$$n = 25 \;\; p_m = p_x = 0.0 \;\; psi$$

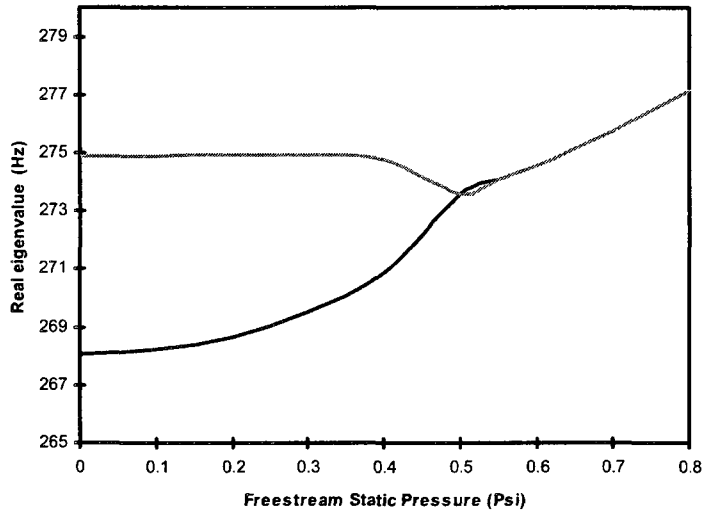

a)

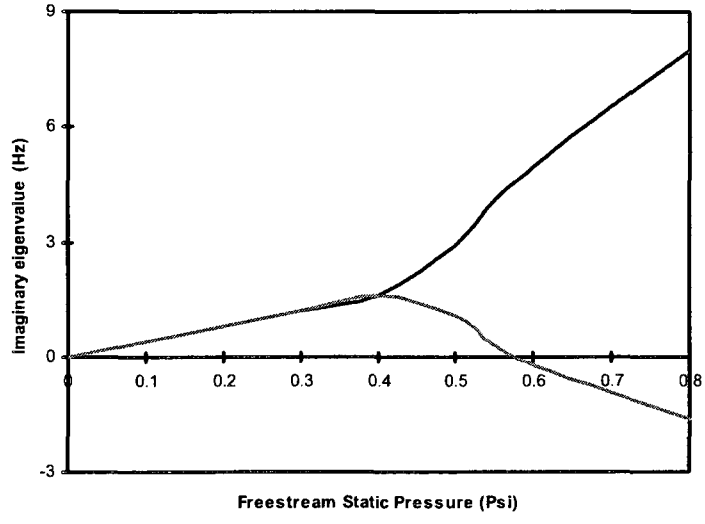

b)

Figure 6 a) Real part and b) imaginary part of the eigenvalues of system vs freestream static pressure, shell case-I, aerodynamic pressure evaluated by Equation (21),

$$n = 25\,,\; p_m = p_x = 0.0 \;\; psi$$

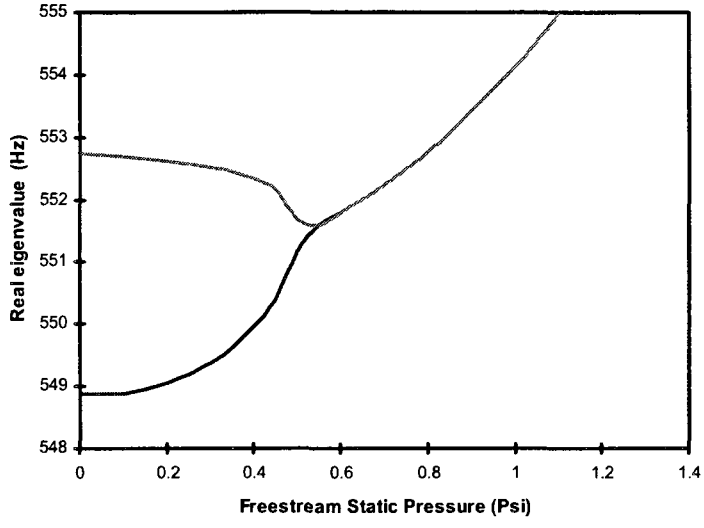

a)

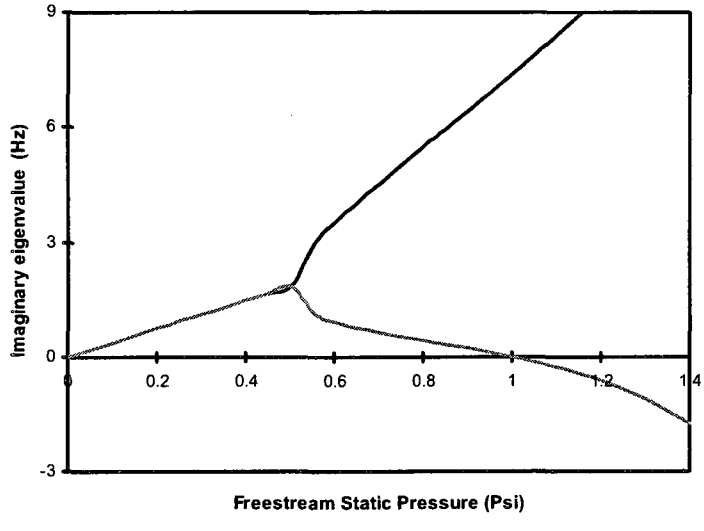

b)

Figure 7 a) Real part and b) imaginary part of the eigenvalues of system vs freestream static pressure, shell case-1, aerodynamic pressure evaluated by Equation (20), $n = 23$, $p_m = 0.50\ \ psi$, $p_x = 0.0\ \ psi$

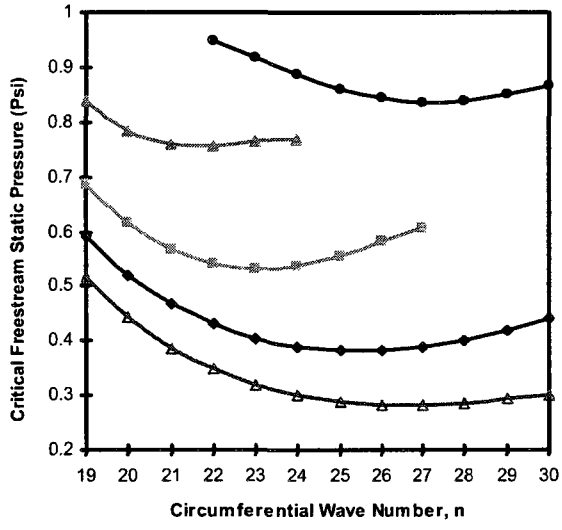

Figure 8 Flutter boundaries for stressed shell. Shell case-I, $p_x = 0.0\ lb/in^2$: ♦, $p_m = 0.0\ lb/in^2$; ■, $p_m = 0.246\ lb/in^2$; ▲, $p_m = 0.50\ lb/in^2$; ●, $p_m = 0.70\ lb/in^2$; Δ, $p_x = 30\ lb, p_m = 0.0\ lb/in^2$.

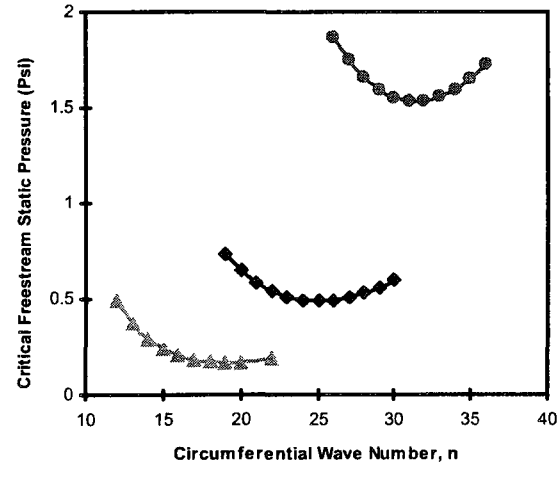

Figure 9 Flutter boundaries for different L/R **ratio, Shell case-I,** $p_m = p_x = 0.0\ psi$; ▲, $L/R = 4$; ♦, $L/R = 2$; ●, $L/R = 1$

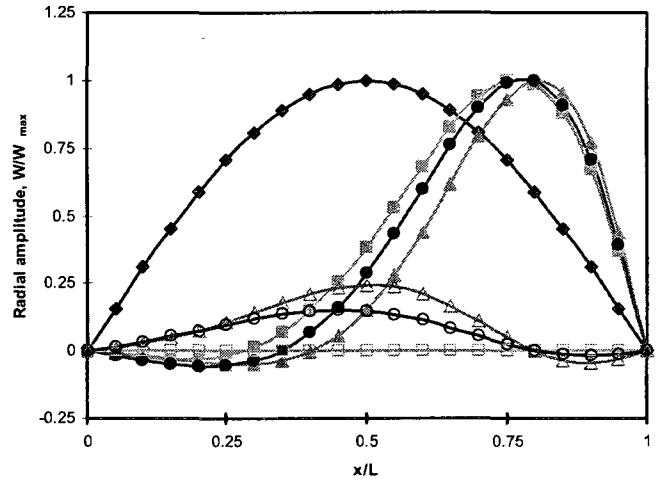
1.25
1
0.75
0.5
0.25
0
-0.25
Radial amplitude, W/W max
0
0.25
0.5
0.75
1
x/L

a)

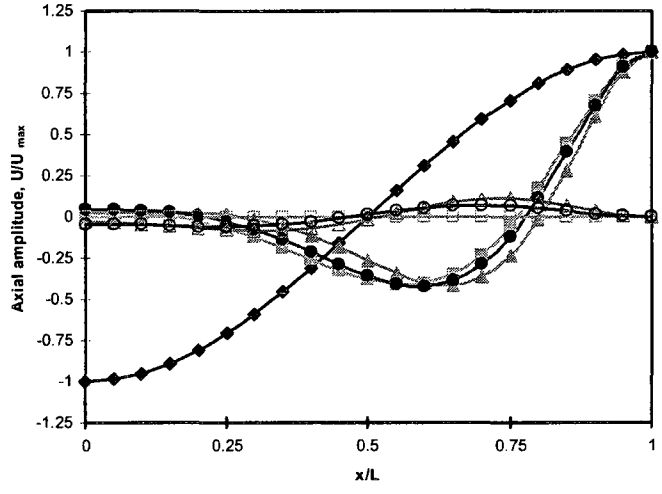
1.25
1
0.75
0.5
0.25
0
-0.25
-0.5
-0.75
-1
-1.25
Axial amplitude, U/U max
0
0.25
0.5
0.75
1
x/L

b)

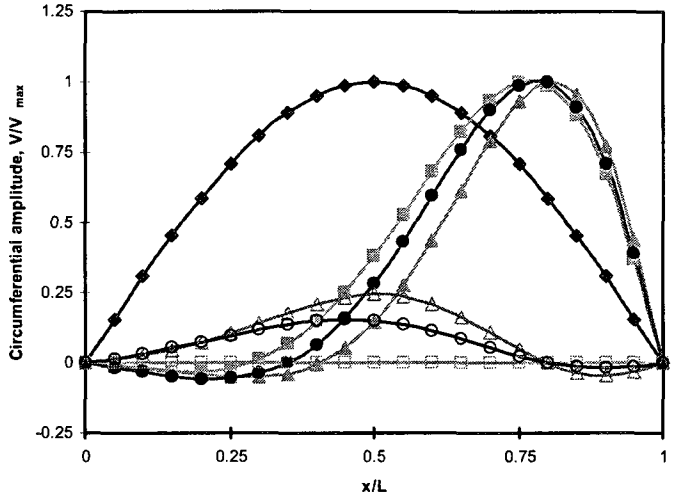

c)

Figure 10 a) Radial, b) axial and c) circumferential mode shapes variation with freestream static pressure, shell case-I, $n = 25, m = 1$ **; ♦, free vibration** $p_\infty = 0.0\ psi$ **; ■, cosine mode,** $p_\infty = 0.45\ psi$ **; □, sine mode,** $p_\infty = 0.45\ psi$ **;●, cosine mode,** $p_\infty = p_{critical} = 0.521\ psi$ **; ○, sine mode,** $p_\infty = p_{critical} = 0.521\ psi$ **; ▲, cosine mode,** $p_\infty = 0.75\ psi$ **; Δ, Sine mode,** $p_\infty = 0.75\ psi$.

Chapter 4: Article III - Hybrid Finite Element Method Applied to Supersonic Flutter of an Empty or Partially Liquid-Filled Truncated Conical Shell.

4.1 Abstracts

In this study, aeroelastic analysis of a truncated conical shell subjected to external supersonic airflow is carried out. The structural model is based on a combination of linear Sanders thin shell theory and the classic finite element method. Linearized first-order potential (piston) theory with the curvature correction term is coupled with the structural model to account for pressure loading. The influence of stress stiffening due to internal or external pressure and axial compression is also taken into account. The fluid-filled effect is considered as a velocity potential variable at each node of the shell elements at the fluid-structure interface in terms of nodal elastic displacements. Aeroelastic equations using a hybrid finite element formulation are derived and solved numerically. Results are validated using numerical and theoretical data available in the literature. The analysis is accomplished for conical shells of different boundary conditions and cone angles. In all cases the conical shell loses its stability through coupled-mode flutter. This proposed hybrid finite element method can be used efficiently for design and analysis of conical shells employed in high speed aircraft structures.

4.2 Introduction

Shells of revolution, particularly conical shells are one of the primary structural elements in high speed aircraft. Their applications include the propellant tank or gas-deployed skirt of spacecraft. Due to the large expanses in their geometry combined with thin wall thicknesses, conical shells are more susceptible to dynamic instability or flutter induced by high-Mach number gas flow. It is therefore important to understand the effect of different parameters and loadings on their dynamic response.

Aeroelastic analysis of shells and plates has been investigated by numerous researchers experimentally and analytically (Bismarck-Nasr, 1996). Dowell addressed a comprehensive study of the aeroelasticity of shells and plates in his book (Dowell, 1975). Aeroelasticity of circular cylindrical shells has also been reported in detail by different researchers (Amabili & Pellicano, 2001, 2002; Barr & Stearman, 1969; Bismarck-Nasr, 1976; Ganapathi et al., 1994; Olson & Fung, 1966, 1967), while less information is available for conical shells. During the 1970s some researchers focused their efforts on conical shell aeroelasticity. The earliest work in this field was found by Shulman (Shulman, 1959). Ueda, Kobayashi and Kihira (Ueda et al., 1977) investigated theoretically and experimentally the supersonic flutter of a conical shell. Dixon and Hudson (Dixon & Hudson, 1970) studied the flutter and vibration of an orthotropic conical shell theoretically. Miserentino and Dixon (Miserentino & Dixon, 1971) investigated experimentally the vibration and flutter of a pressurized truncated conical shell. Bismarck-Nasr and Costa-Savio (Bismarck-Nasr & Costa Savio, 1979) found a finite element solution for the supersonic flutter of conical shells. Sunder, Ramakrishnan

and Sengupta (Sunder et al., 1983a) reported the success of the application of finite element analysis to calculate the flutter of a laminated conical shell. In another study they found the optimum cone angle in aeroelastic flutter (Sunder et al., 1983b). Mason and Blotter (Mason & Blotter, 1986) used a finite element technique to find the flutter boundary for a conical shell (a typical rocket nozzle element) subjected to an internal supersonic gas flow. Most of these works considered only simply supported conical shells. Not all boundary conditions were satisfied by these methods (Mason & Blotter, 1986). There are also other researchers who focused on the dynamic stability and fluid-structure interaction of conical shells. For example, Lakis, Van Dyke and Ouriche (Lakis et al., 1992) investigated the dynamic analysis of anisotropic fluid-filled conical shells. Recently, Kumar and Ganesan (Kumar & Ganesan, 2008) studied the vibration of conical shells conveying fluid.

For such a problem, use of an analytical approach becomes very complicated if one wishes to include complex structures, boundary conditions, material and loading. Therefore, numerical methods such as the finite element method (FEM) are powerful tools for cases involving changes to all factors affecting flutter boundaries.

The objective of the present study is to develop a general hybrid finite element package for predicting the aeroelastic behavior of thin conical shells with boundary conditions which can be varied as desired. The solution scheme is based on the finite element development done by Lakis and et al. (Lakis et al., 1992) for conical shells and Lakis and Paidoussis (Lakis & Paidoussis, 1972) for cylindrical shells. These developed methods demonstrated precise and fast convergence with few numerical difficulties. The

element is a conical frustum instead of the usual rectangular shell element. Sanders linear thin shell theory where all strains vanish for rigid body motions (other theories are incapable of this attribute) is coupled with linearized first order piston theory. In the case of a fluid-filled shell the effect of dynamic pressure acting on the wall is modeled based on a velocity potential formulation and Bernoulli's equation. It is assumed that the fluid is incompressible and has no free-surface effect. Initial stress stiffening in the presence of shell internal or external pressure and axial compression is also applied in the formulation. Finally the linear mass, damping and stiffness matrices are obtained. The aeroelastic equation of motion is driven out to a standard eigenvalue problem. The flutter boundary is found by tracking the real and imaginary parts of the eigenvalues as dynamic pressure is varied.

4.3 Finite Element Formulation

4.3.1 Structural Modeling

Sanders (J. L. Sanders, 1959) developed an improved thin shell theory based on Love's first approximation. One advantage of Sanders theory is that all strains vanish for small rigid-body motion. In this study a structure is modeled using a hybrid finite element method which is a combination of Sanders shell theory and the classic finite element formulation. The displacement functions are found from exact solution of Sanders shell theory. According to the Sanders linear thin shell theory the equilibrium equations for a conical shell (Fig. 1) are written as:

$$
\begin{aligned}
&r\frac{\partial N_x}{\partial x}+N_x\sin\alpha+\frac{\partial N_{x\theta}}{\partial\theta}-N_\theta\sin\alpha-\frac{\cos\alpha}{2r}\frac{\partial M_{x\theta}}{\partial\theta}=0\\
&r\frac{\partial N_{x\theta}}{\partial x}+2N_{x\theta}\sin\alpha+\frac{\partial N_\theta}{\partial\theta}+\frac{3}{2}\cos\alpha\frac{\partial M_{x\theta}}{\partial\theta}-\frac{3}{4}\frac{\sin 2\alpha}{r}M_{x\theta}+\frac{\cos\alpha}{r}\frac{\partial M_\theta}{\partial\theta}=0\\
&r\frac{\partial^2 M_x}{\partial x^2}+2\sin\alpha\frac{\partial M_x}{\partial x}+2\frac{\partial^2 M_{x\theta}}{\partial x\partial\theta}+2\frac{\sin\alpha}{r}\frac{\partial M_{x\theta}}{\partial\theta}+\frac{1}{r}\frac{\partial^2 M_\theta}{\partial\theta^2}-\sin\alpha\frac{\partial M_\theta}{\partial x}-N_\theta\cos\alpha=0
\end{aligned}
\tag{1}
$$

where N and M are the stress resultant and stress couples, respectively. The strain-displacement equations for three infinitesimal displacements in axial U, radial W, and circumferential V directions are (J. L. Sanders, 1959):

$$
\begin{Bmatrix}\varepsilon_x\\ \varepsilon_\theta\\ 2\bar{\varepsilon}_{x\theta}\\ \kappa_x\\ \kappa_\theta\\ \bar{\kappa}_{x\theta}\end{Bmatrix}=\begin{Bmatrix}\dfrac{\partial U}{\partial x}\\ \dfrac{1}{x\sin(\alpha)}\dfrac{\partial V}{\partial\theta}+\dfrac{U}{x}+\dfrac{W\cot(\alpha)}{x}\\ \dfrac{\partial V}{\partial x}+\dfrac{1}{x\sin(\alpha)}\dfrac{\partial U}{\partial\theta}-\dfrac{V}{x}\\ -\dfrac{\partial^2 W}{\partial x^2}\\ \dfrac{\partial V}{\partial\theta}\dfrac{\cos(\alpha)}{x^2\sin^2(\alpha)}-\dfrac{1}{x^2\sin^2(\alpha)}\dfrac{\partial^2 W}{\partial\theta^2}-\dfrac{\partial W}{\partial x}\dfrac{1}{x}\\ -\dfrac{2}{x\sin(\alpha)}\dfrac{\partial^2 W}{\partial x\partial\theta}+\dfrac{3}{2}\dfrac{\cot(\alpha)}{x}\dfrac{\partial V}{\partial x}-\dfrac{\partial U}{\partial\theta}\dfrac{\cos(\alpha)}{2x^2\sin^2(\alpha)}+\dfrac{2\sin(\alpha)}{x^2\sin^2(\alpha)}\dfrac{\partial W}{\partial\theta}-\dfrac{3}{2}\dfrac{\cot(\alpha)}{x^2}V\end{Bmatrix}
\tag{2}
$$

Displacements U, W and V in the global Cartesian coordinate system are related to displacements U_i, W_i, V_i indicated in Fig. 2 by:

$$
\begin{Bmatrix}U\\ W\\ V\end{Bmatrix}=\begin{bmatrix}\cos\alpha & \sin\alpha & 0\\ -\sin\alpha & \cos\alpha & 0\\ 0 & 0 & 1\end{bmatrix}\begin{Bmatrix}U_i\\ W_i\\ V_i\end{Bmatrix}
\tag{3}
$$

The stress-strain relation for an anisotropic shell is expressed by:

$$[\sigma]=[p][\varepsilon] \tag{4}$$

where **P** is the elasticity matrix for an anisotropic shell. Upon substitution of Eqs. (2) and (4) into Eq. (1), a system of equilibrium equations can be obtained as a function of displacements:

$$\begin{aligned} L_1(U,W,V,B_{ij})&=0\\ L_2(U,W,V,B_{ij})&=0\\ L_3(U,W,V,B_{ij})&=0 \end{aligned} \tag{5}$$

These three linear partial differential operators L_1, L_2 and L_3 are given in the Appendix, and B_{ij} are elements of the elasticity matrix which, for an isotropic thin shell with thickness h are given by:

$$[p]=\begin{bmatrix} D & \upsilon D & 0 & 0 & 0 & 0\\ \upsilon D & D & 0 & 0 & 0 & 0\\ 0 & 0 & \dfrac{D(1-\upsilon)}{2} & 0 & 0 & 0\\ 0 & 0 & 0 & K & \upsilon K & 0\\ 0 & 0 & 0 & \upsilon K & K & 0\\ 0 & 0 & 0 & 0 & 0 & \dfrac{K(1-\upsilon)}{2} \end{bmatrix} \tag{6}$$

where:

$$\begin{aligned} K&=\frac{Eh^3}{12(1-\upsilon^2)}\\ D&=\frac{Eh}{1-\upsilon^2} \end{aligned} \tag{7}$$

The element is a circumferential conical frustum shown in Fig. 2. It has two nodal circles with four degrees of freedom; axial, radial, circumferential and rotation at each node. This element type makes it possible to use thin shell equations easily to find the exact solution of displacement functions rather than an approximation with polynomial functions as is done in classic FEM. The displacement functions for n^{th} circumferential wave number in Fourier series form can be written as:

$$\begin{aligned} U(r,x,\theta) &= \sum_{n=0}^{\infty} u(x)\cos(n\theta) \\ W(r,x,\theta) &= \sum_{n=0}^{\infty} w(x)\cos(n\theta) \\ V(r,x,\theta) &= \sum_{n=0}^{\infty} v\,(x)\sin(n\theta) \end{aligned} \tag{8}$$

The solutions for the magnitude of displacements can have the following form (Flugge, 1973):

$$\begin{Bmatrix} u(x) \\ v(x) \\ w(x) \end{Bmatrix} = \left(\frac{x}{l}\right)^{\frac{\lambda-1}{2}} \begin{Bmatrix} A \\ B \\ C \end{Bmatrix} \tag{9}$$

where λ, A, B and C are complex numbers and l is an arbitrary reference length. By replacing Eqs. (8) and (9) into Eqs. (5), three ordinary homogeneous differential equations in the following form are obtained:

$$\begin{bmatrix} H_{11} & H_{12} & H_{13} \\ H_{21} & H_{22} & H_{23} \\ H_{31} & H_{32} & H_{33} \end{bmatrix} \begin{Bmatrix} A \\ B \\ C \end{Bmatrix} = \begin{Bmatrix} 0 \\ 0 \\ 0 \end{Bmatrix} \tag{10}$$

In order to have a non-trivial solution the determinant of the above system of equations must be equal to zero. Application of this condition yields the following characteristic equation:

$$h_8\lambda^8 + h_6\lambda^6 + h_4\lambda^4 + h_2\lambda^2 + h_0 = 0 \tag{11}$$

Each single root of Eq. (11) corresponds to the solution of Eqs. (5). The complete solution is obtained by summation of these roots and constants A_i, B_i and C_i:

$$\begin{aligned} u(x) &= \sum_{n=1}^{8} A_i y^{\lambda_i - 1} \\ v(x) &= \sum_{n=1}^{8} B_i y^{\lambda_i - 1} \\ w(x) &= \sum_{n=1}^{8} C_i y^{\lambda_i - 1} \end{aligned} \tag{12}$$

where y is the dimensionless ratio given in Eq. (9). The independent constants A_i and B_i can be expressed in terms of C_i and complex numbers α and β as:

$$\begin{aligned} A_i &= \alpha_i C_i \\ B_i &= \beta_i C_i \end{aligned} \tag{13}$$

These complex numbers can be obtained by replacing them in Eq. (10) in the following way:

$$\begin{bmatrix} H_{11} & H_{12} \\ H_{21} & H_{22} \end{bmatrix} \begin{Bmatrix} \alpha_i \\ \beta_i \end{Bmatrix} = \begin{Bmatrix} -H_{13} \\ -H_{23} \end{Bmatrix} \tag{14}$$

Finally, the magnitude of displacement functions is written as:

$$\begin{Bmatrix} u(x) \\ w(x) \\ v(x) \end{Bmatrix} = [R]\{C\} \tag{15}$$

The displacement vectors, Eq. (8), that correspond to the circumferential wave number n, are written as:

$$\begin{Bmatrix} U(x,\theta) \\ W(x,\theta) \\ V(x,\theta) \end{Bmatrix} = [T][R]\{C\} \tag{16}$$

where matrices **R** can be found in Ref. (Lakis et al., 1992) and **T** are defined as:

$$\begin{bmatrix} \cos n\theta & 0 & 0 \\ 0 & \cos n\theta & 0 \\ 0 & 0 & \sin n\theta \end{bmatrix} \tag{17}$$

The element in Fig. 2 with two nodal lines (i and j) and eight degrees of freedom will have the following nodal displacement vector:

$$\begin{Bmatrix} \delta_i \\ \delta_j \end{Bmatrix} = \left\{U_i, W_i, \partial W_i/\partial x, V_i, U_j, W_j, \partial W_j/\partial x, V_j\right\}^T = [A]\{C\} \tag{18}$$

where matrix **A** is obtained from the terms of **R**. Now, pre-multiplying Eq. (18) by $\mathbf{A}^{-1}$, the constant vector of $\{C\}$ is found. Eq. (16) can therefore be written in terms of nodal degrees of freedom as:

$$\begin{Bmatrix} U(x,\theta) \\ W(x,\theta) \\ V(x,\theta) \end{Bmatrix} = [T][R][A]^{-1} \begin{Bmatrix} \delta_i \\ \delta_j \end{Bmatrix} = [N] \begin{Bmatrix} \delta_i \\ \delta_j \end{Bmatrix} \tag{19}$$

The strain vector, Eq.(2), will become:

$$\{\varepsilon\} = \begin{bmatrix} [T] & [0] \\ [0] & [T] \end{bmatrix} [Q][A]^{-1}\{\delta\} = [B][\delta] \tag{20}$$

where matrix **Q** can be found in Ref. (Lakis et al., 1992). This relation can be used to find the stress vector, Eq. (4), in terms of the nodal degrees of freedom vector:

$$\{\sigma\} = [P][B]\begin{Bmatrix} \delta_i \\ \delta_j \end{Bmatrix} \tag{21}$$

Based on the standard finite element formulation (Zienkiewicz & Taylor, 2000), the local mass and stiffness matrices are found:

$$\begin{aligned} [m_s] &= \rho h \iint [N]^T [N] h dA \\ [k_s] &= \iint [B]^T [P][B] dA \end{aligned} \tag{22}$$

where ρ is the shell density and $dA = x \sin\alpha d\theta dx$ Finally, the global mass, **M**, and stiffness, **K**, matrices for the entire shell are developed using standard assembling techniques for different boundary conditions.

4.3.2 Stress Stiffening

In the presence of initial membrane forces resulting from circumferentially uniform internal or external pressure and axial compression, a strain-energy contribution is introduced into the formulation. It is assumed that the shell is under equilibrium conditions and has not reached its buckling state. The stress resultants of internal pressure, P_m, and axial load, P_x, (positive in compression) are (Dixon & Hudson, 1970):

$$\begin{aligned}
\overline{N}_\theta &= -x\tan\alpha P_m \\
\overline{N}_x &= -\frac{x}{2}\tan\alpha P_m - \frac{P_x}{2\pi\sin 2\alpha} \\
\overline{N}_{x\theta} &= \overline{N}_{\theta x} = 0
\end{aligned} \tag{23}$$

The potential energy due to this initial strain can be found (MacNeal, 1972):

$$U_i = \frac{1}{2}\iint[\overline{N}_x\phi_{\theta\theta}^2 + \overline{N}_\theta\phi_{xx}^2 + (\overline{N}_x + \overline{N}_\theta)\phi_n^2]dA \tag{24}$$

where $\phi_{\theta\theta}$, ϕ_{xx} and ϕ_n are the strain rotation vectors (J. L. Sanders, 1959):

$$\begin{aligned}
\phi_{\theta\theta} &= -\frac{\partial W}{\partial x} \\
\phi_{xx} &= \frac{V}{x\tan\alpha} - \frac{1}{x\sin\alpha}\frac{\partial W}{\partial\theta} \\
\phi_n &= \frac{V}{2x} + \frac{1}{2}\frac{\partial V}{\partial x} - \frac{1}{2x\sin\alpha}\frac{\partial U}{\partial\theta}
\end{aligned} \tag{25}$$

If the displacements are replaced by Eq. (19) the potential energy in terms of nodal degrees of freedom is generated:

$$U_I = \frac{1}{2}\int_{x_i}^{x_j}\int_0^{2\pi}\{r\}^T\begin{bmatrix}\overline{N}_x & 0 & 0\\ 0 & \overline{N}_\theta & 0\\ 0 & 0 & \overline{N}_x + \overline{N}_\theta\end{bmatrix}\{r\}\,dA \tag{26}$$

where:

$$\{r\} = \begin{bmatrix} 0 & -\frac{\partial}{\partial x} & 0 \\ 0 & -\frac{1}{x\sin\alpha}\frac{\partial}{\partial\theta} & \frac{1}{x\tan\alpha} \\ -\frac{1}{2x\sin\alpha}\frac{\partial}{\partial\theta} & 0 & \frac{1}{2x} + \frac{1}{2}\frac{\partial}{\partial x} \end{bmatrix}\begin{Bmatrix}U\\W\\V\end{Bmatrix} = [\bar{\omega}][N]\begin{Bmatrix}\delta_i\\\delta_j\end{Bmatrix} \tag{27}$$

Therefore, the initial stiffness matrix for each element becomes:

$$[k_I] = \iint [N]^T [\bar{\omega}]^T \begin{bmatrix} \bar{N}_x & 0 & 0 \\ 0 & \bar{N}_\theta & 0 \\ 0 & 0 & \bar{N}_x + \bar{N}_\theta \end{bmatrix} [\bar{\omega}][N] dA \qquad (28)$$

After assembly, the whole stress stiffness matrix, $\mathbf{K_I}$ is added to the geometry stiffness matrix developed in Eq. (22).

4.4 Aerodynamic Modeling

Piston theory, introduced by Ashley and Zartarian (Ashley & Zartarian, 1956), is a powerful tool for aeroelasticity modeling. In this study the fluid-structure effect due to external pressure loading can be taken into account using linearized first-order potential theory (Dowell, 1975). This pressure is expressed as:

$$P_a = \frac{\gamma p_\infty M^2}{(M^2-1)^{1/2}} \left[\frac{\partial W}{\partial x} + \frac{M^2-2}{M^2-1} \frac{1}{U_\infty} \frac{\partial W}{\partial t} - \frac{W}{2R(M^2-1)^{1/2}} \right] \qquad (29)$$

where p_∞, U_∞, M and γ are the freestream static pressure, freestream velocity, Mach number and adiabatic exponent of air, respectively. If the Mach number is sufficiently high $(M \geq 2)$, and the curvature term, $\frac{W}{2R(M^2-1)^{1/2}}$ is neglected, the result is the so-called piston theory:

$$P_a = -\gamma p_\infty \left[M \frac{\partial W}{\partial x} + \frac{1}{a_\infty} \frac{\partial W}{\partial t} \right] \qquad (30)$$

where a_∞ is the freestream speed of sound.

Considering the displacements in Eq. (19), the radial deflection W is:

$$W(x,\theta)=\begin{bmatrix}0 & 1 & 0\end{bmatrix}[N]\begin{Bmatrix}\delta_i\\ \delta_j\end{Bmatrix}=[N_w]\begin{Bmatrix}\delta_i\\ \delta_j\end{Bmatrix} \tag{31}$$

and the pressure loading, Eq. (29), in terms of nodal degrees of freedom is written as:

$$\begin{aligned}\{P_a\}=\begin{Bmatrix}0\\ p_{radial}\\ 0\end{Bmatrix}=&\frac{-\rho_\infty U_\infty^2}{(M^2-1)^{1/2}}\frac{1}{U_\infty}\left(\frac{M^2-2}{M^2-1}\right)[N_w]\begin{Bmatrix}\dot{\delta}_i\\ \dot{\delta}_j\end{Bmatrix}\\ &+\frac{-\rho_\infty U_\infty^2}{(M^2-1)^{1/2}}\frac{\partial[N_w]}{\partial x}\begin{Bmatrix}\delta_i\\ \delta_j\end{Bmatrix}\\ &-\frac{-\rho_\infty U_\infty^2}{(M^2-1)^{1/2}}\left(\frac{1}{2(M^2-1)^{1/2}R_m}\right)[N_w]\begin{Bmatrix}\delta_i\\ \delta_j\end{Bmatrix}\end{aligned} \tag{32}$$

where ρ_∞ is the freestream air density and R_m is the median radius for each element. Based on thermodynamic relations the freestream pressure and velocity can be linked together using the following relation:

$$\begin{aligned}U_\infty &= M\,a_\infty\\ a_\infty &= \sqrt{\gamma\frac{p_\infty}{\rho_\infty}}\end{aligned} \tag{33}$$

The general force vector due to a pressure field is written as:

$$\{F_p\}=\iint[N]^T\{p_a\}\,dA \tag{34}$$

Substituting Eq. (32) into the above relation, the aerodynamic damping, $\mathbf{c_f}$, and stiffness $\mathbf{k_f}$ matrices for each element are obtained:

$$[c_f]=[A^{-1}]^T[D_f][A^{-1}]$$
$$[k_f]=[A^{-1}]^T[G_f][A^{-1}] \quad (35)$$

where:

$$[D_f]=\frac{-\rho_\infty U_\infty^2}{(M^2-1)^{1/2}}\frac{1}{U_\infty}\left(\frac{M^2-2}{M^2-1}\right)\iint[N]^T[N_w]dA \quad (36)$$

$$[G_f]=\frac{-\rho_\infty U_\infty^2}{(M^2-1)^{1/2}}\left(\iint[N]^T\frac{\partial[N_w]}{\partial x}dA-\frac{1}{2(M^2-1)^{1/2}R_m}\iint[N]^T[N_w]dA\right) \quad (37)$$

Finally, global aerodynamic damping, $\mathbf{C_f}$, and aerodynamic stiffness, $\mathbf{K_f}$, matrices are found using assembling procedures.

4.5 Fluid-Filled Modeling

The Laplace equation satisfied by velocity potential for inviscid, incompressible and irrotational fluid in the conical system is written as (Korn & Korn, 1968):

$$\nabla^2\varphi=\frac{2}{x}\frac{\partial\varphi}{\partial x}+\frac{\partial^2\varphi}{\partial x^2}\frac{1}{x^2(\sin\beta)^2}\frac{\partial^2\varphi}{\partial\theta^2}+\frac{1}{x^2\tan\beta}\frac{\partial\varphi}{\partial\beta}+\frac{1}{x^2}\frac{\partial^2\varphi}{\partial\beta^2}=0 \quad (38)$$

where, for quiescent fluid $(U_x=0)$ the velocity components are :

$$V_\alpha=\frac{1}{x}\frac{\partial\varphi}{\partial\beta}\quad V_\theta=\frac{1}{x\sin\alpha}\frac{\partial\varphi}{\partial\theta}\quad V_x=\frac{\partial\varphi}{\partial x} \quad (39)$$

where β is the coordinate along the semivertex angle. Using the Bernoulli equation, hydrodynamic pressure in terms of velocity potential, φ, and fluid density, ρ_f, is found:

$$P_f = \rho_f \frac{\partial \varphi}{\partial t} \tag{40}$$

The impermeability condition, which ensures contact between the shell surface and the peripheral fluid at rest, is written as:

$$V_\alpha = \frac{1}{x}\frac{\partial \varphi}{\partial \beta}\bigg|_{\beta=\alpha} = \frac{\partial W}{\partial t} \tag{41}$$

Method of separation of variables for the velocity potential solution can be done as follows:

$$\varphi(x,\theta,\beta,t) = \sum_{q=1}^{8} R_q(\beta) S_q(x,\theta,t) \tag{42}$$

By placing this relation into the impermeability condition, one can find the function $S_q(x,\theta,t)$ in terms of radial displacement:

$$S_q(x,\theta,t) = \frac{x}{R_q'(\alpha)}\frac{\partial W}{\partial t} \tag{43}$$

With the help of Eq. (43) and substitution of Eq. (42) into Eq. (38), the following second order differential equation in terms of $R_q(\beta)$ is obtained:

$$R_q''(\beta) + \frac{1}{\tan\alpha} R_q'(\beta) - \frac{n^2}{\sin^2\alpha} R_q(\beta) = 0 \tag{44}$$

Solution of the above differential equation yields the following (Korn & Korn, 1968):

$$R_q(\beta) = A\beta^n \left\{ 1 + \frac{n}{12}\beta^2 + \frac{(5n+7)n}{1440}\beta^4 + \frac{n(n+4)(5n+1)}{51840}\beta^6 \right\} \tag{45}$$

Finally, the hydrodynamic pressure, Eq. (40), in terms of velocity potential and radial displacement is written:

$$P_f = -\rho_f k \sum_{q=1}^{8} x \frac{\partial^2 W_q}{\partial t^2} \tag{46}$$

where:

$$k = \frac{\alpha}{n}\left[\frac{1+\frac{n}{12}\alpha^2+\frac{(5n+7)n}{1440}\alpha^4+\frac{n(n+4)(5n+1)}{51840}\alpha^6}{1+\frac{(n+2)}{12}\alpha^2+\frac{(n+4)(5n+7)}{1440}\alpha^4+\frac{(n+4)(n+6)(5n+1)}{51840}\alpha^6}\right] \tag{47}$$

By substituting the expression of W given in Eq. (31) into this pressure relation, Eq. (46), and introducing the general force vector as was done in the previous section, the fluid mass matrix is obtained:

$$[m_f] = [A^{-1}]^T [S_f][A^{-1}] \tag{48}$$

where:

$$[S_f] = -\rho_f k \iint x[N]^T [N_w] dA \tag{49}$$

The global fluid mass matrix $\mathbf{M_f}$ for the case that the shell is partially or completely filled with fluid is now entered into the governing equation.

4.6 Aeroelastic Model

The governing equation of motion in a global system for a fluid-filled conical shell exposed to external supersonic airflow is described using the following relation:

$$[M_s - M_f]\begin{Bmatrix}\ddot{\delta}_i \\ \ddot{\delta}_j\end{Bmatrix} - [C_f]\begin{Bmatrix}\dot{\delta}_i \\ \dot{\delta}_j\end{Bmatrix} + [\,[K_s]+[K_I]-[K_f]\,]\begin{Bmatrix}\delta_i \\ \delta_j\end{Bmatrix} = 0 \quad (50)$$

where subscripts s and f refer to a shell in vacuo and fluid, respectively and I refers to a shell under initial membrane forces (hydrostatic pressure and axial load). Aeroelastic stability of the shell is investigated by studying the eigenvalue in the complex plane. Flutter onset occurs when the imaginary part of the eigenvalue changes from positive to negative.

4.7 Numerical Results

4.7.1 Validation

Two different thin conical shells are treated here for validation. The first problem studies free vibration and buckling of a thin cone examined by Ueda and et al. (Ueda et al., 1977). Numerical calculation is carried out for the wind tunnel test model of a truncated conical shell made of super-Invar for which Young's modulus, Poisson's ratio and density are $1.28\times10^{4}\ kg\,mm^{-2}$, 0.25 and $8.13\times10^{-10}\ kg\,s^{2}mm^{-4}$, respectively. The shell has a ratio of slant length to small radius of $L/R_1 = 1.61$, a semivertex angle of 14 deg and clamped edges. The effect of pressure difference on the natural frequency of the 0.05 mm thick shell is shown in Fig. 3. The positive value is due to the fact that the internal pressure makes the natural frequencies increase, in other words it has a stabilizing effect. External pressure, on the other hand, causes a decrease in the natural frequencies. These trends, which are calculated using only 15 elements show good agreement with the

results obtained in Ref. (Ueda et al., 1977). For large values of external pressure the natural frequency becomes purely imaginary which represents the buckling state of the shell. The second problem treated for validation is the flutter boundary of a simply-supported cone subjected to external supersonic airflow. This case has been studied by various authors (Bismarck-Nasr & Costa Savio, 1979; Dixon & Hudson, 1970; Shulman, 1959). The shell has the following data: Young's modulus, $E = 6.5 \times 10^6\ lb\,in^{-2}$, Poisson's ratio, $\upsilon = 0.29$, material mass density, $\rho = 8.33 \times 10^{-4}\ lb\,s^2\,in^{-4}$, shell thickness, $h = 0.051\ in$, cone semivertex angle, $\alpha = 5\ \mathrm{deg}$, small end radius to thickness, $R_1 / h = 148$, and $L / R_1 = 8.13$ where L is the shell length. The supersonic airflow has freestream Mach number, $M_\infty = 3$, stagnation temperature, $T_\infty = 288.15\ K$ and stagnation pressure, $P_{s\infty} = 14.696\ lb\,in^{-2}$. The boundary conditions at both ends are $u = v = w = 0$. In Table 1, the critical dynamic pressure parameter is defined:

$$\Lambda = \frac{\rho_\infty U^2 R_1^3}{K(M_\infty^2 - 1)^{1/2}} \tag{50}$$

where K is expressed by Eq. (7). When results are summarized and compared with other finite element and analytical solutions, this method shows good convergence using only 15 elements.

4.7.2 Flutter Boundary

The conical shell of the preceding validation for flutter boundary is treated here. The complex frequencies only for the first and second modes versus free stream dynamic

pressure are plotted in Fig. 4. Aerodynamic pressure is evaluated using Eq. (29). In Fig. 4a the real part of the complex frequency increases for the first mode while for the second mode it decreases as the freestream dynamic pressure increases. For higher values of dynamic pressure these real parts, representing the oscillation frequency, eventually coalesce into a single mode. Further increasing the dynamic pressure of flow causes the shell to lose its stability at $p_\infty = 24.8\ psi$. This instability is due to coupled-mode flutter where the imaginary part of complex frequency (representing the damping of the system) crosses the zero value in Fig. 4b. The same behavior is observed in Fig. 5 but instability occurs at $p_\infty = 25.2\ psi$ where the aerodynamic pressure is evaluated using Eq. (30). For the shell treated here, one can see that the curvature term in the aerodynamic pressure expression has a small effect on the flutter boundary.

The flutter boundaries for different circumferential wave numbers for various shell internal or external pressures are reported in Fig. 6. Shell geometry and flow parameters are the same as used in the previous case study. When the shell is pressurized it becomes unstable at higher dynamic pressure levels due to an increase in stiffness because of applied internal pressure. External pressure decreases the stiffness of the shell which results in a lower critical freestream dynamic pressure.

In Fig. 7 the onset of flutter for different semivertex angles, α, and different L/R_1 ratios is plotted. By increasing the conicity effect, flutter instability occurs at lower dynamic pressures for longer shells. This decrease in Λ_{cr} with α is attributed to the fact that the natural frequencies always decrease with increasing the L/R_1 and α.

The effect of boundary conditions on the flutter onset is presented in Table 2. It is seen that for freely simply-supported ends, $u = w = 0$, flutter onset occurs at $27\,psi$ which indicates more flutter resistance compared to clamped ends. When the shell is free at both ends the instability is slightly different and two types of instability are observed. In Fig. 8a the real part of the complex frequency for the first mode decreases as the freestream static pressure increases, while the imaginary part remains positive. The existence of a zero real part and a negative imaginary part of the complex frequency indicates that the shell diverges statically. By further increasing the freestream static pressure, second mode remains stable but the real parts of third and forth modes merge into a single mode and their imaginary parts bifurcate into two branches and one of them becomes negative. At this point, $p_\infty = 45\,psi$, the shell loses stability due to coupled-mode flutter because a negative imaginary part makes the vibration amplitude grow.

4.7.3 Effect of Filling Ratio

In this section the effect of filling ratio on the flutter boundary is investigated. Fig. 9 shows the critical value of freestream static pressure for different filling ratios, H/L, and for various lengths of the shell, L/R_1. Shell geometry and flow parameters are the same as the previous case study with liquid-filled density $\rho_f = 9.355\times10^{-5}\ lb\,s^2\,in^{-4}$. In general, the critical dynamic pressure parameter for an empty shell increases as the length ratio is decreased. It is seen that the value of critical dynamic pressure changes rapidly and widely as the filling ratio increases from a low value. In addition, by increasing the length ratio the decrement of the critical value of Λ is decreased and

vanishes when coupled-mode flutter type instability occurs. This rapid change in critical dynamic pressure at low filling ratios and its almost steady behaviour at large filling ratios indicates that the fluid near the bottom of the shell is largely influenced by elastic deformation when a shell is subjected to external subsonic flow.

4.8 Conclusion

An efficient hybrid finite element method is presented to analyze the aeroelastic stability of an empty or partially liquid-filled conical shell subjected to external supersonic flow. Sanders linear shell theory is coupled with first order piston theory to account for aerodynamic pressure. Fluid-structure interaction due to hydrodynamic pressure of an internal fluid along with the effects of initial stress stiffening is also taken into account. The study has been done for shells with various geometries and boundary conditions. In all study cases one type of instability is found; coupled-mode flutter in the first and second mode. For the free-free boundary condition however, the shell loses its stability first through divergence and then by flutter due to coupling of the third and forth modes. An internally pressurized shell shows more flutter resistance than a shell under external pressure. Decreasing the vertex angle of the cone causes the flutter boundary to occur at a lower dynamic pressure. A lower filling ratio has more flutter resistance for short shells than long shells. The proposed hybrid finite element package can present reliable results at less computational cost compared to commercial software since the latter imposes some restrictions when such an analysis is done.

4.9 Acknowledgments

The authors acknowledge the financial support of NSERC of Canada, grant No. A8814.

4.10 Appendix

The equilibrium equations (Eq. (4)) are:

$$L_1(x,\theta,B_{ij}) = B_{11}\left[2x\sin\alpha\frac{\partial U}{\partial x} + x^2\frac{\partial^2 U}{\partial x^2}\right] + B_{12}\left[x\frac{\partial^2 V}{\partial x\partial\theta} + x\cos\alpha\frac{\partial W}{\partial x} + U\sin\alpha + W\cos\alpha\right] -$$

$$B_{14}\left[3x^2\sin\alpha\frac{\partial^2 W}{\partial x^2} + x^3\sin\alpha\frac{\partial^3 W}{\partial x^3}\right] + B_{15}\left[x\cot\alpha\frac{\partial V}{\partial x\partial\theta} - \frac{x}{\sin\alpha}\frac{\partial^3 W}{\partial\theta^2\partial x} - 2x\sin\alpha\frac{\partial W}{\partial x} - x^2\sin\alpha\frac{\partial^2 W}{\partial x^2} + \cot\alpha\frac{\partial V}{\partial\theta} - \frac{1}{\sin\alpha}\frac{\partial^2 W}{\partial\theta^2}\right] -$$

$$B_{22}\left[\frac{\partial V}{\partial\theta} + \sin\alpha U + \cos\alpha W\right] + B_{24}\left[x^2\sin\alpha\frac{\partial^2 W}{\partial x^2}\right] + B_{25}\left[-\cot\alpha\frac{\partial V}{\partial\theta} + \frac{1}{\sin\alpha}\frac{\partial^2 W}{\partial\theta^2} + x\sin\alpha\frac{\partial W}{\partial x}\right] + B_{33}\left[x\frac{\partial^2 V}{\partial x\partial\theta} + \frac{1}{\sin\alpha}\frac{\partial^2 U}{\partial\theta^2} - \frac{\partial V}{\partial\theta}\right] +$$

$$B_{36}\left[-\frac{2x}{\sin\alpha}\frac{\partial^3 W}{\partial\theta^2\partial x} + x\cot\alpha\frac{\partial^2 V}{\partial x\partial\theta} - \frac{\cot\alpha}{\sin\alpha}\frac{\partial^2 U}{\partial\theta^2} + \frac{2}{\sin\alpha}\frac{\partial^2 W}{\partial\theta^2} - \cot\alpha\frac{\partial V}{\partial\theta}\right] +$$

$$B_{66}\left[\frac{x\cot\alpha}{\sin\alpha}\frac{\partial^3 W}{\partial\theta^2\partial x} - \frac{3x}{4}\cot^2\alpha\frac{\partial^2 V}{\partial x\partial\theta} + \frac{\cot^2\alpha}{4\sin\alpha}\frac{\partial^2 U}{\partial\theta^2} - \frac{\cot\alpha}{\sin\alpha}\frac{\partial^2 W}{\partial\theta^2} + \frac{3\cot^2\alpha}{4}\frac{\partial V}{\partial\theta}\right]$$

$$L_2(x,\theta,B_{ij}) = B_{12}x\frac{\partial^2 U}{\partial x\partial\theta} + B_{13}x\cot\alpha\frac{\partial^2 U}{\partial x\partial\theta} + B_{22}\left[\frac{1}{\sin\alpha}\frac{\partial^2 V}{\partial\theta^2} + \frac{\partial U}{\partial\theta} + \cot\alpha\frac{\partial W}{\partial\theta}\right] - B_{24}x^2\frac{\partial^3 W}{\partial x^2\partial\theta} +$$

$$B_{25}\left[\frac{2\cot\alpha}{\sin\alpha}\frac{\partial^2 V}{\partial\theta^2} - \frac{1}{\sin^2\alpha}\frac{\partial^3 W}{\partial\theta^3} - x\frac{\partial^2 W}{\partial x\partial\theta} + \cot^2\alpha\frac{\partial W}{\partial\theta} + \cot\alpha\frac{\partial U}{\partial\theta}\right] - B_{45}x^2\cot\alpha\frac{\partial^3 W}{\partial x^2\partial\theta} + B_{55}\left[\frac{\cot^2\alpha}{\sin\alpha}\frac{\partial^2 V}{\partial\theta^2} - \frac{\cot\alpha}{\sin^2\alpha}\frac{\partial^3 W}{\partial\theta^3} - x\cot\frac{\partial^2 W}{\partial x\partial\theta}\right]$$

$$B_{33}\left[x^2\sin\alpha\frac{\partial^2 V}{\partial x^2} + x\cot\alpha\frac{\partial^2 U}{\partial x\partial\theta} - 4x\frac{\partial^2 W}{\partial x\partial\theta} + 6x\cos\alpha\frac{\partial V}{\partial x} + 2\cot\alpha\frac{\partial U}{\partial\theta} + 4\frac{\partial W}{\partial\theta} - 6\cos\alpha V\right] +$$

$$B_{66}\left[\begin{array}{l} -6x\cot\alpha\dfrac{\partial^2 W}{\partial x\partial\theta} - 3x^2\cot\alpha\dfrac{\partial^3 W}{\partial x^2\partial\theta} + \dfrac{9x}{2}\cos\alpha\cot\alpha\dfrac{\partial V}{\partial x} + \dfrac{9x^2}{4}\cos\alpha\cot\alpha\dfrac{\partial^2 V}{\partial x^2} - \dfrac{3}{2}\cot^2\alpha\dfrac{\partial U}{\partial\theta} - \dfrac{3x}{4}\cot^2\alpha\dfrac{\partial^2 U}{\partial x\partial\theta} + \\ 6\cot\alpha\dfrac{\partial W}{\partial\theta} - \dfrac{9}{2}\cos\alpha\cot\alpha V \end{array}\right]$$

$$L_3(x,\theta,B_{ij}) = -B_{12}x\cos\alpha\frac{\partial U}{\partial x} + B_{14}\left[6x\sin\alpha\frac{\partial U}{\partial x} + 6x^2\sin\alpha\frac{\partial^2 U}{\partial x^2} + x^3\sin\alpha\frac{\partial^3 U}{\partial x^3}\right] + B_{15}\left[\frac{x}{\sin\alpha}\frac{\partial^3 U}{\partial\theta^2\partial x} - 2x\sin\alpha\frac{\partial U}{\partial x} - x^2\sin\alpha\frac{\partial^2 U}{\partial x^2}\right] -$$

$$B_{22}\left[\cot\alpha\frac{\partial V}{\partial\theta} + \cos\alpha U + \cos\alpha\cot\alpha W\right] +$$

$$B_{24}\left[4x\frac{\partial^2 V}{\partial x\partial\theta} + x^2\frac{\partial^3 V}{\partial x^2\partial\theta} + 4x\sin\alpha\frac{\partial U}{\partial x} + x^2\sin\alpha\frac{\partial^2 U}{\partial x^2} + 4x\cos\alpha\frac{\partial W}{\partial x} + 2x^2\cos\alpha\frac{\partial^2 W}{\partial x^2} + 2\frac{\partial V}{\partial\theta} + 2\sin\alpha U + 2\cos\alpha W\right] +$$

$$B_{25}\left[-\cot^2\alpha\frac{\partial V}{\partial\theta} + \frac{1}{\sin^2\alpha}\frac{\partial^3 V}{\partial\theta^3} + \frac{1}{\sin\alpha}\frac{\partial^2 U}{\partial\theta^2} + 2\frac{\cot\alpha}{\sin\alpha}\frac{\partial^2 W}{\partial\theta^2} - \frac{\partial V}{\partial\theta} - x\frac{\partial^2 V}{\partial x\partial\theta} - \sin\alpha U - x\sin\alpha\frac{\partial U}{\partial x} - \cos\alpha W\right] +$$

$$B_{36}\left[6x\frac{\partial^2 V}{\partial x\partial\theta} + 2x^2\frac{\partial^3 V}{\partial x^2\partial\theta} + \frac{4}{\sin\alpha}\frac{\partial^2 U}{\partial\theta^2} + \frac{2x}{\sin\alpha}\frac{\partial^3 U}{\partial\theta^2\partial x} - 4\frac{\partial V}{\partial\theta} - 2x\frac{\partial^2 V}{\partial x\partial\theta}\right] - B_{44}\left[12x^2\sin\alpha\frac{\partial^2 W}{\partial x^2} + 8x^3\sin\alpha\frac{\partial^3 W}{\partial x^3} + x^4\sin\alpha\frac{\partial^4 W}{\partial x^4}\right] +$$

$$B_{45}\left[4x\cot\alpha\frac{\partial^2 V}{\partial x\partial\theta} + x^2\cot\alpha\frac{\partial^3 V}{\partial x^2\partial\theta} - \frac{4x}{\sin\alpha}\frac{\partial^3 W}{\partial x\partial\theta^2} - \frac{2x^2}{\sin\alpha}\frac{\partial^4 W}{\partial\theta^2\partial x} - 6x\sin\alpha\frac{\partial W}{\partial x} + 2\cot\alpha\frac{\partial V}{\partial\theta} - \frac{2}{\sin\alpha}\frac{\partial^2 W}{\partial\theta^2} - 3x^2\sin\alpha\frac{\partial^2 W}{\partial x^2}\right] -$$

$$B_{55}\left[\cot\alpha\frac{\partial V}{\partial\theta} + x\cot\alpha\frac{\partial^2 V}{\partial x\partial\theta} - \frac{1}{\sin\alpha}\frac{\partial^2 W}{\partial\theta^2} - 2x\sin\alpha\frac{\partial^2 W}{\partial x^2} - x^2\sin\alpha\frac{\partial^2 W}{\partial x^2} - \frac{\cot\alpha}{\sin^2\alpha}\frac{\partial^3 V}{\partial\theta^3} + \frac{1}{\sin^3\alpha}\frac{\partial^4 W}{\partial\theta^4}\right] +$$

$$B_{66}\left[-\frac{8x}{\sin\alpha}\frac{\partial^3 W}{\partial\theta^2\partial x} - \frac{4x^2}{\sin\alpha}\frac{\partial^4 W}{\partial\theta^2\partial x^2} + 6x\cot\alpha\frac{\partial^2 V}{\partial x\partial\theta} + 3x^2\cot\alpha\frac{\partial^3 V}{\partial x^2\partial\theta} - \frac{2\cot\alpha}{\sin\alpha}\frac{\partial^2 U}{\partial\theta^2} - \frac{x\cot\alpha}{\sin\alpha}\frac{\partial^3 U}{\partial\theta^2\partial x} + \frac{8}{\sin\alpha}\frac{\partial^2 W}{\partial\theta^2} - 6\cot\alpha\frac{\partial V}{\partial\theta}\right]$$

4.11 References

Amabili, M., and Pellicano, F. (2001). Nonlinear supersonic flutter of circular cylindrical shells. *AIAA Journal, 39*(4), 564-573.

Amabili, M., and Pellicano, F. (2002). Multimode approach to nonlinear supersonic flutter of imperfect circular cylindrical shells. *Journal of Applied Mechanics, Transactions ASME, 69*(2), 117-129.

Ashley, H., and Zartarian, G. (1956). Piston theory-New aerodynamic tool for aeroelastician. *Journal of the Aeronautical Sciences, 23*(12), 1109-1118.

Barr, G. W., and Stearman, R. O. (1969). Aeroelastic stability characteristics of cylindrical shells considering imperfections and edge constraint. *AIAA Journal, 7*(5), 912-919.

Bismarck-Nasr, M. N. (1976). Finite element method applied to the supersonic flutter of circular cylindrical shells. *International Journal for Numerical Methods in Engineering, 10*(2), 423-435.

Bismarck-Nasr, M. N. (1996). Finite elements in aeroelasticity of plates and shells. *Applied Mechanics Reviews, 49*(10 pt 2), 17-24.

Bismarck-Nasr, M. N., and Costa Savio, H. R. (1979). Finite-Element Solution of the Supersonic Flutter of Conical Shells. *AIAA Journal, 17*(10), 1148-1150.

Dixon, S. C., and Hudson, M. L. (1970). *Flutter, Vibration, And Buckling of Truncated Orthotropic Conical Shells with Generalized Elastic Edge Restraint.* NASA TN D-5759.

Dowell, E. H. (1975). *Aeroelasticity of plates and shells.* Leyden: Noordhoff International Publishing.

Flugge, W. (1973). *Stress in Shell* (2nd edition ed.): Springer-verlag.

Ganapathi, M., Varadan, T. K., and Jijen, J. (1994). Field-consistent element applied to clutter analysis of circular cylindrical shells. *Journal of Sound and Vibration, 171*(4), 509-527.

Korn, G. A., and Korn, T. M. (1968). *Mathematical Handbook for Scientists and engineer* (2nd edition ed.). New York: McGraw-Hill.

Kumar, S. D., and Ganesan, N. (2008). Dynamic analysis of conical shells conveying fluid. *Journal of Sound and Vibration, 310*, 38-57.

Lakis, A. A., and Paidoussis, M. P. (1972). Dynamic analysis of axially non-uniform thin cylindrical shells. *Journal of Mechanical Engineering Science, 14*(1), 49-71.

Lakis, A. A., Van Dyke, P., and Ouriche, H. (1992). Dynamic analysis of anisotropic fluid-filled conical shells. *Journal of Fluid and Structures, 6*(2), 135-162.

MacNeal, R. H. (1972). *Nastran Theoretical manual.* NASA SP-221.

Mason, D. R., and Blotter, P. T. (1986). Finite-Element Application to Rocket Nozzle Aeroelasticity. *Journal of Propulsion and Power, 2*(6), 499-507.

Miserentino, R., and Dixon, S. C. (1971). *Vibration and Flutter Tests of a Pressurized thin-walled Truncated Conical Shell.* NASA TN D-6106.

Olson, M. D., and Fung, Y. C. (1966). Supersonic flutter of circular cylindrical shells subjected to internal pressure and axial compression. *AIAA Journal, 4*(5), 858-864.

Olson, M. D., and Fung, Y. C. (1967). Comparing theory and experiment for supersonic flutter of circular cylindrical shells. *AIAA Journal, 5*(10), 1849-1856.

Sanders, J. L. (1959). *An Improved First-Approximation Theory for Thin Shell.* NASA R-24.

Shulman, Y. (1959). *Vibration and Flutter of Cylindrical and Conical Shells.* MIT ASRL Rept. 74-2 OSR Tech Rept. 59-776.

Sunder, P. J., Ramakrishnan, V. C., and Sengupta, S. (1983a). Finite element analysis of 3-ply laminated conical shell for flutter. *International Journal for Numerical Methods in Engineering, 19*, 1183-1192.

Sunder, P. J., Ramakrishnan, V. C., and Sengupta, S. (1983b). Optimum Cone Angles in Aeroelastic flutter. *Computer & Structures, 17*(1), 25-29.

Ueda, T., Kobayashi, S., and Kihira, M. (1977). Supersonic flutter of truncated conical shells. *Transactions of the Japan Society for Aeronautical and Space Sciences, 20*(47), 13-30.

Zienkiewicz, O. C., and Taylor, R. L. (2000). *The finite element method,Volume:2 Solid Mechanics* (5th edition ed.). Oxford: Butterworht-Heinemann.

4.12 List of Figures and Tables

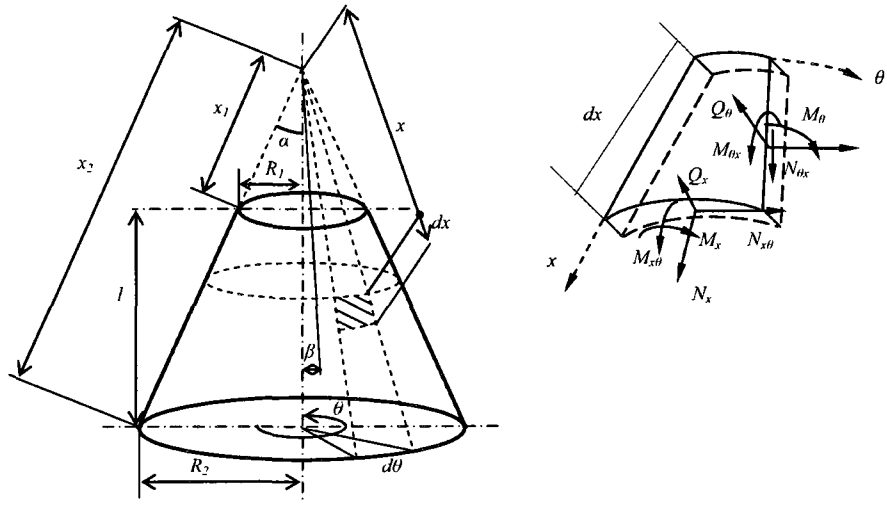

Fig.1. Geometry of a truncated conical shell

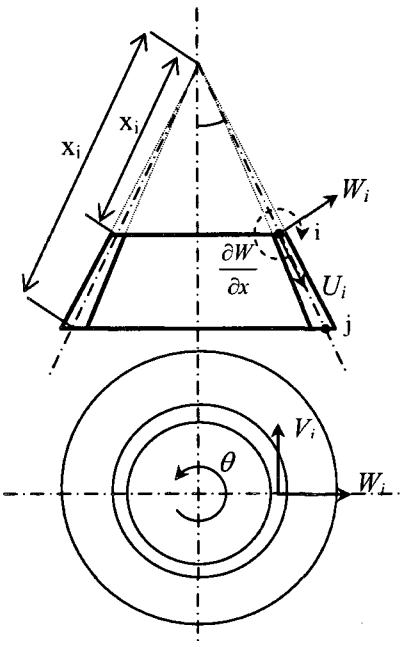

Fig.2. Conical frustum element

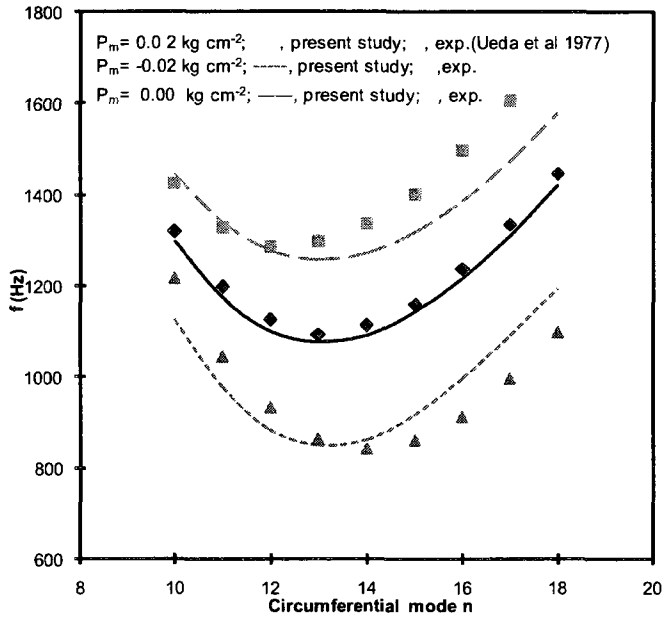

Fig. 3. Effect of pressure difference on natural frequency versus circumferential wave number

Table1. Critical freestream dynamic pressure for the conical shell

Source	Λ_{cr}	n_{cr}
Shulman (Shulman, 1959) :Galerkin, 4 terms	669	6
Dixon and Hudson (Dixon & Hudson, 1970):		
Galerkin, 4 terms	492	5
Galerkin, 8 terms	588	5
Galerkin, 12 terms	590	5
Bismarck-Nasr (Bismarck-Nasr & Costa Savio, 1979), FEM :	702	6
Present study:		
pressure by Eq. (29)	598	6
pressure by Eq. (30)	628	6

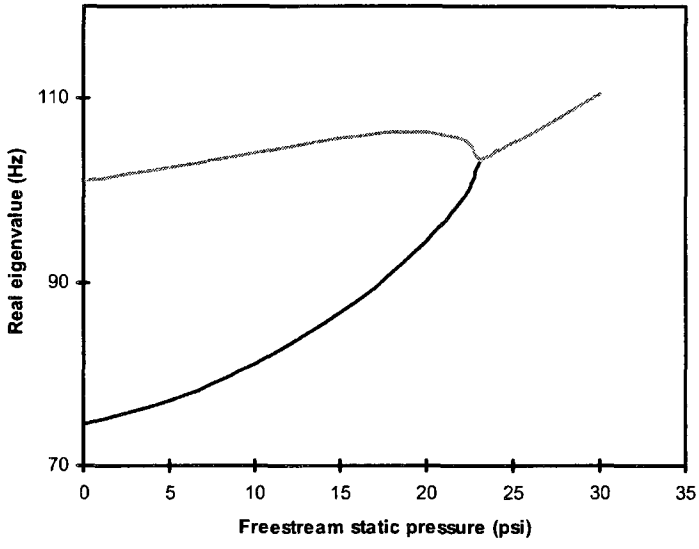

a)

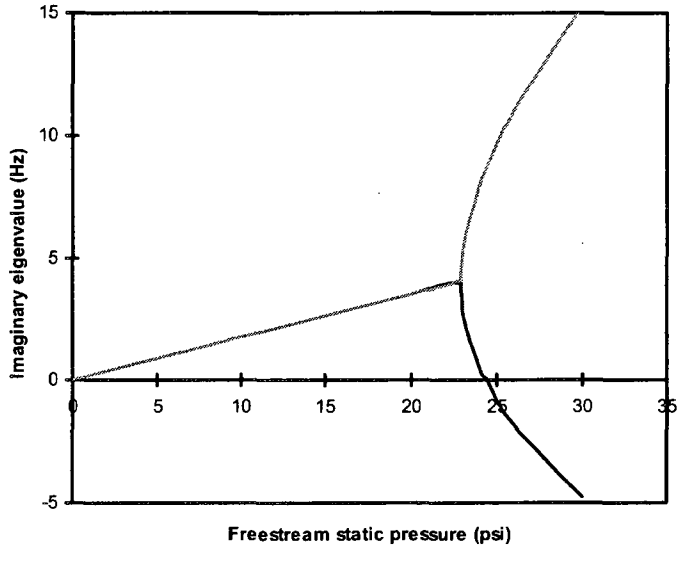

b)

Fig. 4. a) Real part and b) imaginary part of the complex frequencies, $n = 6$, versus freestream static pressure, aerodynamic pressure evaluated by Eq. (29)

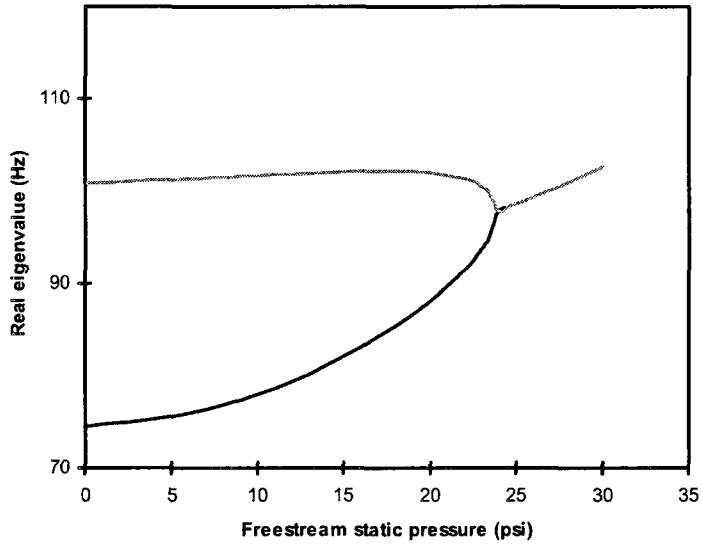

a)

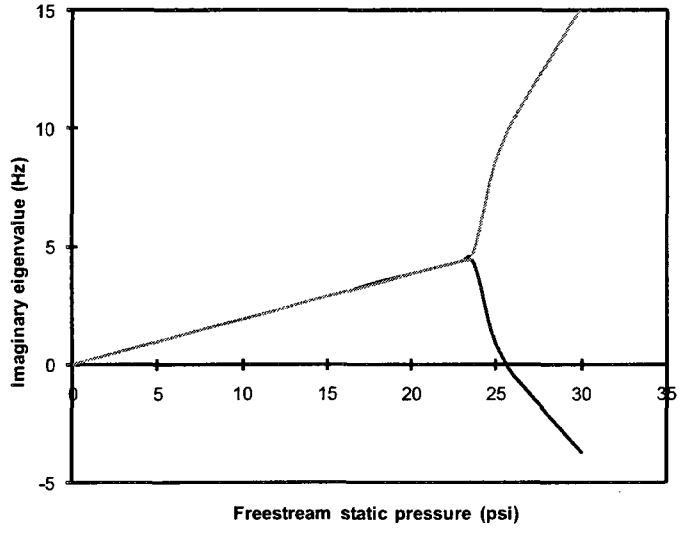

b)

Fig. 5. a) Real part and b) imaginary part of the complex frequencies, $n = 6$, versus freestream static pressure, aerodynamic pressure evaluated by Eq. (30)

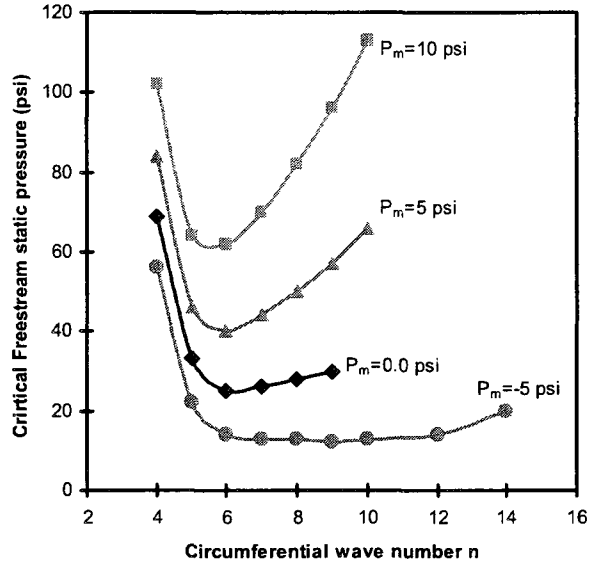

Fig. 6. Flutter boundaries for stressed shell. $R_1/h=148$, $L/R_1=8.13$, $h=0.051\,in$, $\alpha=5\deg$, $P_x=0.0$

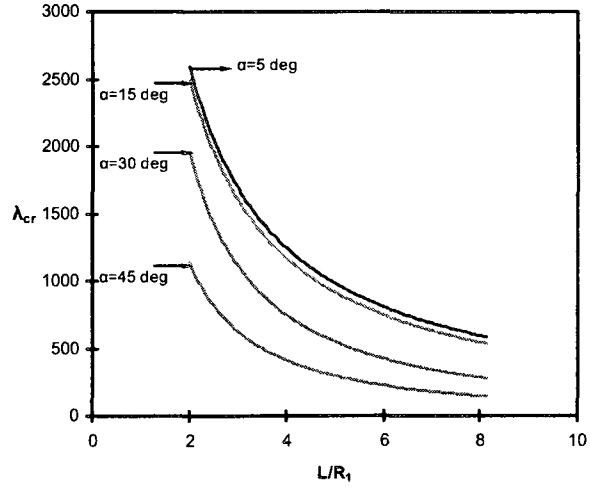

Fig.7. Variation of critical dynamic pressure parameter, Eq. (51), with L/R_1, for an isotropic shell, $R_1/h=148$, $5\le\alpha\le45$, $P_m=P_x=0.0$, $u=v=w=0$

Table 2 Critical freestream static pressure for different boundary conditions

Boundary condition	p_∞ (psi)	Mode No.
freely simply supported	27	coupled 1st and 2nd
clamped-clamped	24.5	coupled 1st and 2nd
free-free		
divergence:	39	1st
flutter:	45	coupled 3rd and 4th

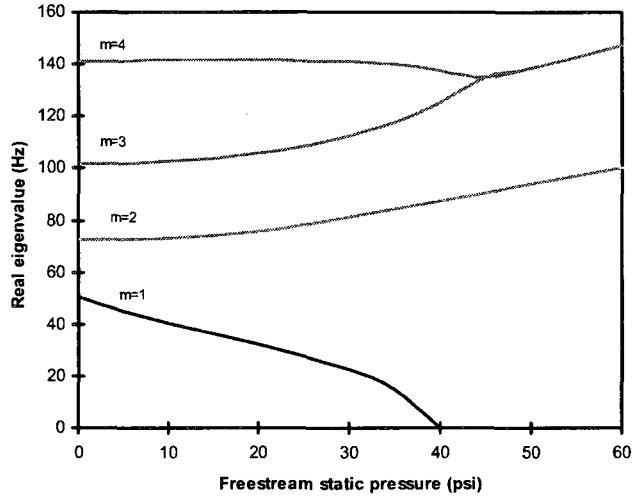

a)

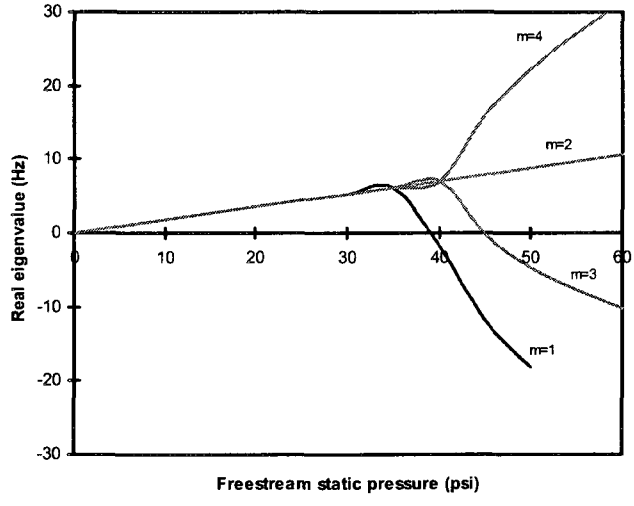

b)

Fig. 8. a) Real part and b) imaginary part of the complex frequencies, $n = 6$, versus freestream static pressure, aerodynamic pressure evaluated by Eq. (29)

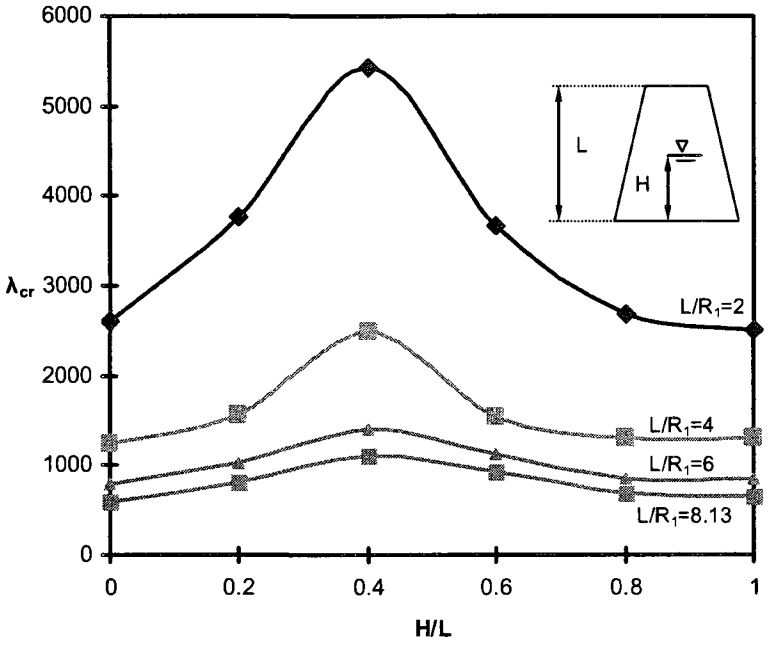

Fig. 9. Flutter boundary for different filling ratios H/L; $R_1/h = 148$, $\alpha = 5$ deg

Chapter 5: General Discussion

This study presented supersonic flutter, vibration and buckling of circular cylindrical and truncated conical shells.

When the shell is completely or partially fluid-filled, the critical buckling loads are not changed compared to the case of empty shell. Filling the shell with fluid only affects the vibration frequency of the shell in the following manner; as the amount of fluid is increased, oscillation frequencies are decreased. The buckling state is found when these oscillation frequencies vanish. It is also observed that a pressurized shell provides more buckling resistance when it is under axial compression. If it is subjected to an external pressure the buckling point will occur at a lower critical value of axial compression compared to the former case. In all obtained results the effect of pre-buckling and shell imperfections are neglected. Analysis of these effects is recommended for future study.

In the case of a partially fluid-filled shell subjected to supersonic flow, we observed that the presence of the inside fluid has an influence on the flutter onset. This effect is greater at low filling ratios and low aspect ratios L/R, where the critical flutter velocity is increased for this boundary condition and geometry configuration.

Dynamic instability occurs in the form of coupled mode flutter for both cylindrical and conical shells placed in an external supersonic flow. A pressurized shell generally shows more flutter resistance than an unpressurized one; however it should be noted that based on existing experimental results, moderate internal pressure can decrease the dynamic stability of the shell to the lower level of an unpressurized shell. Nevertheless, at small

and large internal pressures this numerical simulation provides accurate predictions when compared to other numerical and theoretical results.

When the shell is in the free vibration state the modes shapes are standing waves. At values of supersonic velocity below flutter onset, modes shapes contain traveling wave components similar to those reported in experimental tests. In this case the nodes and anti-nodes travel circumferentially along the shell.

Different end boundary conditions were tested for cylindrical and conical shells. In all cases the shells lose their stability through coupled mode flutter except for the free-free end of the conical shell. It first loses its stability through a divergence (buckling) mode and as the flow velocity is increased it becomes dynamically unstable due to coupled mode flutter.

Chapter 6: Conclusion and Recommendation

6.1 Overview

An efficient hybrid finite element code for aeroelastic analysis and buckling of shell of revolutions was developed. This FEM package can be used effectively for the design of advanced aerospace structures. It demonstrated very fast and precise solution convergence. In addition, this approach works well for prediction of the behavior of shells subjected to supersonic flow at different complex boundary conditions and geometries.

6.2 Concluding Remarks

In this PhD dissertation the following modeling and analysis capabilities have been achieved:

- Linear modeling of shells using a hybrid finite element method.
- Initial strain and stress stiffening due to lateral pressure and axial loading.
- Piston theory for supersonic aerodynamic pressure loading.
- Potential flow theory for internal hydrodynamic pressure.

Using this advanced modeling capability various problems were investigated and an improved prediction was obtained. These include:

- Buckling of empty and partially fluid filled shells
- Aeroelastic instabilities, flutter
- Effect of initial strain on aeroelastic stability

The most significant contribution of this work is the finite element formulation and solution. The FE formulation is designed to handle any analytically or numerically formulated cylindrical or conical shell based on Sanders thin shell theory coupled with piston theory. This hybrid FEM is very successful in predicting aeroelastic instabilities. The computational efficiency and performance of this method has also been proven to be more effective than coupled CFD and FEM packages.

6.3 Future Studies

Future work should include analysis of the effects of geometry and aerodynamic nonlinearities on the flutter boundary. Including these effects would improve the reliability of this FEM package.

It is also recommended to develop an approach to include the effects of aerodynamic heating, in-plane temperature distribution and temperature gradient through the shell thickness on aeroelastic stability. The outer skins of most modern aerospace vehicles may experience very high temperature environments and because of this, use of functionally graded material (FGM) can be efficient. Subsequent to this work we will be studying the supersonic flutter of FG cylindrical and conical shells where their material properties are assumed to be temperature dependent and graded across shell thickness according to different theories, such as the simple power law.

References

Amabili, M. (2008). *Nonlinear Vibration and Stability of Shells and Plates*: Cambridge University Press.

Amabili, M., Paidoussis, M. P., and Lakis, A. A. (1998). Vibrations of partially filled cylindrical tanks with ring-stiffeners and flexible bottom. *Journal of Sound and Vibration, 213*(2), 259-298.

Amabili, M., and Pellicano, F. (2001). Nonlinear supersonic flutter of circular cylindrical shells. *AIAA Journal, 39*(4), 564-573.

Amabili, M., and Pellicano, F. (2002). Multimode approach to nonlinear supersonic flutter of imperfect circular cylindrical shells. *Journal of Applied Mechanics, Transactions ASME, 69*(2), 117-129.

Ashley, H., and Zartarian, G. (1956). Piston theory-New aerodynamic tool for aeroelastician. *Journal of the Aeronautical Sciences, 23*(12), 1109-1118.

Barnes, C. H. (1987). *Handley Page Aircrfat Since 1907.*: Chrysalis Books

.Barr, G. W., and Stearman, R. O. (1969). Aeroelastic Stability Characteristics of Cylindrical Shells Considering Imperfections and Edge Constraint. *AIAA Journal, 7*(5), 912-919.

Barr, G. W., and Stearman, R. O. (1970). Influence of a Supersonic Flowfield on the Elastic Stability of Cylindrical Shells. *AIAA Journal, 8*(6), 993-1000.

Bismarck-Nasr, M. N. (1976). Finite Element Method Applied to the Supersonic Flutter of Circular Cylindrical Shells. *International Journal for Numerical Methods in Engineering, 10*(2), 423-435.

Bismarck-Nasr, M. N. (1996). Finite elements in aeroelasticity of plates and shells. *Applied Mechanics Reviews, 49*(10 pt 2), 17-24.

Bismarck-Nasr, M. N., and Costa Savio, H. R. (1979). Finite-Element Solution of the Supersonic Flutter of Conical Shells. *AIAA Journal, 17*(10), 1148-1150.

Collar, A. R. (1978). The First Fifity Years of Aeroelasticity. *Aerospace, Royal Aeronautical Society, 5*(2), 12-20.

Dixon, S. C., and Hudson, M. L. (1970). *Flutter, Vibration, And Buckling of Truncated Orthotropic Conical Shells with Generalized Elastic Edge Restraint.*

Dowell, E. H. (1975). *Aeroelasticity of plates and shells.* Leyden: Noordhoff International Publishing.

Evensen, D. A., and Olson, M. D. (1967). *Nonlinear Flutter of a Circular Cylindrical shell in Supersonic Flow.*

Evensen, D. A., and Olson, M. D. (1968). Circumferentially traveling wave flutter of circular cylindrical shell. *AIAA Journal, 6*(8), 1522-1527.

Ganapathi, M., Varadan, T. K., and Jijen, J. (1994). Field-consistent element applied to clutter analysis of circular cylindrical shells. *Journal of Sound and Vibration, 171*(4), 509-527.

Horn, W., Barr, G., Carter, L., and Stearman, R. (1974). Recent contributions to experiments on cylindrical shell panel flutter. *AIAA Journal, 12*(11), 1481-1490.

Jeong, K.-H., and Lee, S.-C. (1998). Hydroelastic vibration of a liquid-filled circular cylindrical shell. *Computers and Structures, 66*(2-3), 173-185.

Lakis, A. A., and Paidoussis, M. P. (1971). Free Vibration of Cylindrical Shells Partially Filled with Liquid. *Journal of Sound and Vibration, 19*(1), 1-15.

Mason, D. R., and Blotter, P. T. (1986). Finite-Element Application to Rocket Nozzle Aeroelasticity. *Journal of Propulsion and Power, 2*(6), 499-507.

Mazuch, T., Horacek, J., Trnka, J., and Vesely, J. (1996). Natural modes and frequencies of a thin clamped-free steel cylindrical storage tank partially filled with water: FEM and measurement. *Journal of Sound and Vibration, 193*(3), 669-690.

Miserentino, R., and Dixon, S. C. (1971). Vibration and Flutter Tests of a Pressurized thin-walled Truncated Conical Shell. *NASA TN D-6106.*

Mistry, J., and Menezes, J. C. (1995). Vibration of cylinders partially-filled with liquids. *Journal of Vibration and Acoustics, Transactions of the ASME, 117*(1), 87-93.

Nemeth, M. P., Britt, V. O., Collins, T. J., and Starnes, J. H., Jr. (1996). Nonlinear analysis of the space shuttle super-lightweight external fuel tank. *NASA Technical Paper 3616.*

Nemeth, M. P., Young, R. D., Collins, T. J., and Starnes J.H, Jr. (2002). Effects of initial geometric imperfections on the non-linear response of the Space Shuttle superlightweight liquid-oxygen tank. *International Journal of Non-Linear Mechanics, 37*(4-5), 723-744.

Olson, M. D., and Fung, Y. C. (1966). Supersonic flutter of circular cylindrical shells subjected to internal pressure and axial compression. *AIAA Journal, 4*(5), 858-864.

Olson, M. D., and Fung, Y. C. (1967). Comparing theory and experiment for supersonic flutter of circular cylindrical shells. *AIAA Journal, 5*(10), 1849-1856.

Paidoussis, M. P. (1998). *Fluid-Structure Interactions: Slender Structures and Axial Flow; Volume 1* (Vol. 1). Bridgend, Mid Glamorgan,UK: Academic Press.

Paidoussis, M. P. (2004). *Fluid-Structure Interactions: Slender Structures and Axial Flow; Volume 2* (Vol. 2). Amsterdam: Elsevier Academic Press.

Pellicano, F., and Amabili, M. (2003). Stability and vibration of empty and fluid-filled circular cylindrical shells under static and periodic axial loads. *International Journal of Solids and Structures, 40*(13-14), 3229-3251.

Pellicano, F., and Amabili, M. (2006). Dynamic instability and chaos of empty and fluid-filled circular cylindrical shells under periodic axial loads. *Journal of Sound and Vibration, 293*(1-2), 227-252.

Shulman, Y. (1959). *Vibration and Flutter of Cylindrical and Conical Shells.*

Sunder, P. J., Ramakrishnan, V. C., and Sengupta, S. (1983a). Finite element analysis of 3-ply laminated conical shell for flutter. *International Journal for Numerical Methods in Engineering, 19*, 1183-1192.

Sunder, P. J., Ramakrishnan, V. C., and Sengupta, S. (1983b). Optimum Cone Angles in Aeroelastic flutter. *Computer & Structures, 17*(1), 25-29.

Ueda, T., Kobayashi, S., and Kihira, M. (1977). Supersonic flutter of truncated conical shells. *Transactions of the Japan Society for Aeronautical and Space Sciences, 20*(47), 13-30.

Vodenitcharova, T., and Ansourian, P. (1996). Buckling of circular cylindrical shells subject to uniform lateral pressure. *Engineering Structures, 18*(8), 604-614.

Yamaki, N. (1984). *Elastic Stability for Circular Cylindrical Shells*: North Holland.